Molecular Orientation and Electronic Interactions in Organic Thin Films Studied by Spectroscopic Ellipsometry

von der Fakultät für Naturwissenschaften der Technischen Universität Chemnitz
Genehmigte Dissertation zur Erlangung des akademischen Grades

doctor rerum naturalium
(Dr. rer. nat.)

vorgelegt von M. Sc. Phys. Ovidiu Dorin Gordan

geboren am 20. August 1978 in Cluj-Napoca

eingereicht am 18. Juli 2006

Gutachter: Prof. Dr. Dietrich R. T. Zahn
Prof. Dr. Frank Richter
Prof. Dr. Norbert Esser

Tag der Verteidigung: 03. November 2006

Bibliografische Beschreibung

M. Sc. Phys. Ovidiu Dorin Gordan

Molecular Orientation and Electronic Interactions in Organic Thin Films Studied by Spectroscopic Ellipsometry

Technische Universität Chemnitz

Dissertation (in englischer Sprache), 2006

In dieser Arbeit wurde das Wachstum von organischen Molekülschichten mit Hilfe einer Kombination aus spektroskopischer Ellipsometrie mit variablem Einfallswinkel *Variable Angle Spectroscopic Ellipsometry* (VASE) und Infrarotspektroskopie (IR) untersucht. Als organische Systeme wurden verschiedene Phthalocyaninmoleküle (Pc), 3,4,9,10-Perylentetracarbonsäure Dianhydrid (PTCDA) und tris-(8-hydroxochinolin)-Aluminium(III) (Alq_3) / N,N'-Di-[(1-naphthyl)-N,N'-diphenyl]-(1,1'-biphenyl)-4,4'-diamin (α-NPD) betrachtet.

Das geordnete Wachstum der Pcs und von PTCDA führt, bedingt durch die intrinsische optische Anisotropie der planaren organischen Moleküle, zu hochgradig anisotropen Schichten. Im Gegensatz zu den planaren Molekülen bilden Alq_3 und α-NPD homogene isotrope Filme mit einer sehr geringen Oberflächenrauigkeit aus. Als eine nicht destruktive und sehr oberflächensensitive Technik, erlaubt es die Ellipsometrie, die Dicke, die Oberflächenrauigkeit und die optischen Konstanten genau zu bestimmen. Aus der starken *in-plane / out-of-plane* Anisotropie der dielektrischen Funktion wurde der mittlere molekulare Orientierungswinkel der Pc-Moleküle bestimmt. Die Kenntnis der molekularen Orientierung, verknüpft mit der in der Form des Q-Bandes der Pc-Moleküle enthaltenen Information, gewährt Einblick in das molekulare Wachstumsverhalten. Während die Pc-Schichten unter Hochvakuumbedingungen mit der b-Achse (Stapelachse) senkrecht zum Substrat wachsen und $F_{16}PcVO$ sich flach auf die KBr-Substrate legt, nehmen die unter Ultrahochvakuumbedingungen hergestellten Pc-Proben eine parallel zum Substrat liegende b-Achsenanordnung ein. Diese Ergebnisse wurden mit IR-Messungen bestätigt, welche in s- und p-Polarisation durchgeführt wurden. Die ellipsometrischen Untersuchungen an Heterostrukturen haben bewiesen, dass PTCDA einen Template-Effekt auf das Wachstum der aufwachsenden Pc-Schicht hat und dass die Wechselwirkung zwischen diesen beiden Molekülen die Reaktion an der Grenzflächenschicht beeinflusst. Im Gegensatz zu diesem System, bei dem raue Grenzflächen im Modell verwendet wurden, ergibt die Kombination Alq_3 / α-NPD scharfe Grenzflächen.

Die *in-situ*-Messungen, welche bei BESSY durchgeführt wurden, bewiesen, dass Submonolagensensitivität im Vakuum-ultravioletten Spektralbereich mit Hilfe der spektroskopischen Ellipsometrie erreicht und zudem die dielektrische Funktion bestimmt werden kann, Verglichen mit dicken Schichten als Referenz, wurde auf Siliziumsubstraten für Submonolagen eine spektrale Verschiebung der Alq_3- and α-NPD-Absorptionsbanden zu höheren Energien beobachtet. Die kleinere Verschiebung, die für Alq_3-Submonolagen auf ZnO-Substraten beobachtet wurde, deutet an, dass der Einfluss des Siliziumsubstrates in Betracht gezogen werden muss, wenn man das spektrale Verhalten der Submonolagen erklären will.

Schlagwörter

Spektroskopische Ellipsometrie, Infrarotspektroskopie, organische dünne Schichten, dielektrische Funktion (optische Konstanten), Anisotropie

Parts of this work are already published:

11) **O.D. Gordan,** T. Sakurai, M. Friedrich, K. Akimoto, and D.R.T. Zahn
Ellipsometric Study of an Organic Template Effect: H_2Pc/PTCDA
Organic Electronics, submitted

10) **O.D. Gordan,** C. Himcinschi, D.R.T. Zahn, C. Cobet, N. Esser, W. Braun
Reduced Intermolecular Interaction in Organic Ultrathin Films
Appl. Phys. Lett., 88, 141913 (2006)

9) **O.D. Gordan**, S. Hermann, M. Friedrich and D.R.T. Zahn
Optical properties of the interfaces in organic/organic multilayered heterostructures
Journal de Physique IV (Proceedings ICFSI-10), Vol. 132 (March 2006), 73

8) **O.D. Gordan**, D.R.T. Zahn
The Anisotropic Dielectric Function for Copper Phthalocyanine Thin Films
New Trends in Advanced Materials (The West University of Timisoara), (2005) 83, ISBN 973-7608-41-0

7) **O.D. Gordan**, S. Hermann, M. Friedrich, D.R.T. Zahn
Comparative Study of Dielectric Function of Complex Organic Heterostructures
Phys. stat. sol. (b), 242 (13) (2005), 2688

6) C. Himcinschi, **O. Gordan**, G. Salvan, F. Müller, D.R.T. Zahn, C. Cobet, N. Esser, W. Braun
Stability of tris(8-hydroxyquinoline)-Aluminium(III) Films Investigated by Vacuum Ultraviolet Spectroscopic Ellipsometry
Appl. Phys. Lett., 86 (2005) 111907

5) S. Hermann, **O.D. Gordan**, M. Friedrich, D.R.T. Zahn
Optical Properties of Multilayered Alq_3/α-NPD Structures Investigated with Spectroscopic Ellipsometry
Phys. stat. sol. (c) 2, 12 (2005) 4037

4) **O.D. Gordan**, S. Hermann, M. Friedrich, D.R.T. Zahn
Optical Properties of PTCDA/CuPc Superlattices
J. Appl. Phys., 97 (2005) 063518

3) **O.D. Gordan**, M. Friedrich, D.R.T. Zahn
The Anisotropic Dielectric Function for Copper Phthalocyanine Thin Films
Organic Electronics, 5 (2004) 291

2) **O.D. Gordan**, M. Friedrich, W. Michaelis, R. Krüger, T.U. Kampen, D. Schlettwein, D.R.T. Zahn
Determination of the Anisotropic Optical Properties for Perfluorinated Vanadyl Phthalocyanine Thin Films
J. Mater. Res., 19 (2004) 2008

1) **O.D. Gordan**, M. Friedrich, D.R.T. Zahn
Determination of the Anisotropic Dielectric Function for Metal Free Phthalocyanine Thin Films
Thin Solid Films, 455-456 (2004) 551

Table of Contents

List of Abbreviations

α-NPD	N,N'-Di-[(1-naphthyl)-N,N'-diphenyl]-(1,1'-biphenyl)-4,4'-diamine
ε	Dielectric Function
$\langle\varepsilon\rangle$	Effective Dielectric Function
Alq_3	Tris(8-hydroxyquinoline)-aluminum(III)
BESSY	Berliner Elektronenspeicherring Gesellschaft für Synchrotronstrahlung g.m.b.H.
CT	Charge transfer
CuPc	Copper Phthalocyanine
EMA	Effective Medium Approximations
$F_{16}PcVO$	Perflourinated Vanadyl Phthalocyanine
H_2Pc	Metal-free Phthalocyanine
HOMO	Highest Occupied Molecular Orbital
H-Si(111)	Hydrogen Passivated Silicon (111)
HV	High Vacuum
IR	Infrared
IRRAS	Infrared Reflection Absorption Spectroscopy
LUMO	Lowest Unoccupied Molecular Orbital
MSE	Mean Square Error
OLED	Organic Light Emitting Diode
OMBD	Organic Molecular Beam Deposition
OVPD	Organic Vapour Phase Deposition
Pc	Phthalocyanine
PEM	Photo Elastic Modulator
PTCDA	3,4,9,10– Perylenetetracarboxylic Dianhydride
PVD	Physical Vapour Deposition
Si	Silicon
UHV	Ultra High Vacuum
UV	Ultra Violet
VASE	Variable Angle Spectrometric Ellipsometry
VUV	Vacuum Ultra Violet
ZnO	Zinc Oxide
ZnPc	Zinc Phthalocyanine

1. Introduction

The development of new devices in communication, imaging, (opto)electronics and sensor technologies involves the application of new materials. Promising candidates are organic molecular materials which exhibit in solid form semiconducting properties. Such materials which also possess a high thermal and chemical stability, as well as high optical absorption in the visible range are *e.g.* Phthalocyanines (Pc's) [McK98, Lez96]. The Pc's have been known for almost a hundred years and used in many remarkable experiments in molecular physics such as the first direct X-ray structure analysis of an organic crystal and the first image of a molecule using field-emission microscopy [McK98]. Nevertheless, there are currently only very few papers that describe the dielectric function of metal free phthalocyanine and, moreover, these treat the material as isotropic [Arw86, Deb91, Deb92, EiN01, Dju02, Yiq03, Bor04]. Another class of planar stacking molecules which exhibit a highly ordered organic growth [For97] are the polycyclic aromatic compounds based on naphthalene and perylene. One of the most studied molecules from the latter class, mostly used in industry as a red dye, is 3,4,9,10– perylene-tetracarboxylic dianhydride (PTCDA). In contrast with these planar molecules, two non-planar molecules relevant for organic light emitting diodes (OLEDs) were also studied in this work. Due to its light emitting and electron transporting properties one of the most promising organic material is tris(8-hydroxyquinoline)-aluminum(III) (Alq_3) which is commonly used in commercial OLEDs. This low molar weight molecule attracted a lot of scientific and technological attention due to the landmark work of Tang and van Slyke [Tan87]. While Alq_3 has great potential with respect to the development of large-area display applications [Gu96, Hun02], it is often used together with a hole transporting material like N,N'-Di-[(1-naphthyl)-N,N'-diphenyl]-(1,1'-biphenyl)-4,4'-diamine (α-NPD).

For many potential applications, like organic solar cells and OLEDs, the knowledge of the optical constants (or dielectric function) is necessary for device production. A non-destructive and very surface sensitive technique suited for this purpose is spectroscopic ellipsometry. Therefore this work presents the results on the molecular growth mode of several organic molecules using a combination of ellipsometry and infrared spectroscopy as investigations tools. While the chapters 2 and 3 present the theoretical background, the sample preparation and the experimental techniques are described in the chapters 4 and 5, respectively. The results obtained for single layers are summarized in the chapter 6 and the combinations of the above introduced molecules in multilayered structures are presented in the chapter 7. Chapter 8 contains the results obtained in the Vacuum-Ultra-Violet (VUV) range for ultra-thin films. Chapter 9 presents the final conclusions.

2. Theoretical Background

2.1. Introduction

Ellipsometry is a very sensitive thin film measurement technique which has been developed over the past twenty years and it is gaining more and more attention recently. This is due to the fact that new numerical methods have been perfected for treating anisotropic materials. Generally ellipsometry can be defined as the measurement of the state of polarization of a polarized vector wave.

In short terms the Variable Angle Spectrometric Ellipsometry (VASE) technique has the advantages to be non-destructive, very sensitive and accurate, since the variation in absolute intensity of the light has no effect in the determination of the relative phase change in a beam of reflected polarized light. Many desired parameters can be extracted by VASE analysis, including layer thickness, surface roughness and optical constants.

2.2. Light polarization in the Jones formalism

Light propagation trough a non-conducting, non-dispersive isotropic medium obeys Maxwell's equations:

$$\vec{\nabla} \cdot \vec{E} = 0$$
$$\vec{\nabla} \cdot \vec{B} = 0$$
$$\vec{\nabla} \times \vec{E} + \frac{1}{c}\frac{\partial \vec{B}}{\partial t} = 0$$
$$\vec{\nabla} \times \vec{B} - \frac{\mu\varepsilon}{c}\frac{\partial \vec{B}}{\partial t} = 0$$

(2.2.1)

where E is the electric field, B – the magnetic field, c – the speed of light, μ – the permeability and ε – the dielectric function.

These equations can be combined to yield the wave equation for the electric field:

$$\vec{\nabla}^2\vec{E} - \frac{1}{v^2}\frac{\partial^2\vec{E}}{\partial t^2} = 0$$

(2.2.2)

where the optical impedance v is defined as :

$$v = \frac{c}{\sqrt{\varepsilon\mu}}$$

(2.2.3)

A solution of the electric field wave equation is the electromagnetic plane wave:

$$\vec{E}(\vec{r},t) = \vec{E}_0 \exp\left(\frac{i2\pi\tilde{n}}{\lambda}\vec{q}\cdot\vec{r}\right)\exp(-i\omega t)$$

(2.2.4)

where $\vec{q}$ is a unit vector along the direction of wave propagation, $\tilde{n}$ is the complex index of refraction $\tilde{n} = n+ik$, λ is the wavelength of the light in vacuum, ω is the angular frequency of the wave, and $\vec{E}_0$ is a complex vector constant specifying the amplitude and polarization state of the wave.

The E-field, B-field, and the direction of propagation are all orthogonal with respect to each other. Because of the relationship between the fields, only the E-field and the direction of propagation are required to completely define a plane wave. Polarization states are usually defined in terms of the direction and phase of the E-field vector, only.

In the expression for the plane wave appears the complex index of refraction. If the imaginary part of the complex index (the extinction coefficient) is non-zero, the amplitude of the wave will decay exponentially as it propagates, according to the following expression (assuming propagation along the z-direction):

$$E \propto \exp\left(-\frac{2\pi kz}{\lambda} \right)$$
(2.2.5)

where k is the extinction coefficient, z is the distance of propagation in length units, and λ is the wavelength, in the same length units as the distance of propagation. The wave will then decay to 1/e of its original amplitude after propagating a distance, D_P, known as the penetration depth, given by:

$$D_P = \frac{\lambda}{2\pi k}$$
(2.2.6)

This is an important concept, as many materials exhibit large values of the extinction coefficient such that the light beam may penetrate only a few tens of nm or less into the material. We cannot expect to gain any information from a film or interface unless the light beam used in the ellipsometric experiment penetrates into the film or interface we are studying, and it is also able to propagate back out of the sample after reflection from the interface. For this reason it is usually not possible to measure the thickness of metal films of more than 50 nm (or so), as very little of the incident light beam reaches the bottom of the metal film and gets back out of the top to reach the detector [Azz92, Asp76].

Starting from the equation of a plane wave we can describe the polarization state of any beam by specifying its components along any two orthogonal axes in the plane perpendicular to the direction of beam propagation.

In ellipsometric experiments (fig. 2.2.1) it is common to use the so-called p- and s-directions as the two orthogonal basis vectors to express beam polarization states. The p-direction is defined as lying in the plane of incidence, defined as the plane containing the incident and reflected beams and the vector normal to the sample surface. The s- direction (from senkrecht, German for perpendicular) lies perpendicular to the p-direction so that the p-direction, s-direction, and direction of propagation (in that order) define a right-handed Cartesian coordinate system.
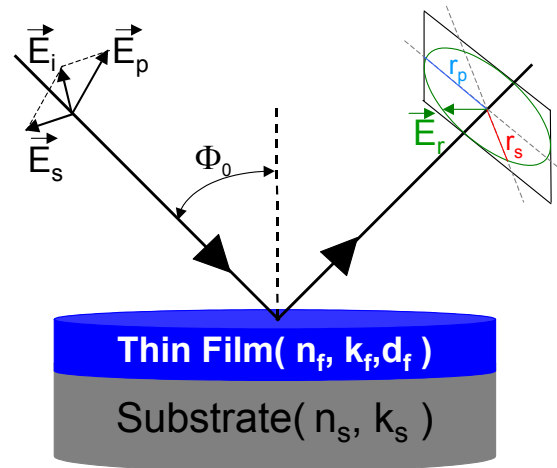
Figure 2.2.1. Geometry of an ellipsometric experiment

We can now express any totally polarized beam by specifying the components of the electric field of the beam along the p- and s-directions as:

$$\vec{E} = \exp(i\omega t)\begin{vmatrix} E_p \exp(-i\varphi_p) \\ E_s \exp(-i\varphi_s) \end{vmatrix} \text{ or } \vec{E} = \begin{bmatrix} \tilde{E}_p \\ \tilde{E}_s \end{bmatrix}$$

(2.2.7)

where φ is the phase delay.

For example, in figure 2.2.2, a linear polarisation is presented. In this case $\varphi_P = \varphi_S$.
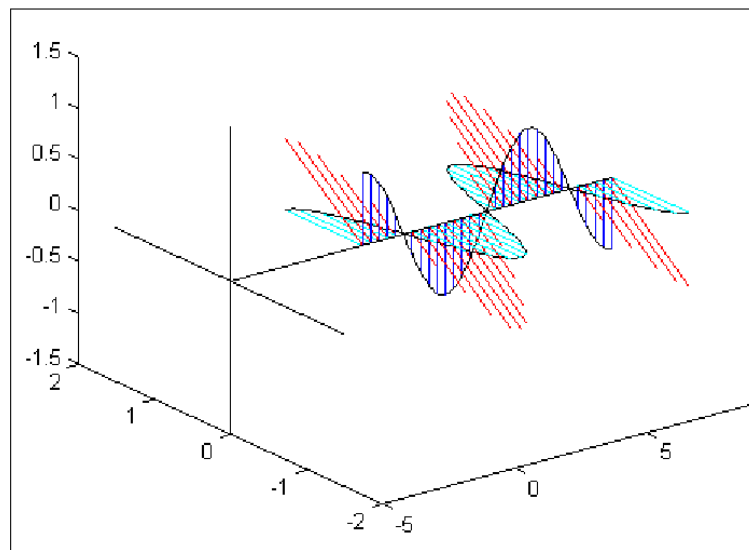

Figure 2.2.2. Linear polarization – and the electric field components along p and s directions

Any change in the polarization of the light as result of a reflection or transmission trough an optical system can be described by means of a 2 x 2 transfer matrix, also known as a Jones matrix.

$$\begin{bmatrix} \tilde{E}_p^{out} \\ \tilde{E}_s^{out} \end{bmatrix} = \begin{bmatrix} \tilde{r}_p & \tilde{r}_{ps} \\ \tilde{r}_{sp} & \tilde{r}_s \end{bmatrix}\begin{bmatrix} \tilde{E}_p^{in} \\ \tilde{E}_s^{in} \end{bmatrix}$$

(2.2.8)

The diagonal elements of the Jones matrix represent the change of amplitude and phase of the p- and s- components of the beam, while the off-diagonal elements describe the transfer of energy from the p-component to the s-component, and *vice versa*.

2.3. Ellipsometric parameters

The ellipsometric parameters are the two values – psi(Ψ) and delta(Δ) – measured in ellipsometric experiments. They describe completely the change in polarization state of light reflected from the surface of a sample, and are related to the ratio of Fresnel reflection coefficients $\tilde{r}_p$ and $\tilde{r}_s$ for p- and s-polarized light, respectively.

$$\rho = \frac{\tilde{r}_p}{\tilde{r}_s} = \tan \Psi \exp(i\Delta) \text{ where } \Delta = \varphi_p - \varphi_s \tag{2.3.1}$$

Fresnel coefficients can be calculated starting form an oblique reflection and transmission of an optical plane wave at the planar interface between two semi-infinite homogeneous optically isotropic media 0 and 1 with complex indices of refraction n_0 and n_1, respectively (figure 2.3.1).
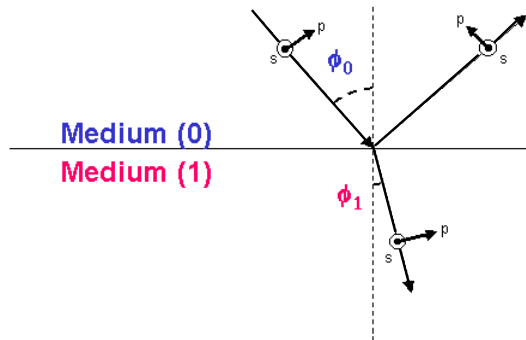

Figure 2.3.1. Oblique reflection and transmission

For a given amplitude and polarization of the incident wave, the amplitude and polarization of the reflected and transmitted waves can be determined from the continuity of the tangential components of the electric (E) and magnetic (H) field vectors across the interface [Azz92].

It is enough to express the amplitudes of the reflected and transmitted waves in terms of those of the incident wave for p and s polarization. This is because an arbitrarily polarized incident wave can be resolved into its p and s components.

$$\frac{E_{rp}}{E_{ip}} = r_p = \frac{n_1 \cos\phi_0 - n_0 \cos\phi_1}{n_1 \cos\phi_0 + n_0 \cos\phi_1} \tag{2.3.2a}$$

$$\frac{E_{rs}}{E_{is}} = r_s = \frac{n_0 \cos\phi_0 - n_1 \cos\phi_1}{n_0 \cos\phi_0 + n_1 \cos\phi_1}$$

$$\frac{E_{tp}}{E_{ip}} = t_p = \frac{2n_0 \cos\phi_0}{n_1 \cos\phi_0 + n_0 \cos\phi_1}$$

$$\frac{E_{ts}}{E_{is}} = t_s = \frac{2n_0 \cos\phi_0}{n_0 \cos\phi_0 + n_1 \cos\phi_1}$$

(2.3.2b)

where (E_{ip}, E_{is}), (E_{rp}, E_{rs}) and (E_{tp}, E_{ts}) represent the complex amplitudes of the components of the electric vectors of the incident, reflected and transmitted waves; r and t are the Fresnel complex-amplitude reflection, respectively transmission coefficients for p and s polarization.

2.4. The three phase model

One of the most simple models, but very important for understanding how the values of the thickness or optical constants can be computed, is the three phase model consisting of ambient – film – substrate [Azz92, Asp76]. Like in figure 2.4.1 the film has parallel-plane boundaries sandwiched between semi-infinite ambient and substrate media.
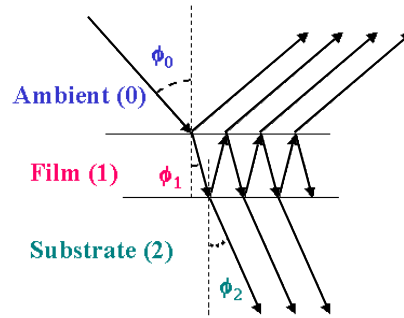

Figure 2.4.1. Oblique reflection and transmission of a plane wave by an
ambient(0)-film(1)-substrate(2) system

The ambient, the film and the substrate are all homogeneous and optically isotropic, with indices of refraction n_0, n_1 and n_2 respectively. The film thickness is d.

The objective is to relate the complex amplitudes of the resultant reflected and transmitted waves to the amplitude of the incident wave. If the Fresnel reflection and transmission coefficients at the 0-1, (1-0) and 1-2 interfaces are denoted by r_{01}, t_{01}, (r_{10}, t_{10}) and r_{12}, t_{12}, respectively, the total reflected amplitude r in medium 0 is given by an infinite geometric series of successive partial plane waves, like in equation 2.4.1. Similarly, the total transmitted amplitude is also given by an infinite geometric series.

$$r = r_{01} + t_{01}t_{10}r_{12}e^{-2i\beta} + t_{01}t_{10}r_{10}r_{12}^2 e^{-4i\beta} + t_{01}t_{10}r_{10}^2 r_{12}^3 e^{-6i\beta} + ...$$

$$t = t_{01}t_{12}e^{-i\beta} + t_{01}t_{10}r_{10}r_{12}e^{-3i\beta} + t_{01}t_{10}r_{10}^2 r_{12}^2 e^{-5i\beta} + ...$$

(2.4.1)

where β is the phase change of the multiply-reflected wave that traverses the film from one boundary to another. β can be expressed in terms of the free-space wavelength λ, the film thickness d, the film complex index of refraction n_1 and the angle of refraction in the film ϕ_1.

$$\beta = 2\pi \left(\frac{d}{\lambda} \right) n_1 \cos \phi_1 \qquad (2.4.2)$$

If the direction of propagation of the refracted wave in medium 1 is reversed, the reflection and transmission coefficients r_{10} and t_{10} at the 1-0 interface are related to the corresponding coefficients r_{01} and t_{01} at 0-1 interface by:

$$r_{10} = -r_{01}$$
$$t_{10}t_{01} = 1 - r_{01}^2 \qquad (2.4.3)$$

Considering equations 2.4.3, the sums from the equations 2.4.1 can be reduced to:

$$r = \frac{r_{01} + r_{12}e^{-2i\beta}}{1 + r_{01}r_{12}e^{-2i\beta}}$$

$$t = \frac{t_{01}t_{12}e^{-i\beta}}{1 + r_{01}r_{12}e^{-2i\beta}} \qquad (2.4.4)$$

These equations are valid when the incident wave is linearly polarized, either parallel (p), or perpendicular (s) to the plane of incidence. Thus, we may have the information on polarization by adding the p and s subscripts as follows:

$$r_p = \frac{r_{01p} + r_{12p}e^{-2i\beta}}{1 + r_{01p}r_{12p}e^{-2i\beta}}$$

$$r_s = \frac{r_{01s} + r_{12s}e^{-2i\beta}}{1 + r_{01s}r_{12s}e^{-2i\beta}}$$

$$t_p = \frac{t_{01p}t_{12p}e^{-i\beta}}{1 + r_{01p}r_{12p}e^{-2i\beta}} \qquad (2.4.5)$$

$$t_s = \frac{t_{01s}t_{12s}e^{-i\beta}}{1 + r_{01s}r_{12s}e^{-2i\beta}}$$

The Fresnel reflection and transmission coefficients that appear in equations 2.4.5 can be very easily obtained from equations 2.3.2.

$$r_{01p} = \frac{n_1 \cos \phi_0 - n_0 \cos \phi_1}{n_1 \cos \phi_0 + n_0 \cos \phi_1}$$

$$r_{12p} = \frac{n_2 \cos \phi_1 - n_1 \cos \phi_2}{n_2 \cos \phi_1 + n_1 \cos \phi_2}$$

$$r_{01s} = \frac{n_0 \cos \phi_0 - n_1 \cos \phi_1}{n_0 \cos \phi_0 + n_1 \cos \phi_1}$$

$$r_{12s} = \frac{n_1 \cos \phi_1 - n_2 \cos \phi_2}{n_1 \cos \phi_1 + n_2 \cos \phi_2} \qquad (2.4.6)$$

$$t_{01p} = \frac{2n_0 \cos\phi_0}{n_1 \cos\phi_0 + n_0 \cos\phi_1}$$

$$t_{12p} = \frac{2n_1 \cos\phi_1}{n_2 \cos\phi_1 + n_1 \cos\phi_2}$$

$$t_{01s} = \frac{2n_0 \cos\phi_0}{n_0 \cos\phi_0 + n_1 \cos\phi_1} \qquad (2.4.6)$$

$$t_{12s} = \frac{2n_1 \cos\phi_1}{n_1 \cos\phi_1 + n_2 \cos\phi_2}$$

The angles ϕ_0, ϕ_1 and ϕ_2 between the directions of propagation of the plane waves in media 0, 1 and 2, respectively, and the normal to the film boundaries are related by Snell's law:

$$n_0 \sin\phi_0 = n_1 \sin\phi_1 = n_2 \sin\phi_2 \qquad (2.4.7)$$

To apply the above theory [Azz92] to a practical film – substrate system, the following conditions have to be met – (1) the lateral dimension of the film must be many times its thickness so that the multiple reflected and transmitted partial waves can be summed to infinity; (2) the source bandwidth, beam diameter, and degree of collimating must all be such that the multiple-reflected and transmitted waves combine coherently.

2.5. Numerical inversion in ellipsometry

The above theory presents the *forward* problem and if we substitute r_p and r_s from equation 2.4.5 in equation 2.3.1 we have the ellipsometric parameters in the form:

$$\tan\psi e^{i\Delta} = \rho = \left(\frac{r_{01p} + r_{12p}e^{-2i\beta}}{1 + r_{01p}r_{12p}e^{-2i\beta}} \right)\left(\frac{1 + r_{01s}r_{12s}e^{-2i\beta}}{r_{01s} + r_{12s}e^{-2i\beta}} \right) \qquad (2.5.1)$$

The *reverse* problem in which the ellipsometric parameters are to be used to find some unknown properties like film thickness and dielectric function is of considerable practical interest. Because of their nonlinear and transcendental nature, the equations that govern the *forward* problem can be resolved in the *reverse* way only with digital computers using numerical fitting methods.

$$\tan\psi e^{i\Delta} = \rho\left(\tilde{n}_0, \tilde{n}_1, \tilde{n}_2, d, \phi_0, \lambda\right) \qquad (2.5.2)$$

As we see in equation 2.5.2, the function ρ is, in general, explicitly dependent on nine arguments: three complex refractive indices $\tilde{n}_0$, $\tilde{n}_1$ and $\tilde{n}_2$, film thickness d, angle of incidence ϕ_0 and wavelength. In most cases the ambient medium is air, so we know the value $\tilde{n}_0$. Usually we also have the complex refractive index of the substrate $\tilde{n}_2$ and the values for the angle of incidence ϕ_0 and the wave length λ. We still have three unknown parameters and for anisotropic materials the number is even higher.

Finding the unknown parameters is like a "fitting" procedure and the accuracy is given by the convergence method chosen, and the way in which the error is defined. So the computational problem in reflection ellipsometry consists in finding a set of optical parameters that characterize the optical system under measurement so that the quantity Mean Square Error (MSE) is minimized.

$$MSE = \sqrt{\frac{1}{N}\sum_{j=1}^{N}\left|\rho_j^m - \rho_j^c\left(\tilde{n}_0, \tilde{n}_1, \tilde{n}_2, d, \phi_0, \lambda\right)\right|^2}$$

(2.5.3)

where N is the number of measurements, ρ_j^m is the value of the j-th measurement and ρ_j^c is the computed value corresponding to the j-th measurement.

An alternative way to define the error function is based on dealing directly with Ψ and Δ.:

$$MSE = \sqrt{\frac{1}{N}\sum_{j=1}^{N}\left[\left(\Delta_j^c - \Delta_j^m\right)^2 + \left(\psi_j^c - \psi_j^m\right)^2\right]}$$

(2.5.4)

2.6. Reflection and transmission by anisotropic homogeneous systems

In the case of a birefringent system the four magnetic and electric parts of the plane wave are no longer spatially independent of each other, and the so-called mode coupling appears [Sch96]. This will happen inside the anisotropic material during the propagation of light. Consequently 4x4 matrices are needed in order to establish a matrix method. Dealing with the first-order Maxwell equations, Berreman [Ber72] showed a general way to calculate the reflection and transmission coefficients of an anisotropic slab from a wave matrix of rank 4.

The description of the method is quite extensive and it can be found in reference [Ber72]. In this section we will resume to the case of a stratified layer of an optically anisotropic medium (fig 2.6.1), sandwiched between two isotropic ambient and substrate media of refractive indices n_0 and n_2 [Azz92].
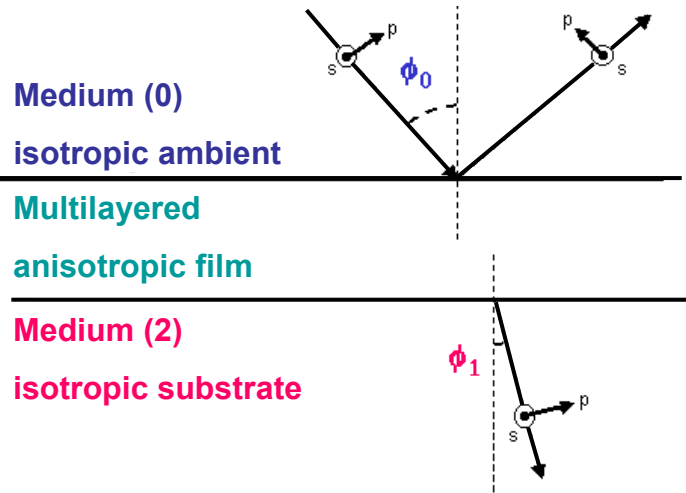
Figure 2.6.1. Reflection and transmission of a plane wave by multilayered anisotropic slab

Let (E_{ip}, E_{is}), (E_{rp}, E_{rs}), and (E_{tp}, E_{ts}) represent the components of the electric field vectors of the incident, reflected, and transmitted waves, respectively, parallel (p) and perpendicular (s) to the plane of incidence. In a non-magnetic ($\mu=1$), optically isotropic medium, the magnetic field components are simply related to their associated orthogonal electric field components through the index of refraction n:

$$\frac{H_p}{E_s} = \frac{H_s}{E_p} = n \qquad (2.6.1)$$

Thus the three generalized field vectors ψ_i, ψ_r, and ψ_t of the incident, reflected, and transmitted waves, respectively, can be expressed in a four rank matrix without explicit reference to the magnetic field components [Azz92].

$$\psi_i = \begin{bmatrix} E_{ip}\cos\phi_0 \\ n_0 E_{ip} \\ E_{is} \\ n_0 E_{is}\cos\phi_0 \end{bmatrix}$$

$$\psi_r = \begin{bmatrix} -E_{rp}\cos\phi_0 \\ n_0 E_{rp} \\ E_{rs} \\ -n_0 E_{rs}\cos\phi_0 \end{bmatrix} \qquad (2.6.2)$$

$$\psi_t = \begin{bmatrix} E_{tp}\cos\phi_2 \\ n_2 E_{tp} \\ E_{ts} \\ n_2 E_{ts}\cos\phi_2 \end{bmatrix}$$

The p and s direction are shown in figure 2.6.1 and $\vec{E} \times \vec{H}$ is in the direction of propagation. The internal fields inside the layer are included in the layer matrix T also called the transfer matrix.

$$\begin{bmatrix} E_{tp}\cos\phi_2 \\ n_2 E_{tp} \\ E_{ts} \\ n_2 E_{ts}\cos\phi_2 \end{bmatrix} = T \begin{bmatrix} (E_{ip} - E_{rp})\cos\phi_0 \\ n_0(E_{ip} + E_{rp}) \\ (E_{is} + E_{rs}) \\ n_0(E_{is} - E_{rs})\cos\phi_0 \end{bmatrix} = \begin{bmatrix} t_{11} & t_{12} & t_{13} & t_{14} \\ t_{21} & t_{22} & t_{23} & t_{24} \\ t_{31} & t_{32} & t_{33} & t_{34} \\ t_{41} & t_{42} & t_{43} & t_{44} \end{bmatrix} \begin{bmatrix} (E_{ip} - E_{rp})\cos\phi_0 \\ n_0(E_{ip} + E_{rp}) \\ (E_{is} + E_{rs}) \\ n_0(E_{is} - E_{rs})\cos\phi_0 \end{bmatrix} \qquad (2.6.3)$$

Equation 2.6.3 can be further expanded into four separate linear algebraic equations in the six components (E_{ip}, E_{is}), (E_{rp}, E_{rs}) and (E_{tp}, E_{ts}). E_{tp} can be readily eliminated from the first and second of these four equations, while E_{ts} can be eliminated from the third and fourth equations. This yields two linear algebraic equations connecting the incident and reflected fields alone:

$$a_{ip}E_{ip} + a_{is}E_{is} + a_{rp}E_{rp} + a_{rs}E_{rs} = 0$$
$$b_{ip}E_{ip} + b_{is}E_{is} + b_{rp}E_{rp} + b_{rs}E_{rs} = 0 \qquad (2.6.4)$$

where

$$\left.\begin{matrix} a_{ip} \\ a_{rp} \end{matrix}\right\} = \pm\cos\phi_0\left(t_{11}n_2 - t_{21}\cos\phi_2\right) + n_0\left(t_{12}n_2 - t_{22}\cos\phi_2\right)$$

$$\left.\begin{matrix} a_{is} \\ a_{rs} \end{matrix}\right\} = \pm n_0\cos\phi_0\left(t_{14}n_2 - t_{24}\cos\phi_2\right) + \left(t_{32}n_2 - t_{23}\cos\phi_2\right) \qquad (2.6.5)$$

$$\left.\begin{matrix} b_{ip} \\ b_{rp} \end{matrix}\right\} = \pm\cos\phi_0\left(t_{31}n_2\cos\phi_2 - t_{41}\right) + n_0\left(t_{32}n_2\cos\phi_2 - t_{42}\right)$$

$$\left.\begin{matrix} b_{is} \\ b_{rs} \end{matrix}\right\} = \pm n_0\cos\phi_0\left(t_{34}n_2\cos\phi_2 - t_{44}\right) + \left(t_{33}n_2\cos\phi_2 - t_{43}\right)$$

In the equations 2.6.5, the upper and lower symbols on the left correspond, respectively, to the upper (+) and lower (-) signs on the right. So equation 2.6.4 can be recast in the form:

$$\begin{bmatrix} E_{rp} \\ E_{rs} \end{bmatrix} = \begin{bmatrix} R_{pp} & R_{ps} \\ R_{sp} & R_{ss} \end{bmatrix} \begin{bmatrix} E_{ip} \\ E_{is} \end{bmatrix} \qquad (2.6.6)$$

where

$$\begin{bmatrix} R_{pp} & R_{ps} \\ R_{sp} & R_{ss} \end{bmatrix} = \left(a_{rs}b_{rp} - a_{rp}b_{rs}\right)^{-1} \begin{bmatrix} \left(a_{ip}b_{rs} - a_{rs}b_{ip}\right) & \left(a_{is}b_{rs} - a_{rs}b_{is}\right) \\ \left(a_{rp}b_{ip} - a_{ip}b_{rp}\right) & \left(a_{rp}b_{is} - a_{rp}b_{is}\right) \end{bmatrix} \qquad (2.6.7)$$

Equation 2.6.6 is similar to equation 2.6.7 and it can be directly linked to the ellipsometric parameters.

2.7. The dielectric tensor

The dielectric constant ε_t characterizes the material, and gives the polarization induced by an electric field applied on the material.

$$P = \left(\varepsilon_t - \varepsilon_0\right)E = \varepsilon_0\chi E \qquad (2.7.1)$$

where χ is the dielectric susceptibility which in the general case is a function of the electric field frequency.

$$\chi = \frac{\varepsilon_t}{\varepsilon_0} - 1 = \varepsilon - 1 \qquad (2.7.2)$$

where ε is the relative dielectric constant of the material. ε can be directly linked to the complex index of refraction $\tilde{n}$ by the formula:

$$\varepsilon = \tilde{n}^2 = (n + ik)^2 = \varepsilon_1 + i\varepsilon_2$$

$$\varepsilon_1 = n^2 - k^2$$

$$\varepsilon_2 = 2nk \qquad (2.7.3a)$$

$$n = \sqrt{\frac{\varepsilon_1 + \sqrt{\varepsilon_1^2 + \varepsilon_2^2}}{2}}$$

$$\qquad (2.7.3b)$$

$$k = \frac{\varepsilon_2}{2n}$$

For an isotropic absorbing material ε is a complex scalar (ε_1 - real part, ε_2 - imaginary part). For anisotropic materials, however, ε becomes a tensor which, referred to three arbitrary orthogonal axes (x,y,z), is:

$$\varepsilon_{xyz} = \begin{pmatrix} \varepsilon_{xx} & \varepsilon_{xy} & \varepsilon_{xz} \\ \varepsilon_{yx} & \varepsilon_{yy} & \varepsilon_{yz} \\ \varepsilon_{zx} & \varepsilon_{zy} & \varepsilon_{zz} \end{pmatrix} \qquad (2.7.4)$$

By making the appropriate choice of axes the dielectric tensor can be diagonalized. With this choice of axes, called the eigen axes of the material (X,Y,Z), equation 2.7.4 can be recast as:

$$\varepsilon_{XYZ} = \begin{pmatrix} \varepsilon_X & 0 & 0 \\ 0 & \varepsilon_Y & 0 \\ 0 & 0 & \varepsilon_Z \end{pmatrix} \qquad (2.7.5)$$

The two sets of coordinates can be linked together by a rotation matrix R:

$$\varepsilon_{xyz} = R\varepsilon_{XYZ}R^{-1} \qquad (2.7.6)$$

and R is a function of the Euler angles ψ_E, θ_E and ϕ_E:

$$R = \begin{pmatrix} \cos\psi_E & \sin\psi_E & 0 \\ -\sin\psi_E & \cos\psi_E & 0 \\ 0 & 0 & 1 \end{pmatrix} \begin{pmatrix} 1 & 0 & 0 \\ 0 & \cos\theta_E & \sin\theta_E \\ 0 & -\sin\theta_E & \cos\theta_E \end{pmatrix} \begin{pmatrix} \cos\phi_E & \sin\phi_E & 0 \\ -\sin\phi_E & \cos\phi_E & 0 \\ 0 & 0 & 1 \end{pmatrix} \qquad (2.7.7)$$

As we can see in formula 2.7.7, three rotations, in the trigonometric sense, are made with the (X,Y,Z) coordinate system – the first one is with an angle ψ_E around the Z axis, the

second one with an angle θ_E around the new X axis and the last rotation with an angle ϕ_E is done around the new Z axis.

2.8. Isotropic, uniaxial and biaxial materials

For non-magnetic and non absorbing materials the components of the dielectric tensor can be usefully represented as Cartesian coordinates of an ellipsoid. The figure is often called "index ellipsoid", "reciprocal ellipsoid", or "ellipsoid of wave normals".
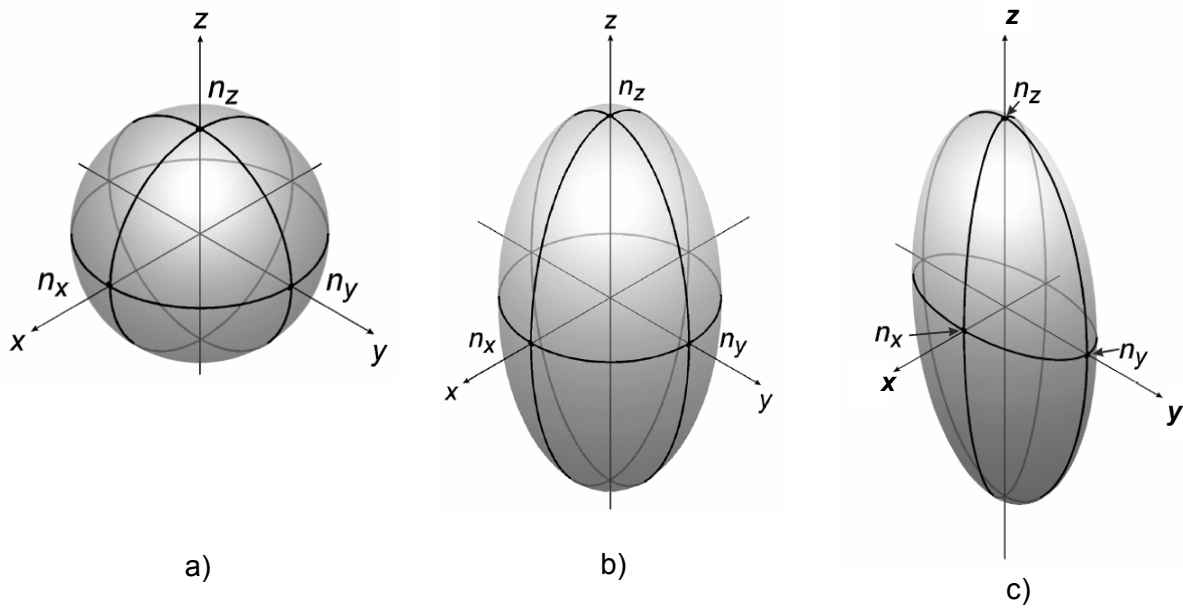

Figure 2.8.1. Index ellipsoid – a) isotropic, b) uniaxial, c) biaxial

According to the form of the complex dielectric function, the materials can be classified as in the following table:

Table 2.8.1. Anisotropy classification

Isotropic		$\varepsilon = \begin{pmatrix} a & 0 & 0 \\ 0 & a & 0 \\ 0 & 0 & a \end{pmatrix}$	$\tilde{n} = \sqrt{a}$
Anisotropic	Uniaxial	$\varepsilon = \begin{pmatrix} a & 0 & 0 \\ 0 & a & 0 \\ 0 & 0 & b \end{pmatrix}$	$\tilde{n}_O = \sqrt{a}$ $\tilde{n}_E = \sqrt{b}$
	Biaxial	$\varepsilon = \begin{pmatrix} a & 0 & 0 \\ 0 & b & 0 \\ 0 & 0 & c \end{pmatrix}$	$\tilde{n}_X = \sqrt{a}$ $\tilde{n}_Y = \sqrt{b}$ $\tilde{n}_Z = \sqrt{c}$

For an isotropic ambient – film – isotropic substrate system, the Jones reflection matrix of the film (from equation 2.2.8) is diagonal ($R_{ps}=R_{sp}=0$). This is also valid for the case

of anisotropic materials when the beam coordinates correspond to the eigen axes of the material. However, for anisotropic materials, when the Euler angles are different from zero, the off diagonal terms (R_{ps} and R_{sp}) are also different from zero. In this case the Jones matrix of the material cannot be completely described in terms of ellipsometric parameters Ψ and Δ and the ratios A_{ps} and A_{sp} also have to be measured.

$$A_{ps} = \frac{R_{ps}}{R_p} \quad \text{and} \quad A_{sp} = \frac{R_{sp}}{R_{ss}} \tag{2.8.1}$$

3. First Order Approximations

3.1. Introduction

In this chapter the equations of the three phase model will be solved in a first order approximation. Before presenting the solutions, the concept of effective dielectric function will be introduced. While this chapter can be regarded as a part of the Theoretical Background, as it uses the notions presented before, due to the importance in understanding the fundamentals behind the ellipsometry equations, I decided that this part should be a stand alone section.

3.2. Effective dielectric function <ε>

Due to their nonlinear and transcendental nature, the ellipsometric equations (2.5.1) can be reverted only for a semi-infinite isotropic sample. In this case the dielectric function ε can be related to ρ and the angle of incidence ϕ_0 by [Azz92, Ros96]:

$$\varepsilon = \sin^2 \phi_0 + \sin^2 \phi_0 \tan^2 \phi_0 \left[\frac{1-\rho}{1+\rho} \right] \tag{3.2.1}$$

In the general case when the sample is anisotropic, or it consist of several layers on a substrate, equation 3.2.1 is no longer valid. Moreover, even if the sample is an isotropic bulk, the surface can be reconstructed, contaminated and rough, and the optical response is an approximation of the bulk [Ros96]. However, equation 3.2.1 gives an average over the region penetrated by the incident light, and can be useful in evaluating experimental data as if the sample would be a homogeneous half-space. Therefore ε is denoted as <ε> and is called pseudodielectric function [Asp83] or effective dielectric function [Ros96].

Figure 3.2.1 shows the real and imaginary dielectric function ε for silicon [Jel92], compared with the measured effective dielectric function <ε> of a silicon (111) substrate covered with 1.7 nm natural silicon oxide. After the measurement the silicon was hydrogen passivated by dipping the substrate in a 40% solution of hydrofluoric acid for 2 minutes. During this procedure [Mön93] the natural surface oxide is removed, and the silicon dangling bonds were saturated with hydrogen. In this case a direct inspection of <ε> is possible without carrying out complicated evaluation procedures [Ros96]. As can be seen in figure 3.2.1 the oxidation leads to a decrease in the imaginary part of <ε_2> near the E_2 gap of silicon. This effect can be used to estimate the cleanliness of the Si surface as the decrease of E_2 peak indicates the presence of an overlayer on the Si surface.
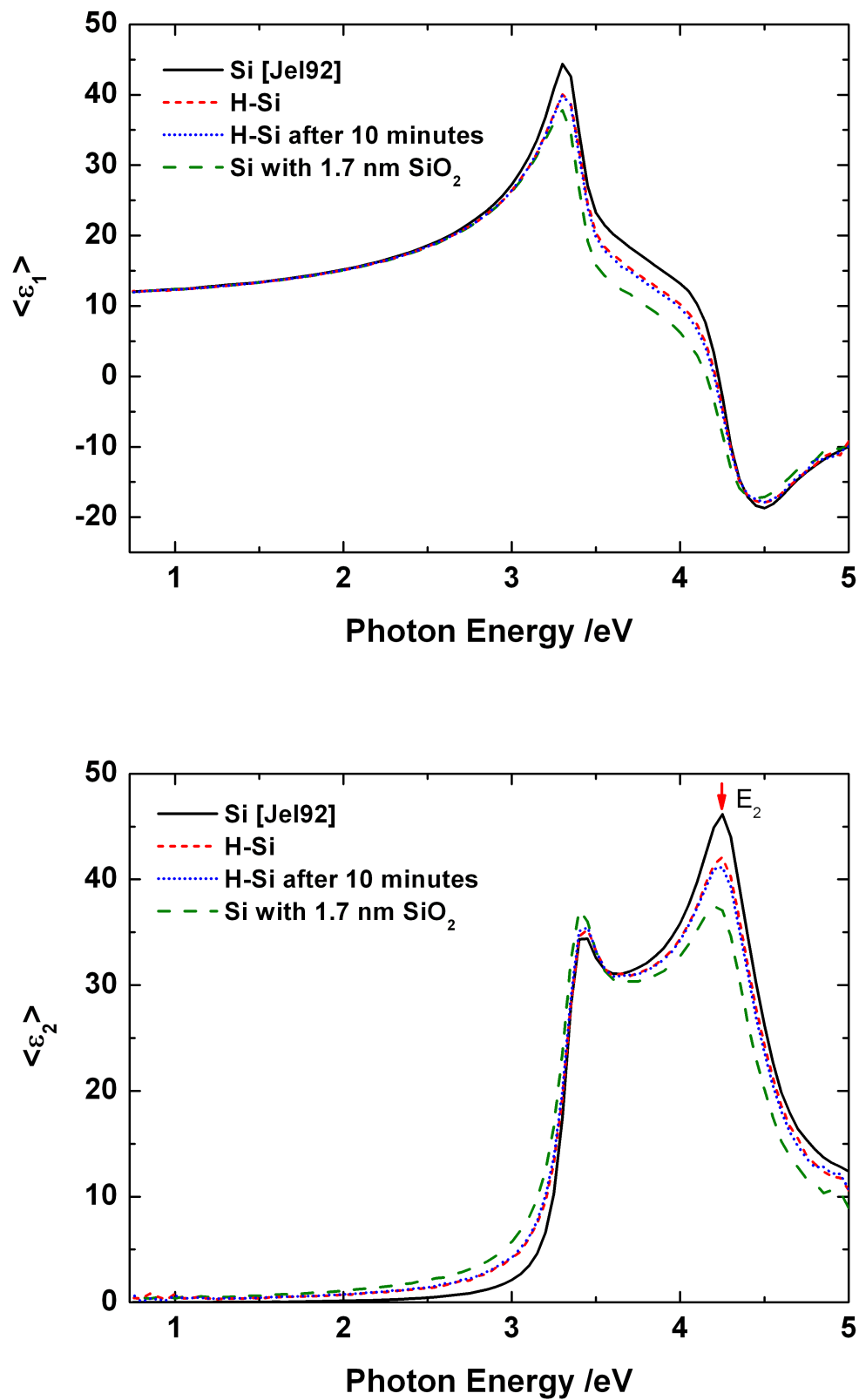
Figure 3.2.1. The complex dielectric function of clean silicon [Jel92] compared with the complex effective dielectric function of hydrogen passivated silicon (111) and silicon (111) with natural oxide.

The same method can be applied to investigate the stability of the hydrogen passivated silicon surface (H-Si). Even if the H-Si surface is rather stable, a slightly decrease of E_2 peak can be observed after 10 minutes of exposure to atmosphere. The presence of various contaminants on the H-Si surface can affect the growth mode of organic molecules. Therefore it is very important that the substrates are transferred in the vacuum chamber immediately after the *ex situ* wet chemical passivation procedure.

3.3. Approximate solution of ellipsometric equations for optically biaxial crystals

The direct inspection of the effective dielectric function $<\varepsilon>$ provides useful information on bulk isotropic samples and on growth evolution of an overlayer. However, in data evaluation of complex systems, including anisotropic bulk samples, the complex ellipsometric equations have to be considered. In spite of the implementation of new numerical algorithms [Sch96] based on a 4x4 transfer matrix formalism developed by Berreman [Ber72], determining the anisotropic dielectric function from ellipsometric data, especially in the perpendicular direction on the sample surface, remains a challenging task. This is due to the reduced measurement sensitivity in the out-of-plane direction.

While rigorously correct the Berreman formalism [Ber72] involves the numerical solution of matrices of nonlinear equations which are hard to follow from physical view. Aspnes developed an approximate solution of the ellipsometric equations for a biaxial crystal, based on a first order expansion which assumes that the anisotropies are corrections to an isotropic mean value [Asp80]. This procedure is not exact, but the calculation is performed in the framework of the easily solved isotropic problem, and the resulting expansion gives considerable insight in the physics of the ellipsometric measurement. In the calculation example the biaxial sample is oriented so that the eigen axis of the dielectric tensor are perpendicular to both surface and plane of incidence. This assumption simplifies the solution as the Euler rotation matrices are not included in the equations.

If we consider the z axis normal to the surface and the xz plane as the plane of incidence, n_a the refraction index of the ambient, ε_x, ε_y and ε_z the components of the dielectric tensor along x, y and z, then equation 2.5.1 can be rewritten as [Azz92]:

$$\rho = \frac{r_p}{r_s} = \frac{\left(\varepsilon_{x\perp}\cos\phi - n_a n_{z\perp}^{\circ}\right)\left(n_{a\perp} + n_{y\perp}\right)}{\left(\varepsilon_{x\perp}\cos\phi + n_a n_{z\perp}^{\circ}\right)\left(n_{a\perp} - n_{y\perp}\right)} \tag{3.3.1}$$

where

$$n_{a\perp} = \sqrt{\varepsilon_a - \varepsilon_a \sin^2\phi} = n_a \cos\phi$$

$$n_{j\perp} = \sqrt{\varepsilon_j - \varepsilon_a \sin^2\phi}, \text{with } j = x, y \tag{3.3.2}$$

$$n_{z\perp}^{\circ} = \sqrt{\frac{\varepsilon_x}{\varepsilon_y}}\sqrt{\varepsilon_z - \varepsilon_a \sin^2 \phi} = n_a \cos\phi \tag{3.3.2}$$

If we assume that the refractive index of the ambient medium is 1 and the small deviation $\Delta\varepsilon$ from a mean isotropic value ε, then ε_x, ε_y, and ε_z are given by:

$$\begin{aligned} \varepsilon_x &= \varepsilon + \Delta\varepsilon_x \\ \varepsilon_y &= \varepsilon + \Delta\varepsilon_y \\ \varepsilon_z &= \varepsilon + \Delta\varepsilon_z \end{aligned} \tag{3.3.3}$$

If Δ is small the correction can be treated in first order. In this way the original anisotropic problem is reduced to a correction of the isotropic one. Substituting equation 3.3.3 into 3.3.2 and using the intermediate expansion in 3.3.1, the effective dielectric function from equation 3.2.1 becomes:

$$< \varepsilon > = \varepsilon + \frac{\left(\varepsilon\cos^2\phi - \sin^2\phi\right)\sqrt{\varepsilon - \sin^2\phi}}{\sin^2\phi\cos\phi}\frac{\Delta\rho}{\rho} \tag{3.3.4}$$

$$< \varepsilon > = \varepsilon + \frac{\varepsilon - \sin^2\phi}{(\varepsilon - 1)\sin^2\phi}\Delta\varepsilon_x - \frac{\varepsilon\cos^2\phi - \sin^2\phi}{(\varepsilon - 1)\sin^2\phi}\Delta\varepsilon_y - \frac{1}{(\varepsilon - 1)}\Delta\varepsilon_z \tag{3.3.5}$$

If the crystal is uniaxial with $\Delta\varepsilon_x = \Delta\varepsilon_y = \Delta\varepsilon$, then:

$$< \varepsilon > = \varepsilon + \frac{\varepsilon}{\varepsilon - 1}\Delta\varepsilon - \frac{1}{\varepsilon - 1}\Delta\varepsilon_z \tag{3.3.6}$$

If the crystal is isotropic with $\Delta\varepsilon_x = \Delta\varepsilon_y = \Delta\varepsilon_z = \Delta\varepsilon = 0$, then:

$$< \varepsilon > = \varepsilon \tag{3.3.7}$$

If $|\varepsilon|$ is moderately large, of order of 10, then for typical angles of incidence $\phi \sim 70°$ the main contribution to the measured values is given by the x direction [Asp80]. The presented formalism is valid only for small anisotropy, and the solution indicates that ellipsometry has a reduced sensitivity for the y and z direction. While the reduced sensitivity for y direction can be easily overcome by rotating the sample azimuthally, in order to have reliable values for the z direction special analysis procedures were developed. Even if the contribution of the z direction is small it is correlated with the xy direction. This means that an accurate determination for the in-plane dielectric function would lead to the determination of the dielectric function in z direction. In order to reliably deduce the values for the z direction multi-sample analysis [Mcg93] can be used to reduce the correlation between parameters. In this procedure several films with different thicknesses, but the same optical constants can be coupled together during the numerical fitting procedure.

3.4. First order approximation for very thin overlayers

Ellipsometry is a non-destructive and very sensitive surface and thin film measurement technique which can detect the changes in the optical response produced by an overlayer on a smooth surface. However, interpreting the ellipsometry spectra for very low coverages (below few nanometers) down to a monolayer or even submonolayer regime remains a challenging task as the optical path of the light through the material is much smaller than the wavelength [Azz92]. In this case the light has a reduced sensitivity to the refractive index of the film which is strongly correlated with the film thickness. Consequently only the product of these parameters can be uniquely determined.

Due to this difficulty it is hard to obtain reliable results using the numerical fitting procedure. In this case, when the overlayer thickness d is below 1 nm, the ellipsometric equations for the three phase model can be simplified to yield a quadratic form. If we consider a three phase system with ε_a, ε_L, and ε_s the complex dielectric functions of ambient, overlayer, and substrate, respectively, the exponential terms of the Fresnel coefficients from equation 2.4.5 can be written in a power series expansion. In the limit where d ≤ 1 nm, only the first terms have to be retained [Bur64, Asp76], and the Fresnel coefficients can be written as:

$$r_p^\circ \cong r_p \left\{ 1 + \left(\frac{4\pi i d n_a \cos\phi}{\lambda} \right) \left[\frac{\varepsilon_a (\varepsilon_s - \varepsilon_L) \left[\varepsilon_s \varepsilon_L - \varepsilon_a (\varepsilon_s + \varepsilon_L) \sin^2\phi \right]}{\varepsilon_L (\varepsilon_s - \varepsilon_a) \left[\varepsilon_s \varepsilon_L - \varepsilon_a (\varepsilon_s + \varepsilon_a) \sin^2\phi \right]} \right] \right\}$$

$$r_s^\circ \cong r_s \left\{ 1 + \left(\frac{4\pi i d n_a \cos\phi}{\lambda} \right) \left[\frac{\varepsilon_s - \varepsilon_L}{\varepsilon_s - \varepsilon_a} \right] \right\}$$

(3.4.1)

where r_p and r_s are the two phase (ambient-substrate) quantities given in 2.3.2.

Using equation 3.4.1 in equation 3.2.1 the effective dielectric function for very thin layers can be approximated by [Ros96]:

$$< \varepsilon > = \varepsilon_s + \frac{4\pi i d}{\lambda} \sqrt{\varepsilon_s - \sin^2\phi} \, \frac{\varepsilon_s (\varepsilon_s - \varepsilon_L)(\varepsilon_L - 1)}{\varepsilon_L (\varepsilon_s - 1)}$$

(3.4.2)

This formula is valid for thicknesses below 1 nm [Ros96]. This quadratic equation can be easily solved to find ε_L.

4. Sample Preparation

4.1. Phthalocyanines

Phthalocyanines are a broad class of materials with high thermal and chemical stability, as well as high optical absorption in the visible range. The attested discovery dates almost one century back and was reported by Braun and Tcherniac in 1907 [McK98]. The full elucidation of the structure of Pc began in 1928 at the Grangemouth plant of Scottish Dyes Ltd, when a glass-lined reaction vessel cracked and a blue-green material was formed during the industrial preparation of phthalimide. The preliminary study, performed by two employees – Dandridge and Dunsworth – revealed that the iron containing by-product was an exceptionally stable and insoluble pigment. Following this, many other metal substituted phthalocyanines were synthesized and a comprehensive study of their chemical properties was initiated by Linstead and coworkers in 1932 [Lin34]. Linstead also coined the term "phthalocyanine" to refer to this class of organic materials.

Since then, the phthalocyanines (abbreviated Pc from the phthalocyanato anion $C_{32}H_{16}N_8^{2-}$) have been used in applications as diverse as dyes, chemical sensors and optoelectronics. They played an important role in many landmark experiments in molecular physics *e.g.* first organic structure to yield to an absolutely direct X-ray analysis reported by Robertson in 1953 or the first image of a molecule using field-emission microscopy reported by Müller in 1950 [McK98].

4.1.1. Molecular structure

The Phthalocyanines share a common large polyaromatic ring, and the metal-free variant has a planar molecular structure, as shown in figure 4.1.1. The central cavity of the Pc ring can accommodate as many as 70 different elemental ions or oxides such as TiO or VO. The geometry of the molecule can change from planar to pyramidal when the ions are to large to be accommodated in the central cavity (e.g. PbPc). Many ions (e.g. Cu^{2+}, Co^{2+}, Fe^{2+}) are held so tightly that they cannot be removed without the destruction of the macromolecule. This explains the high thermodynamic stability of certain MPcs [McK98].

In this work three different varieties of Phthalocyanines were used to prepare thin films, namely Metal-free Phthalocyanine (H_2Pc), Copper Phthalocyanine (CuPc) and Perflourinated Vanadyl Phthalocyanine ($F_{16}PcVO$). The molecular structure of these molecules is presented in figure 4.1.1.

$C_{32}H_{18}N_8$

$C_{32}CuH_{18}N_8$

$C_{32}F_{16}N_8VO$

a)   b)   c)
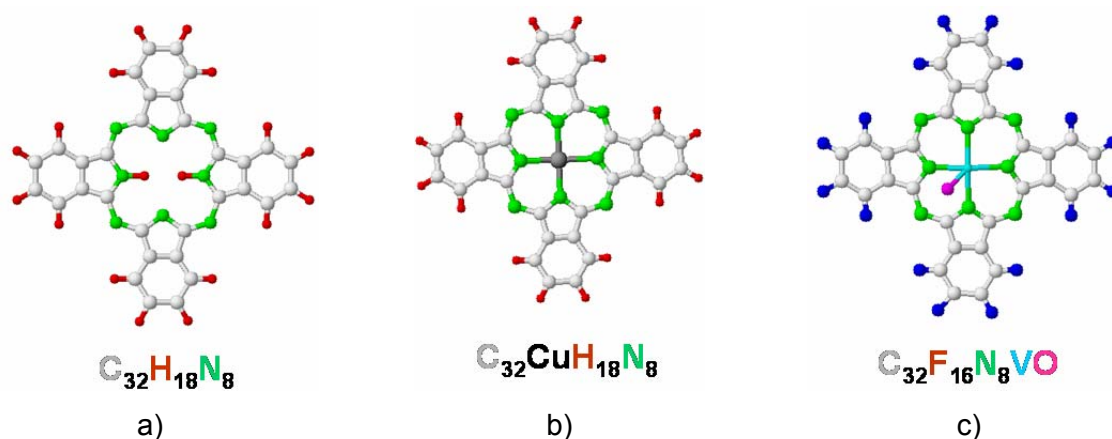
Figure 4.1.1. Molecular structure of a) Metal-free Phthalocyanine, b) Copper Phthalocyanine, and c) Perflourinated Vanadyl Phthalocyanine

4.1.2. Crystalline structure

For many potential applications, highly ordered crystalline Pc materials are required, especially for the fabrication of reproducible optical and electronic devices. In contrast to the covalent bonding in inorganic electronic materials, such as single crystalline silicon, the forces within organic crystals (e.g. van der Waals and π-π interactions) are relatively weak. Consequently, a number of different forms of crystalline state (polymorphs) may be displayed by the same compound. The knowledge of Pc polymorphism is useful for understanding the structure of all Pc derivatives, but this is especially true for the structure within microcrystalline films prepared by vacuum sublimation [McK98].

As mentioned before, the ability of H_2Pc and its planar metal derivatives to form crystals by vacuum sublimation led to their structural determination by X-ray diffraction by Robertson (1935). His studies showed that the β-form crystal is monoclinic and belongs to the $P2_1/a$ space group, with two Pc molecules per unit cell (fig. 4.1.2). In this case the Pc stacks make an angle between 45° and 49° with the b-axis of the crystal. The Pc molecules in neighboring stacks are roughly orthogonal, producing a herringbone like arrangement.

The metal-free phthalocyanine and the other planar MPcs have also a α-type polymorph. It is only relatively recent that a consensus has been reached concerning the exact structure of the α-form, although it was agreed that the main difference between the α- and β-forms is the smaller tilt angle (about 27°-30°) of the molecule relative to the b-axis of the crystal. The α-phase also has a monoclinic crystal structure of the C2/c space group, with four molecules per unit cell. This was deduced from the single-crystal X-ray diffraction study of a α-form crystal performed by Yase and coworkers (1988). Earlier studies describe the α-form as a tetragonal structure, of the P4/m space group, containing six molecules per unit cell (Robinson and Klein, 1952) and, tentatively, as an orthorhombic crystal structure (Assour, 1965) [McK98]. Both of these assignments were based on X-ray diffraction data.
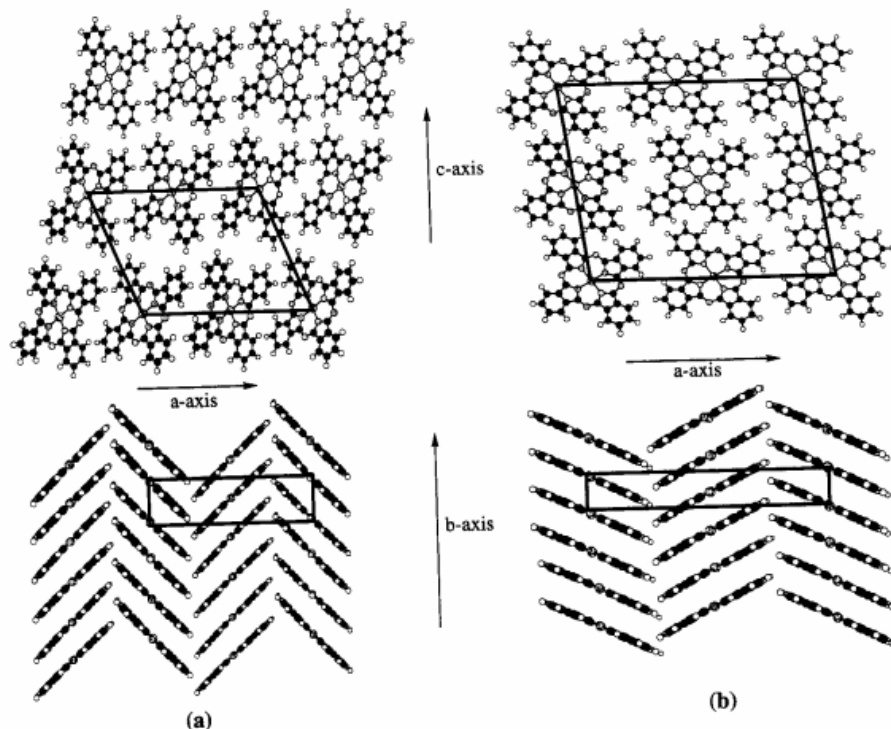
Figure 4.1.2. The crystal structure of H_2Pc and planar MPc [McK98]. a) β-type crystal, monoclinic $P2_1/a$ space group; b) α-type crystal C2/c space group.
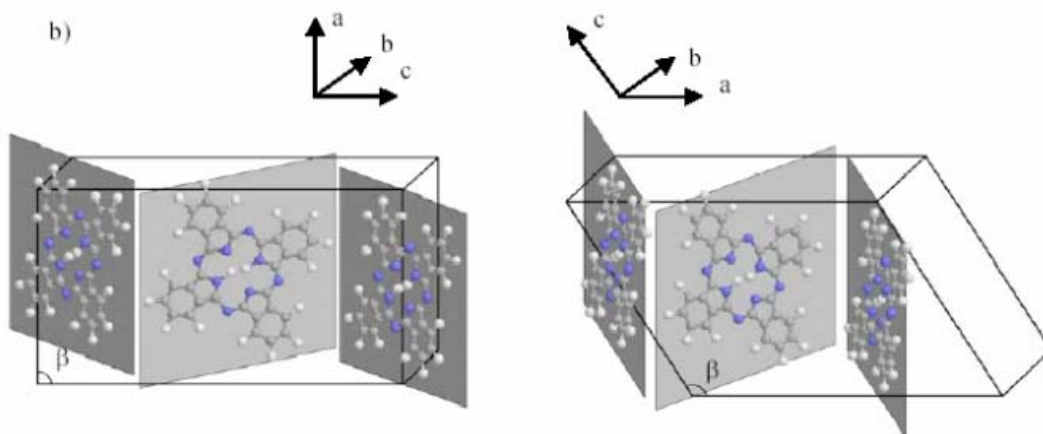
Figure 4.1.3. 3D Schematic of the unit cell and molecular arrangement for α and β-H_2Pc. For the convenience of comparison with the β unit cell, only half of the α unit cell is displayed, although it should contain four molecules per unit cell.

4.1.3. Thin films

For many applications it is required to have thin films deposited on appropriate substrates. The stability of Pcs towards sublimation upon heating in vacuum gives a simple technique for the film fabrication. They can be investigated by numerous techniques like ultra

violet - visible absorption spectroscopy, glancing angle X-ray diffraction, infrared spectroscopy, Raman spectroscopy and ellipsometry [Lez96, Mck98].

The structure of the films depends on the nature of the substrate and deposition conditions. Usually the deposition of planar Pcs at room temperature leads to small crystallites of α-form. If there is no particular affinity between the Pc molecule and the substrate, the crystallites adopt a parallel b-axis to the substrate. This has been proved by glancing angle XRD, showing a repeated distance equal to the width of a Pc molecule [Dog92, Has92, McK98], and by spectroscopic methods [Dow91, Kol97]. However, these methods do not provide any information about the orientation of the other crystallographic axes. Powder XRD, a technique sensitive to the planes parallel to the substrate, refined the study by certifying that the a-axis is perpendicular to the substrate in H_2Pc films [Bay99], thereby rotating the commonly accepted picture by 90 ° around the b-axis. In thicker films (>1 µm) of H_2Pc [Nes94] and CuPc [Has92], the b-axis was found to be perpendicular to the substrate (Figure 4.1.4).

a)   b)   c)
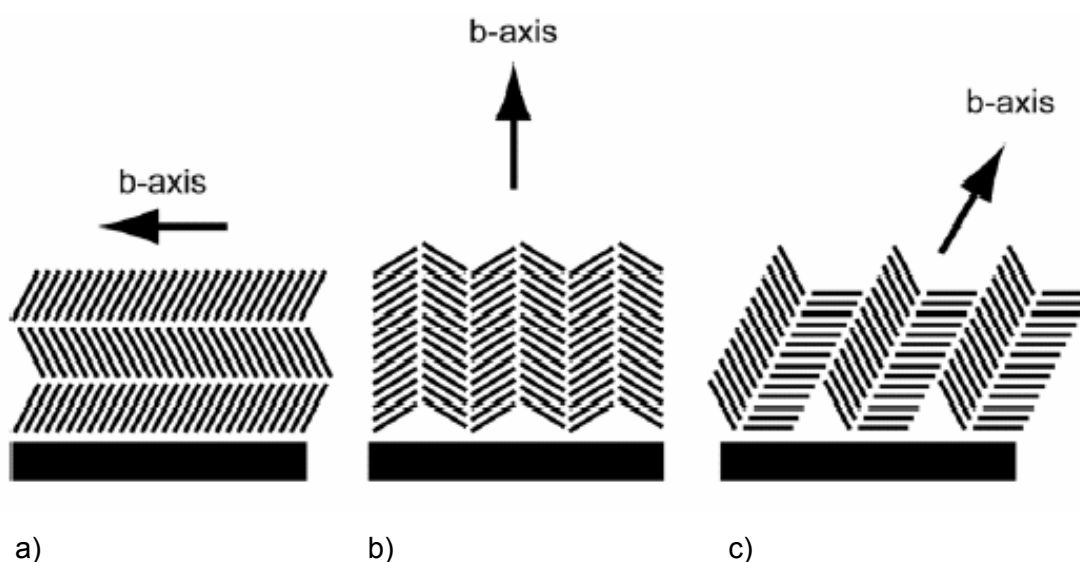
Figure 4.1.4. Types of molecular arrangements of vacuum-sublimed α-type films [McK98]. (a) thin film deposited slowly onto a substrate that does not interact strongly with the first Pc monolayers, (b) thick film, (c) thin film deposited onto a substrate that interacts strongly with the initially deposited Pc monolayers.

Interaction with the substrate can modify the orientation of the phthalocyanine crystallites. Early work by Ashida *et al.* showed that CuPc tends to lie flat when deposited at room temperature on KCl, due to electrostatic forces between K^+ and the electron-rich bridging nitrogens [Ash66]. Although the crystals are still of the α form, they adopt a standing b-axis orientation in that case, where the b-axis is tilted by 26 ° with respect to the substrate normal (Figure 4.1.4(c)). Usually, the structure in layers were the Pc molecules have an initial lying configuration also relax to standing b-axis α crystals after a few monolayers [Tok95].

4.1.3. Structural information from visible absorption spectra

Phthalocyanines can be regarded as an 18 or 16 π-electron system perturbed by the attachment of four benzoid rings. The absorption of Pcs in the UV-visible range is due to the Q band and B, or Soret band, following the nomenclature of porphyrins. The lowest energy band (Q) appearing at 700-800 nm is due to $\pi-\pi^*$ transitions. The B band is also a $\pi-\pi^*$ transition occurring in the 300 nm region.

The absorption spectra is specific to a polymorph and the difference between α and β can be seen by comparison of figures 4.1.5 (a) and (b). The α phase appears as a broad peak centered at 630 nm and a shoulder at 690 nm. The two peaks are of comparable intensity in the β polymorph, red shifted and centered at 650 and 710 nm, respectively. The size of the crystallites has also a dramatic influence on their absorption features: significant broadening and increased splitting characterize the spectrum of large particles embedded in a polymer matrix.

a)   b)
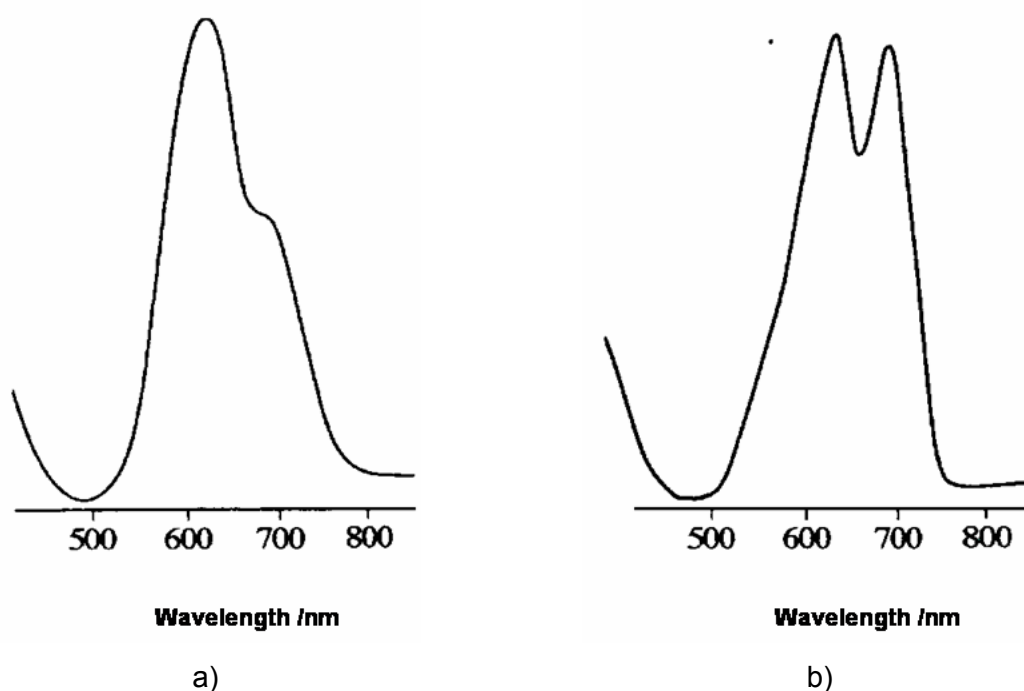
Figure 4.1.5. Solid-state visible absorption spectra of H_2Pc thin film:

(a) α - form; (b) β - form [McK98]

4.2. PTCDA

Next to the Phthalocyanines, another class of planar stacking molecules are the polycyclic aromatic compounds based on naphthalene and perylene. One of the most studied molecules from the latter class is 3,4,9,10– perylenetetracarboxylic dianhydride

(PTCDA). While this molecule is mostly used in industry as a red dye, it constitutes an example for highly ordered organic growth [For97].

4.2.1. Molecular and crystalline structure

The molecular structure of PTCDA is presented in figure 4.2.1. It consists of 24 carbon atoms, 8 hydrogen atoms and 6 oxygen atoms.

$C_{24}H_8O_6$
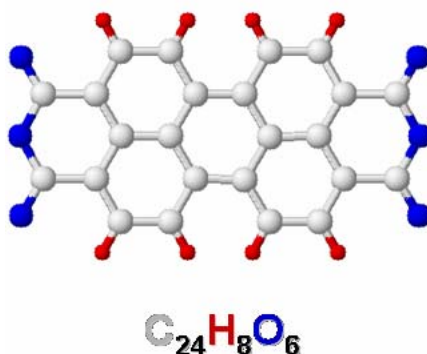
Figure 4.2.1. Molecular structure of PTCDA

Extensive studies indicate that the perylene derivates grow flat when thermally evaporated under vacuum condition on a large variety of substrates ranging from metals to ionic insulators. For PTCDA two crystal polymorphs were reported [Oga99]. Detailed information can be found in an exhaustive review made by Forrest in 1997 [For97]. The crystalline structure of the α modification is presented in figure 4.2.2.
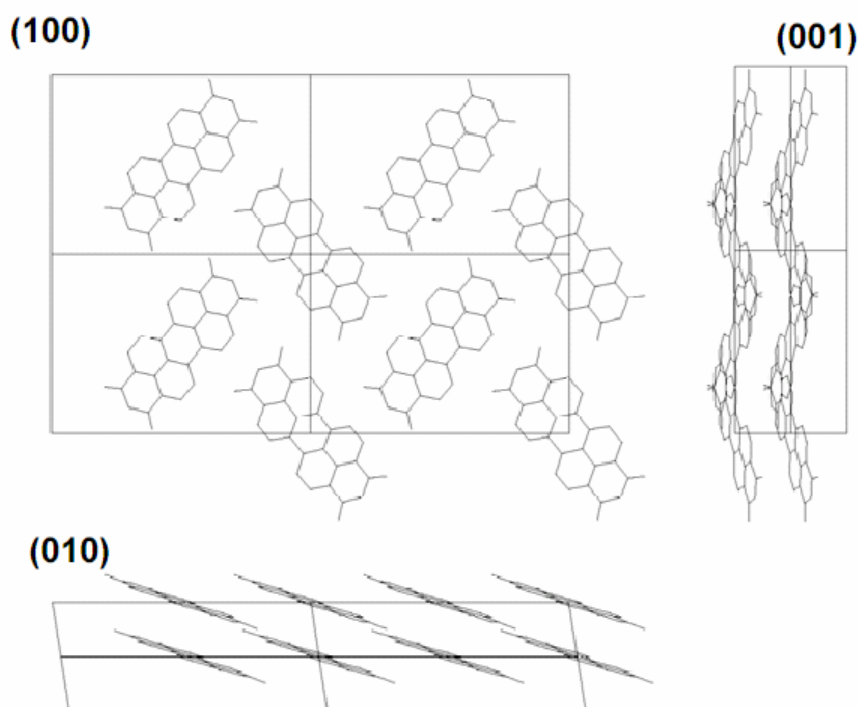
Figure 4.2.2. The crystalline structure of α-PTCDA

The α modification crystallizes in the space group P2$_1$/c with lattice constants a=0.372, b=1.196, c=1.734 nm and β=98.8°. The β modification is found to crystallize in the same space group, but with different lattice parameters: a=0.378, b=1.930, c=1.077 nm and β=83.6° [Oga99].

4.2.1. Excitons in crystalline films of PTCDA

Like in the case for Pcs, the first electronic transitions between the highest occupied molecular orbital (HOMO) and the lowest unoccupied molecular orbital (LUMO) of perylene derivatives are mainly governed by the extended conjugated π-electron system composed of atomic 2p$_z$ wave functions [Sch00]. The experimental ultraviolet-visible (UV-VIS) absorption spectra of isolated-like molecules (monomer) obtained from diluted solutions of PTCDA in dimethyl-sulfoxide (DMSO) is presented in the lower part of figure 4.2.3. A comprehensive analysis of the PTCDA monomer absorption was carried out by Scholz *et al*. in [Sch01] taking into account the participation of totally symmetric vibrations in the vibronic progression.

The change in absorption line-shape of films (crystal) compared to that of monomers in solution is known as crystallochromy and was observed for a large number of perylene derivatives [Hof00]. For PTCDA it was shown that this change can be related to the transfer of Frenkel excitons between neighbouring molecules [Sch01], considering a regular arrangement of the molecules in the crystalline domains having finite-size.

a)   b)
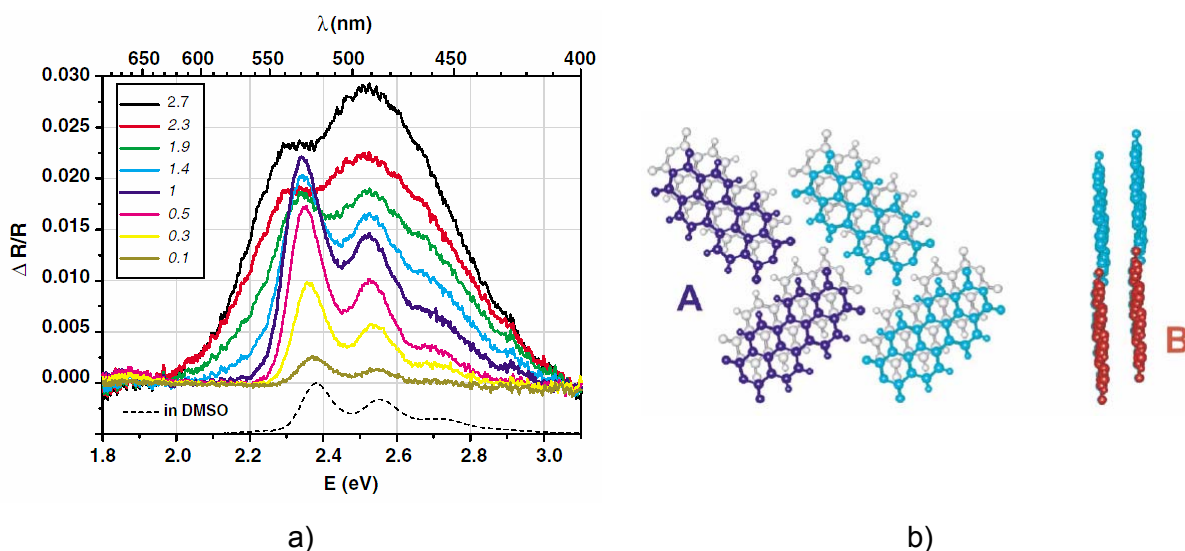
Figure 4.2.3. a) Differential reflectance spectra of PTCDA on mica during growth from 0.1 to 2.7 monolayers (ML) compared with the absorbance spectrum of PTCDA in DMSO (shifted). After Proehl *et al.* [Pro04]

b) Crystal structure of α-PTCDA – two types of dimers are indicated: (A) – in plane, (B) stacked [Pro04]

In figure 4.2.3 the differential reflectance spectra of PTCDA on mica during growth from 0.1 to 2.7 monolayers (ML) is shown [Pro04]. The change in the experimental spectra proves that the molecular interaction between the in-plane dimers (A) is week, while in the stacking direction (B) there is a strong interaction of the overlapping π electrons.

4.3. Alq$_3$ and α-NPD

Since the pioneering work of Tang and van Slyke [Tan87] who reported the first efficient organic light emitting diode (OLED) using a low molar weight molecule, tris(8-hydroxyquinoline)-aluminum(III) (Alq$_3$) has attracted a lot of scientific and technological interest due to its great potential with respect to the development of large-area displays applications [Gu96, Hun02]. While Alq$_3$ is considered to be the most successful organic material used in commercial OLEDs due to its light emitting and electron transporting properties, it is often used together with a hole transporting material like N,N'-Di-[(1-naphthyl)-N,N'-diphenyl]-(1,1'-biphenyl)-4,4'-diamine (α-NPD).

4.3.1. Molecular structure and thin films

Unlike the planar molecular structure of the Phthalocyanines and PTCDA, Alq$_3$ and α-NPD have a more complex (3D) molecular structure as can be seen in figure 4.3.1. Alq$_3$ is known to have two geometric isomers, namely facial (fac-Alq$_3$) and meridional (mer-Alq$_3$) having C$_3$ and C$_1$ symmetries, respectively. Both experimental and theoretical studies indicate that the mer-Alq$_3$ is the dominant form [Hal01].
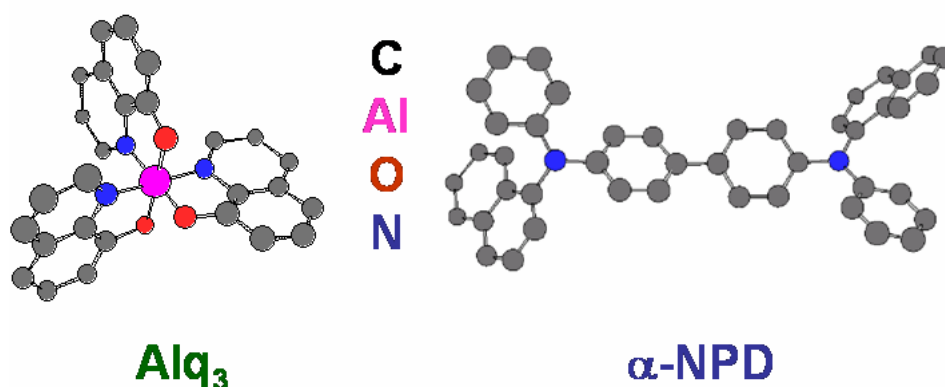
Figure 4.3.1. Molecular structure of mer-Alq$_3$ and α-NPD

Extensive X-ray studies done by Brinkmann *et al.* [Bri00] indicate that Alq$_3$ has several crystalline polymorphs. However, the detailed description of these polymorphs will not be presented here, as the sublimed thin films yield amorphous structure [Che98, Cur98, Bri00].

Like Alq$_3$, α-NPD forms amorphous films trough sublimation. Due to this fact these films are isotropic and the optical response can be modelled in ellipsometry using isotropic models [Him05].

4.4. Substrates and sample preparation

The organic materials described in the above sections were used in order to prepare thin films by organic molecular beam deposition (OMBD). The substrates, hydrogen passivated silicon (H-Si), were kept at room temperature during the deposition. Some of the H$_2$Pc and PTCDA films were prepared at the University of Tsukuba (Japan) on glass (Corning 7059) and on silicon oxide covered silicon substrates. The F$_{16}$PcVO samples were prepared by physical vapour deposition (PVD) at University of Oldenburg (Germany) on fused silica substrates and potassium bromide (KBr). During the deposition the temperature of the KBr substrates was kept at 42 °C and at 85 °C for the fused silica substrates. The thickness of the organic films was monitored using a quartz micro-balance located in the vicinity of the sample.

The silicon substrates were cut from one side polished (111) oriented silicon wafers provided by Wacker Siltronic. The wafers were p-type (B-doped) with a doping concentration of approximately $1.5 \cdot 10^{15}$ cm^{-3}. The Si(111) substrates with an offcut angle less than 0.35^0 [Sil05], were cleaned with isopropanol and deionised water in order to remove organic contaminants. The natural surface oxide was removed by keeping the wafer in hydrofluoric acid (HF) solution 40% for 2 minutes. This treatment yields a 1x1 reconstructed Si surface that is chemically passivated with hydrogen (H) [Mön93], and has a surface roughness around 4 Å [Sil05]. Figure 4.4.1 shows the low energy electron diffraction (LEED) pattern of a 1x1 reconstructed H-Si(111) surface prepared as described.

I=5mA, E=29eV
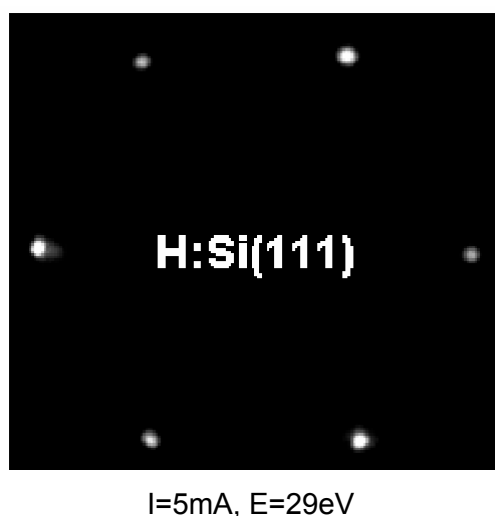
Figure 4.4.1. LEED pattern of 1x1 reconstructed Si surface

The source material used for OMBD was sublimed β-phase CuPc with 97% purity, supplied by Aldrich. For the ultra high vacuum (UHV) deposition higher purity (99%) β-CuPc was used. The PTCDA powder was supplied by Lancaster. The preparation conditions ranged from high vacuum (HV) conditions at a pressure less than 10^{-8} mbar to UHV conditions at a pressure better than 10^{-9} mbar. During the deposition the substrates were kept at room temperature.

Sublimed Alq$_3$ and α-NPD materials were purchased from Sensient-Syntec. These materials were used without further sublimation. The ultra-thin films of Alq$_3$ and α-NPD were prepared by OMBD on hydrogen passivated Si (111) and ZnO substrates in the UHV preparation chamber in BESSY. The base pressure in the preparation chamber was ~$6 \cdot 10^{-10}$ mbar. The starting materials were deposited from quartz crucibles located 20 cm away from the sample holder. During the deposition the pressure was ~$1.1 \cdot 10^{-8}$ mbar. The thickness of the organic material was monitored by a quartz crystal micro-balance located in the vicinity of the samples.

The F$_{16}$PcVO films were prepared by Dr. Wilfried Michaelis by physical vapor deposition (PVD) under HV conditions. The F$_{16}$PcVO was synthesized as described in reference [Sch00a] and prior to deposition purified by sublimation in a three zone temperature gradient oven (Lindberg). The KBr(100) substrates were cleaved by means of a steel knife from a single crystal purchased from Dr. W. Schrader (Braunschweig, Germany). Immediately after cleavage the substrates were transferred into a high vacuum chamber ($5 \cdot 10^{-8}$ mbar) and annealed for 16 h at 500-600 K in order to desorb water and other adsorbates. The fused silica substrates were bought from Menzel Gläser, Germany, and washed in an ultrasonic bath subsequently with acetone, ethanol and de-ionized water.

The H$_2$Pc and PTCDA samples prepared in Japan by Dr. Takeaki Sakurai were deposited on glass (Corning 7059) and SiO$_2$/Si (001) substrates by organic molecular beam deposition (OMBD) at a base pressure of $1.5 \cdot 10^{-9}$ mbar. The organic source materials were purified three times by gradient sublimation and were charged into Knudsen cells. The glass substrates were cleaned in ultrasonic baths of acetone and ethanol and then dried in nitrogen flow before being loaded into the OMBD chamber. The SiO$_2$/Si structure was fabricated depositing SiO$_2$ on Si(001) wafers by electron beam evaporation.

5. Experimental Techniques and Analysis Procedures

5.1. Spectroscopic Ellipsometry

Ellipsometry measures the change in the polarisation state of light after reflection on a sample. There are various ellipsometer configurations like RAE (Rotating Analyzer Ellipsometer), RPE (Rotating Polarizer Ellipsometer), RCE (Rotating Compensator Ellipsometer), PME (Phase Modulation Ellipsometer) and NE (Null Ellipsometer). Each ellipsometer configuration has different features and merits [Woo99].

The ellipsometric measurements carried out in this work were performed with two RAE ellipsometer setups: (1) a fully automated variable angle spectrometric ellipsometer (VASE) from J. A. Wollam Co. Inc. and (2) a vacuum ultra-violet (VUV) ellipsometer setup located at the synchrotron facility "Berliner Elektronenspeicherring Gesellschaft für Synchrotronstrahlung G.m.b.H." (BESSY), Berlin. The schematics of a RAE setup is presented in figure 5.1.1.

L – light source
P – polarizer
C – compensator (retarder)
S – Sample
A – analyzer (polarizer)
D – detector
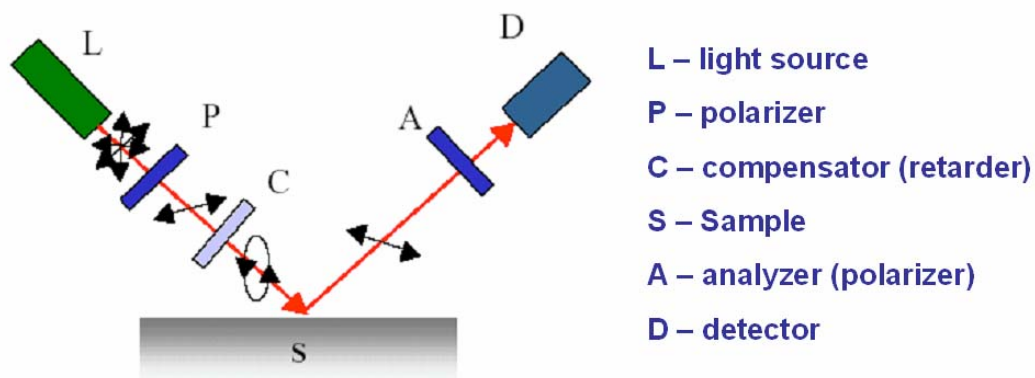
Figure 5.1.1. Schematics of a rotating analyser ellipsometer setup.

In this configuration the signal at the detector can be written in the general case for elliptically polarised light as a sinusoid with a DC offset (fig. 5.1.2).

$$V(t) = DC + a\cos 2A(t) + b\sin 2A(t) \tag{5.1.1}$$

$$A(t) = \omega t \tag{5.1.2}$$

For simplicity the signal is written as function of the 2ω components in equation 5.1.1. If the sample is misaligned, higher ω components will be present in the signal. From the normalized Fourier coefficients of the signal, $\alpha = \dfrac{a}{DC}$, $\beta = \dfrac{b}{DC}$ and the input polarizer azimuth P, the ellipsometer parameters Ψ and Δ can be deduced [Azz92]:

$$\tan \Psi = \sqrt{\frac{1+\alpha}{1-\alpha}}\,|\tan P|$$

$$\cos\Delta = \frac{\beta}{\sqrt{1-\alpha^2}}\frac{\tan P}{|\tan P|} \qquad (5.1.3)$$
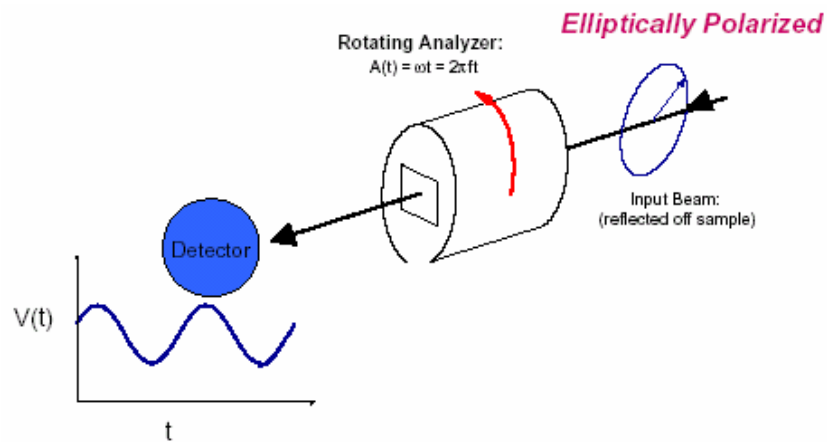
Figure 5.1.2. Signal at the detector for RAE setup

5.1.1. Experimental setups

The picture 5.1.3 presents the Woollam VASE ellipsometer. The schematic diagram of figure 5.1.1can be used to identify the ellipsometer components.
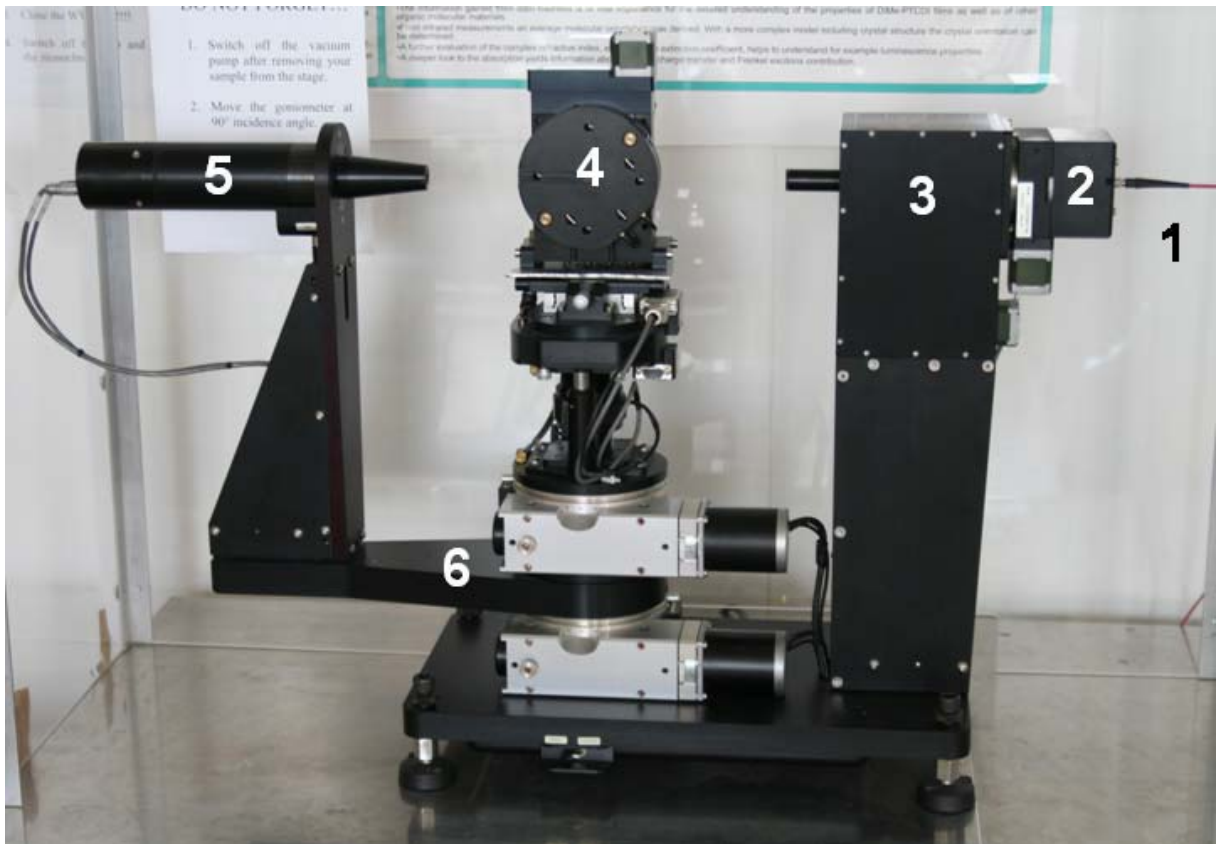
Figure 5.1.3. Woollam VASE ellipsometer. (1) optical fiber, (2) polarizer, (3) compensator, (4) sample stage, (5) analyser, (6) goniometers

As can be seen in figure 5.1.3 the VASE ellipsometer has two goniometers – one for rotating the sample stage and one for rotating the analyser arm. The precision in measuring the incidence angle is 0.01°. This is useful in increasing the sensitivity of the ellipsometric measurements as it depends of the magnitude of changes in Ψ and Δ. In this way the samples can be measured near to the Brewster angle where the biggest changes in Ψ and Δ are expected. The combination of a short arc xenon lamp with an adequate optical fiber gives an extended energy range from 0.7 eV up to 5 eV. The measurements presented in this work were performed with an energy step of 0.02 eV with or without autoretarder. Without autoretarder one cannot distinguish between left and right polarisation and the respective Δ values range in an interval from 0° to 180°. Using the autoretarder makes it possible to distinguish these two polarizations and therefore Δ can range in an interval from 0° to 360°. For transparent samples it is particularly useful to use the autoretarder as these samples exhibit values of Δ near to 0° or 180° (very small ellipticity).

Extended *in situ* spectroscopic ellipsometry (SE) measurements were performed up to 10 eV at the VUV setup in BESSY. The schematics of this setup is presented in figure 5.1.4.
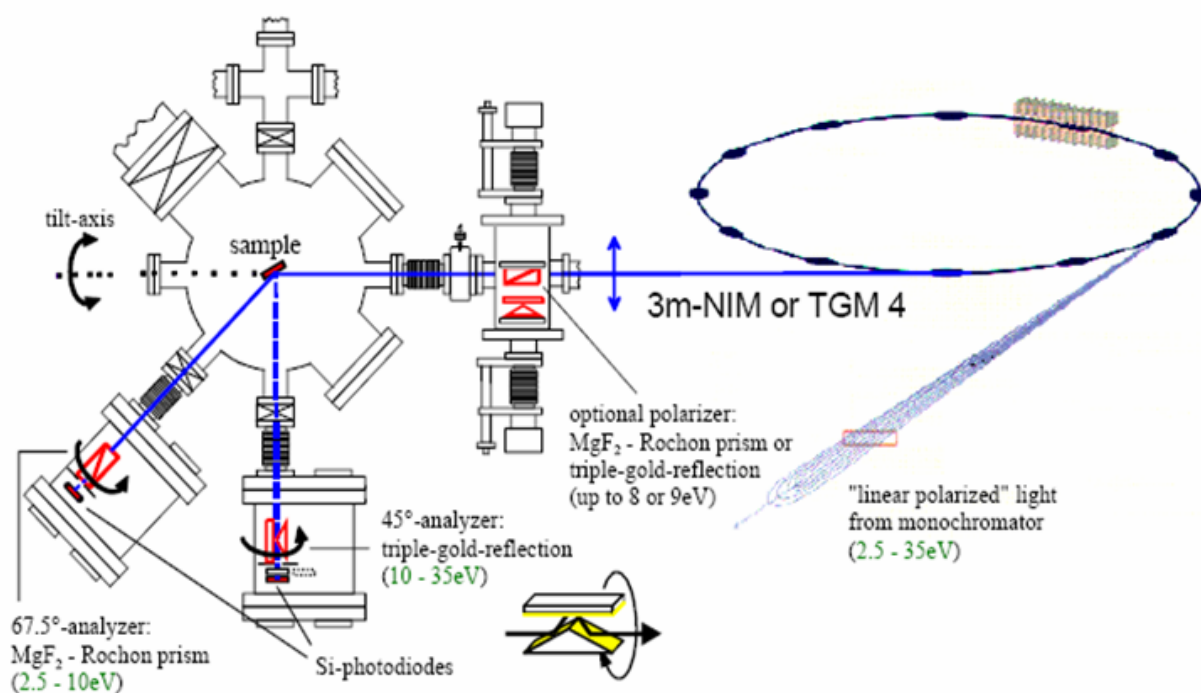
Figure 5.1.4. Schematics of the VUV setup from BESSY

During these measurement the UHV chamber was attached to the 3 meter Normal Incidence Monochromator (3m-NIM 1A). The setup has a rotating-analyser at 67.5° angle of incidence and most measurements were performed in the range from 4eV to 9.5 eV with energy steps of 0.025 eV. MgF$_2$ Rochon prisms were used as polarizers. A detailed

description of the setup can be found in references [Joh89, Bar91, Wet98]. Dependent on the alignment the incidence angle can vary (67.5° ±1°).

5.1.2. Models for data evaluation

In order to determine the sample thickness, surface roughness and the dielectric function from ellipsometric data a model which describes the interaction of light with matter has to be employed. Figure 5.1.5 shows the flow chart of the numerical fitting procedure.

Numerical fitting procedure
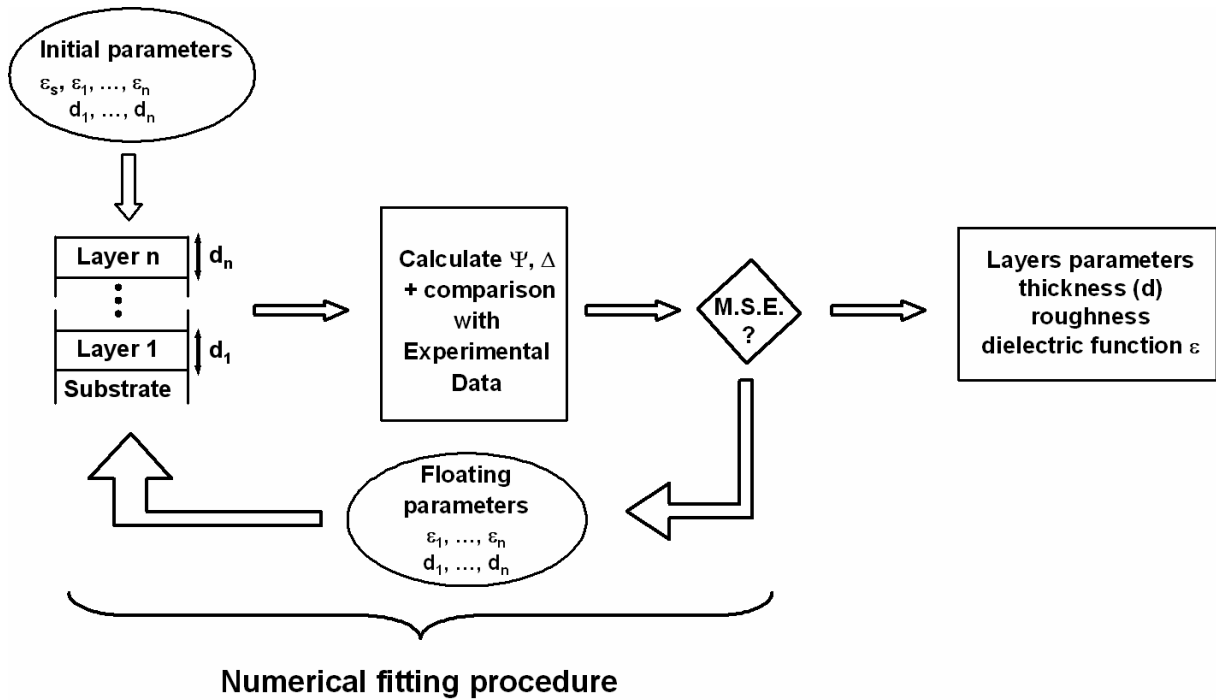
Figure 5.1.5. Flow chart of the numerical fitting procedure

As the inverse ellipsometric problem is impossible to be solved in the general case, the equations presented in chapter 2 are used in an iterative way to find the thicknesses and the optical properties of the layers. The result depends on the model chosen. In this way the ellipsometric data are simulated and compared to the experimental data. The iterative cycle minimizes the differences between the simulated and experimental data.

In the Woollam WVASE software the mean-square error (MSE) which gives the differences between the model and the experimental points is defined as follows:

$$MSE = \sqrt{\frac{1}{2N-M} \sum_{i=1}^{N} \left[\left(\frac{\Psi_i^{mod} - \Psi_i^{exp}}{\sigma_{\Psi,i}^{exp}} \right)^2 + \left(\frac{\Delta_i^{mod} - \Delta_i^{exp}}{\sigma_{\Delta,i}^{exp}} \right)^2 \right]} \qquad (5.1.2.1)$$

where N is the number of the experimental points, M is the number of fit parameters and σ is the standard deviation for each point. The standard deviation is used to weigh the contributions of each data point to the mean-square error during the fitting process, such that very noisy data points are effectively excluded from the fit [Woo99]. A MSE of 1 means that the simulated data pass through experimental data within the experimental error.

In order to get the correct dielectric function of the layers the thickness has to be precisely determined. This is possible in the absorption free range of the materials where most of them have a normal dispersion and can be described by a Cauchy dispersion function. In the Cauchy relation the index of refraction n is simulated by a slowly varying function of wavelength, λ:

$$n(\lambda) = A + \frac{B}{\lambda^2} + \frac{C}{\lambda^4}$$

(5.1.2.2)

During the fit the parameters are the film thickness, A and B. Usually the A and B parameters describe the dispersion well enough, so C is set to 0.

The surface roughness and interfacial mixing can be also determined using Effective Medium Approximations (EMA). EMA models for surface and interfacial roughness are most useful when the film is transparent and the experimental data exhibit interference oscillations, as the shape of these oscillations is very sensitive to roughness. For films which are absorbing everywhere or thinner than ~ 30 nm, the roughness layer thickness will usually correlate very strongly to the film thickness, and it is hard to obtain both uniquely. While in the EMA models for surface roughness 50% of the layer is considered to be voids, in the interfacial roughness the mixing ratio can be floating parameter. In the following paragraph the simplest linear EMA model and the most used Bruggeman [Bru35] EMA model will be shortly introduced.

Considering a mixing of two different materials a and b, the optical response of the mixed layer can be approximated by a linear combination of the dielectric functions of the materials:

$$\widetilde{\varepsilon} = f_a \widetilde{\varepsilon}_a + (1 - f_a)\widetilde{\varepsilon}_b$$

(5.1.2.3)

where f_a is the volume fraction of material a.

The Bruggeman approximation is valid for the case of two media, a and b, having the dielectric constants $\widetilde{\varepsilon}_a$ and $\widetilde{\varepsilon}_b$ embedded in a host medium with the dielectric constants $\widetilde{\varepsilon}_h$. In the approximation of spherical inclusions, the dielectric constant $\widetilde{\varepsilon}$ can be written as:

$$\frac{\widetilde{\varepsilon} - \widetilde{\varepsilon}_h}{\widetilde{\varepsilon} + 2\widetilde{\varepsilon}_h} = f_a \frac{\widetilde{\varepsilon}_a - \widetilde{\varepsilon}_h}{\widetilde{\varepsilon}_a + 2\widetilde{\varepsilon}_h} + f_b \frac{\widetilde{\varepsilon}_b - \widetilde{\varepsilon}_h}{\widetilde{\varepsilon}_b + 2\widetilde{\varepsilon}_h}$$

(5.1.2.4)

Assuming that the inclusion of the materials a and b are embedded in the effective medium itself ($\widetilde{\varepsilon} = \widetilde{\varepsilon}_h$), such that neither phase should be given preference, the first term in the previous equation becomes 0.

Figure 5.1.6 shows an example of thickness determination for a 1.5 μm thick Alq$_3$ film prepared in BESSY and measured with VASE after a few days of atmosphere exposure. Due to the high thickness, clear interference features can be seen in the experimental Ψ and Δ spectra. The amplitude of Ψ oscillations decreases towards higher energies indicating that the film exhibits thickness non-uniformity. This is a common sample non-ideality and it is the

variation of the film thickness across the sample surface. If a film thickness varies over the width of the light beam, the resulting reflected beam will be partially polarized, as the beam may be divided up into thin slices, each of which effectively 'sees' a film of slightly differing thickness. These beams must be properly added at the detector in order to correctly predict the measured Ψ and Δ values. The simulation software WVASE allows the user to specify that the film structure on a given sample is non-uniform, such that all films in a multilayer are assumed to exhibit the same non-uniformity. The user must specify the percentage variation in film thickness across the probing light beam, and may fit for this percentage.
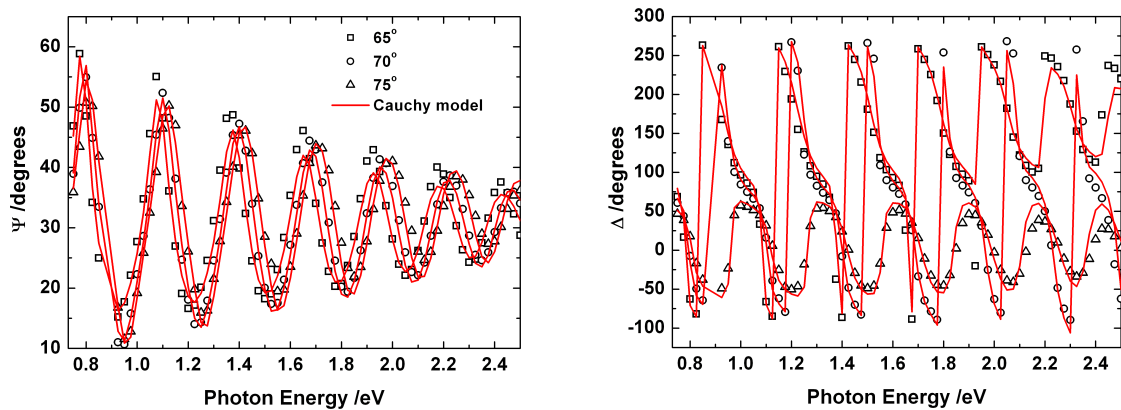
Figure 5.1.6. Non-ideal Cauchy model for a 1.5 μm thick Alq$_3$ film. Open symbols represent experimental data while continuous lines represent the model simulations.

The experimental data were simulated using a Cauchy model with A=1.56 and B=0.026. The values of the refractive index and dielectric function are presented in figure 5.1.7. Additionally the film was found to have 1532 ($\pm$13) nm thickness, 25 ($\pm$4) nm surface roughness and 8% variation in the thickness across the measured surface.
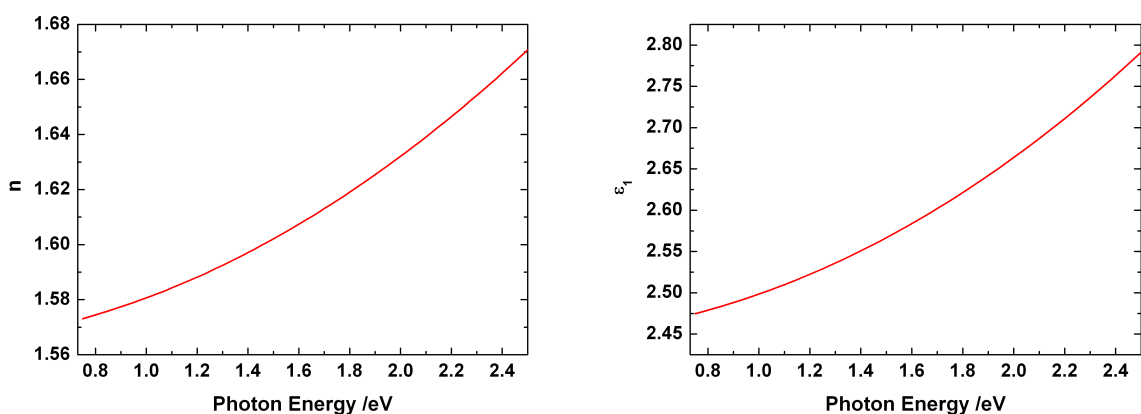
Figure 5.1.7. The refractive index n and the real part of the dielectric function ε_1 as determined from the Cauchy model

The measured data will not be very sensitive to film thickness variations unless there are spectral features in the measured data which are very strongly dependent on the film thickness, most commonly interference oscillations in Ψ and Δ and sharp handedness changes in delta. For thinner films, non-uniformity of the film will simply lead to the determination of an effective thickness of the film which is roughly an average value over the illuminated area. The spot size for the ellipsometer presented in the figure 5.1.3 depends on the angle of incidence $-\Phi$. For example for Φ=70° the spot has an ellipse like shape, with ~0.4 cm short axis and ~1 cm the long axis.

Using the Alq$_3$ refractive index presented in figure 5.1.7 the effect of the surface roughness on the ellipsometric spectra was simulated in figure 5.1.8. For clarity only the spectra for 70° angle of incidence is plotted. The roughness simulation was performed using an EMA model with 50% voids as described before. As can be seen in the figure clear differences in the Ψ and Δ values can be seen when the surface roughness was added even if this is less than 4% of the total thickness of the layer.
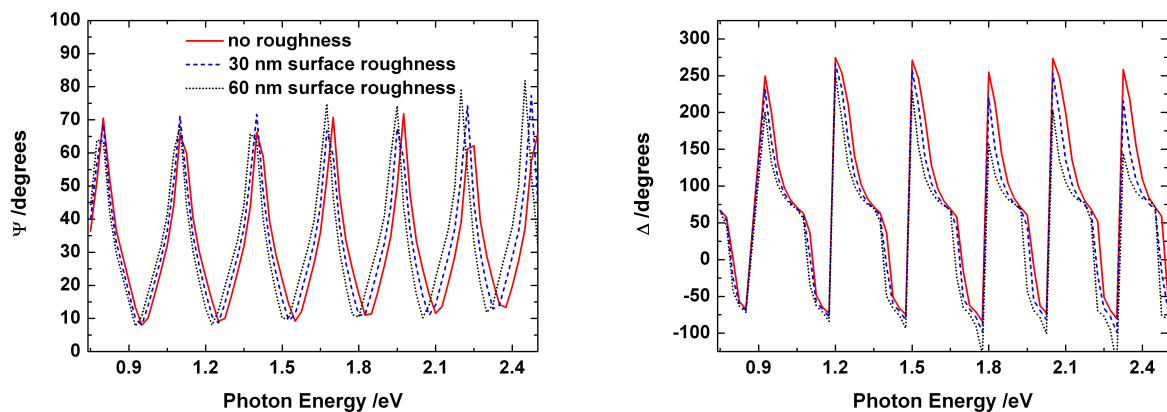
Figure 5.1.8. Simulation of the influence of the surface roughness on the ellipsometric Ψ and Δ spectra for 70° angle of incidence.

If the substrate is transparent the reflected light from the backside of the substrate is no longer coherent with the reflected light from the surface and the light at the detector will be partially polarized. The back side reflection is another type of non-ideality that can be included in the model. However in this case the back side reflections can be avoided by roughening the back side of the substrate.

After thickness determination an initial point-by-point fit can be performed. In the point-by-point fit the refractive index n and the extinction coefficient k are found by fitting the experimental data at each wavelength. The overall result, however, is not always Kramers-Kronig (KK) consistent. In order to ensure the KK consistency a mathematical based model is used. In this model the shape of the imaginary part of the dielectric function ε_2 is simulated using Gaussian functions while the real part is solved applying KK consistency.

For anisotropic materials, *e.g.* uniaxial layers, two sets of Cauchy functions are used to determine the layer thickness – one for simulating the dielectric function in the surface plane and one for simulating the dielectric function in a direction perpendicular to the surface plane. Following this procedure two sets of Gaussian functions are used to simulate the optical properties in the mentioned directions.

5.2. Infrared Spectroscopy

The Infrared (IR) radiation is the electromagnetic radiation in the spectral range from 10 cm^{-1} to 10000 cm^{-1}. In this range we find the frequency of the vibrational and rotational movement of atoms and molecules. If for a vibrational motion the dipole moment changes, this mode is called IR active. In this case, if the IR frequency of the radiation matches a natural vibrational frequency of the molecules, a net transfer of energy takes place resulting in a change of the amplitude of the molecular vibration and a corresponding absorption of the radiation. The ratio between the intensity of the beam measured after and before interaction of IR light with the sample plotted as a function of the frequency of the light represents an IR spectrum.

5.2.1. Experimental setup

The IR measurements were performed with a Fourier Transform Infrared (FTIR) Bruker IFS-66 spectrometer. The schematics of the experimental setup is shown in figure 5.2.1.
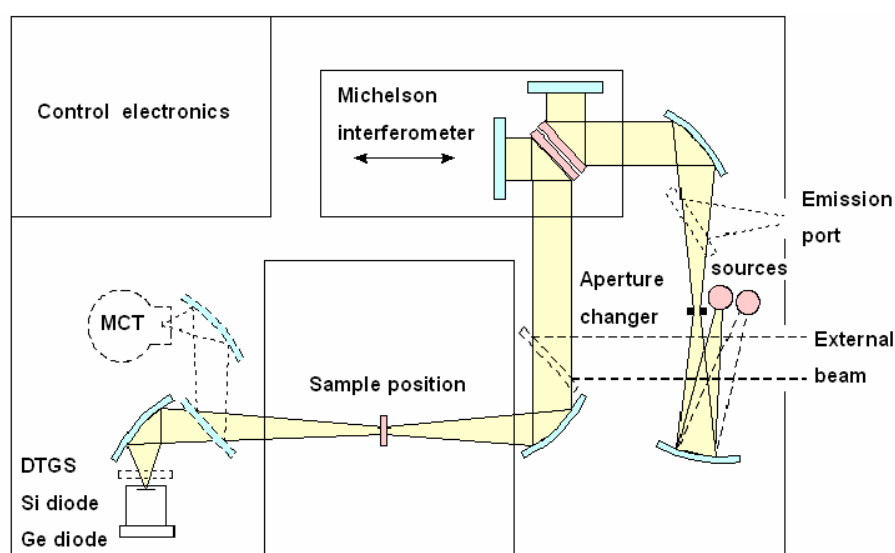
Figure 5.2.1. Schematics of FTIR Bruker IFS-66 spectrometer

The FTIR spectrometer is based on a Michelson interferometer which can be seen in the upper part of the 5.2.1 schematics. During the measurement one of the mirrors moves and the spectrometer records the signal as a function of the beam retardation (path

difference) between the fixed and the moving mirror. The recorded spectrum is called interferogram. The Fourier transformation (FT) of the interferogram gives the IR spectrum function of frequency. A detailed description of the FTIR principles can be found in reference [Gri86].

The IR measurements performed in this work were performed in reflection at 20^0 and at 60^0 using s- and p- polarized light for the samples on Si substrates. Comparing the spectra for s- and p- polarization is particularly useful for evaluating the anisotropy of the organic films. While in s- polarization the IR modes which have a change in the dipole moment in the surface plane will show up, in p- polarization the IR modes which have a change in the dipole moment perpendicular to the plane can be also excited. For isotropic layers the relative intensities of the IR features should be the same is s- and p- polarization. In order to compare the molecular orientation in thin films, KBr pellets containing crystallites with random orientation were also prepared. These pellets were measured in transmission IR.

The IR source used is a Globar: an electrically heated silicon carbide rod. For the measurements performed in the mid infrared range (500-4000 cm^{-1}) a beam splitter made of KBr is used. For transmission and reflection measurements a deuterated triglycine sulphate (DTGS) detector is employed. DTGS is a pyroelectric detector which is sensitive in the mid infrared range.

6. Molecular Orientation in Thin Films

6.1. H$_2$Pc

Even though the Pc's are known for almost one century and were used in many landmark experiments in molecular physics such as the first direct X-ray structure analysis of an organic crystal and the first image of a molecule using field-emission microscopy [McK98], there are at present only very few papers that describe the dielectric function of metal free phthalocyanine and, moreover, these treat the material as isotropic [Arw86, Deb91]. To our knowledge there is no report in literature for the dielectric function deduced from an anisotropic model.

While the high thermal and chemical stability of the Pc materials [McK98, Lez96] make them promising candidates for new devices in communication, imaging, (opto) electronics and sensors, optimizing the efficiencies of such devices remains a challenging task as many properties like electrical transport and optical response depend on the molecular orientation and electronic interactions at interfaces. The growth mode of the Pc depends on many parameters as presented in chapter 4.1.3. In this work the dielectric function for H$_2$Pc films was determined over a wide spectral range from ellipsometry simulation using anisotropic model approaches. Moreover, the molecular orientation was found to be dependent on the pressure conditions.

6.1.1. High Vacuum Deposition

Thin films of metal - free phthalocyanine (H$_2$Pc) were grown by OMBD in high vacuum (HV) simultaneously on different substrates. The substrates (hydrogen passivated Si(111), NaCl were kept at room temperature during the deposition. The NaCl substrates were obtained by cleavage from a salt crystal. The passivation and cleaning procedure was done as described in the chapter 4.4. After passivation the substrates were immediately transferred into the deposition chamber. The thickness of the organic material was monitored by a quartz crystal micro-balance which was located in the vicinity of the samples, the frequency shift of which is proportional to the film thickness (see table 6.1.1).

In order to determine the dielectric function of the H$_2$Pc layers ellipsometric spectra were recorded at different angles of incidence (55°, 60°, 65°, 70°, 75°) in the range of 0.73 eV - 4.5 eV with a 0.02 eV step for each sample. As in ellipsometry the main contribution to the signal is given by the dielectric function from the x direction (see chapter 3.3 or Asp80) the samples were also measured by rotating them azimuthally around the z direction. These measurements revealed that the samples exhibit in-plane isotropy. Consequently the possibilities are reduced to isotropic or uniaxial anisotropic samples.

Table 6.1.1. H_2Pc samples – S and N for silicon and NaCl substrates, respectively and frequency shift as measured by a quartz crystal microbalance.

Set	Substrate	Sample name	Frequency shift
1	H-Si(111)	S1	884 Hz
	NaCl	N1	
1	H-Si(111)	S2	1069 Hz
	NaCl	N2	
3	H-Si(111)	S3	2122 Hz
	NaCl	N3	

In order to assess the in-plane / out-of-plane anisotropy the samples were measured using IR spectroscopy. As the NaCl is transparent in the IR range the samples grown on NaCl substrates were measured in normal transmission. Additionally, in order to have a reference with random orientation of H_2Pc molecules, KBr pellets were prepared. The Si(111) substrates were one side polished. For the samples S1, S2 and S3 reflection measurements were performed at 60° in s- and p- polarization.

Figure 6.1.1 shows the FTIR spectra of H_2Pc films on NaCl (N1, N2, N3) and of H_2Pc embedded in a KBr pellet. All spectra are normalized with respect to the peak at 1006 cm^{-1}.
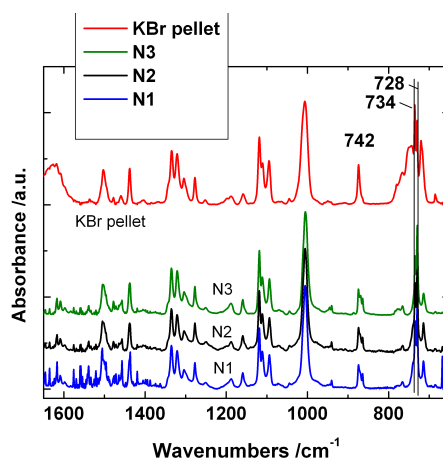
Figure 6.1.1. FTIR spectra of H_2Pc films on NaCl (N1, N2 and N3) and of H_2Pc embedded in a KBr pellet.

Figure 6.1.2 presents the reflection absorption FTIR spectra of samples S1, S2 and S3 measured in s- respectively p-polarization at 60^0 angle of incidence. According to Debe and Field [Deb91] the dominance of the out-of-plane vibrational band at 742 cm^{-1} in p-polarization compared to the in-plane bands at 728, 734 and above 800 cm^{-1} in s-polarization implies that the H_2Pc molecules are oriented on Si(111) substrates in the perpendicular b-axis configuration (see figure 4.1.4). The IR spectra of the samples on NaCl substrates are similar to the spectra in s-polarization for samples on Si(111) substrates. Here, the presence

of the in-plane bands at 728 and 734 cm^{-1} and the absence of the 742 cm^{-1} band compared to bulk H_2Pc leads to the conclusion that the H_2Pc molecules are also adopting a perpendicular b-axis configuration.
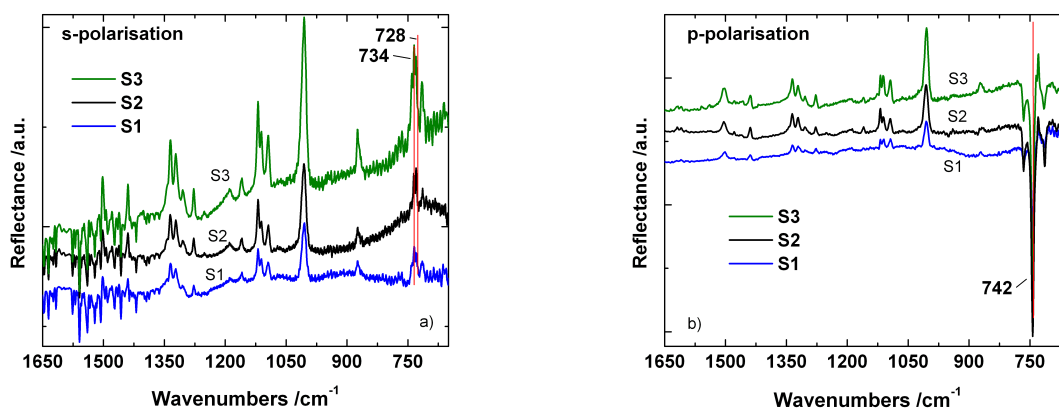
Figure 6.1.2. Reflection absorption FTIR spectra in s-polarization at 60° angle of incidence for samples S1, S2, and S3.
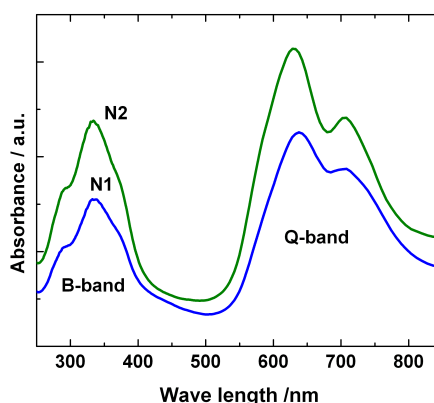
Figure 6.1.3. UV-Vis absorption spectra of N1 and N2 samples. The lowest energy band, the Q band, is characteristic for α-phase H_2Pc [McK98]

The UV-Vis absorbance spectra of H_2Pc films on NaCl substrates are presented in figure 6.1.3. The long wavelength band, the Q band, with a broad peak centered around 630 nm and a shoulder towards the red corresponds to a $\pi-\pi^*$ transition. In the case of an isolated H_2Pc molecule, the absorption band is a sharp doublet corresponding to the non-degenerate Q_x and Q_y transitions [Ass65]. Compared to the spectra of a single molecule the broad features of the film can be explained by a cofacial (face-to-face) arrangement of the H_2Pc molecules leading to strong excitonic interactions [McK98]. The shape of the Q band clearly indicate that the films consist of $\alpha-$type H_2Pc [McK98].The absorption band occurring in the 300 nm region is also a $\pi-\pi^*$ transition and denoted as B band.

The H_2Pc molecule has an intrinsic optical anisotropy due to its planar structure (figure 4.1.1.a) and the presence of 18 delocalized π electrons. According to UV-Vis

absorption we have an α-type H_2Pc crystal and IR measurements show that the b-axis is perpendicular with respect to the substrate. Taking into account the in-plane isotropy deduced from ellipsometric measurements the films are thus best represented by uniaxial models.

An uniaxial model was built using the WVASE^{tm} software [Gor04a] and the film thicknesses of S1, S2 and S3 samples were determined in the absorption free range (below 1 eV) using two Cauchy formulas (5.1.2.2) as described in the chapter 5.1.2. The results are summarized in table 6.1.2. The thickness determination for the films on NaCl was found not to be accurate due to the low contrast between the refractive index of the substrate and the refractive index of the H_2Pc films and due to the presence of multiple cleavage planes in the NaCl substrates. The surface roughness was considered using an effective medium approximation (EMA) layer. It consists of a mixture of 50% film material and 50% voids.

Table 6.1.2. Thickness and surface roughness of H_2Pc films on Si(111) substrates determined from ellipsometry.

Sample	Thickness /nm	Surface roughness /nm
S1	60.0 ±0.9	6.0 ±1.6
S2	77.1 ±1.0	8.3 ±2.0
S3	155 ±2	16.3 ±6.6

In order to determine the dielectric function describing the optical response of the films, a more complex model was used. The shape of ε_2 was simulated using Gaussian lineshapes, three for the Q band and two for B band. Especially for the z component it is very difficult to obtain reliable optical constants for thin uniaxial films. All three samples S1, S2 and S3 thus were fitted simultaneously. During the fit, the thickness and the surface roughness previously determined were kept fixed. As an example, Figure 6.1.4 presents the ψ and Δ ellipsometric spectra and the best fit for sample S3.

Figure 6.1.5 presents the anisotropic dielectric function determined for H_2Pc on H-Si(111). The shape of the in-plane components of the uniaxially oriented films is in very good agreement with the one determined for an isotropic H_2Pc film by Arwin and Aspnes [Arw86]. The effective values in our case are higher, but if we consider that for an isotropic film we have an average between the in-plane and out-of-plane components the values obtained are also in good agreement with ref. [Arw86].
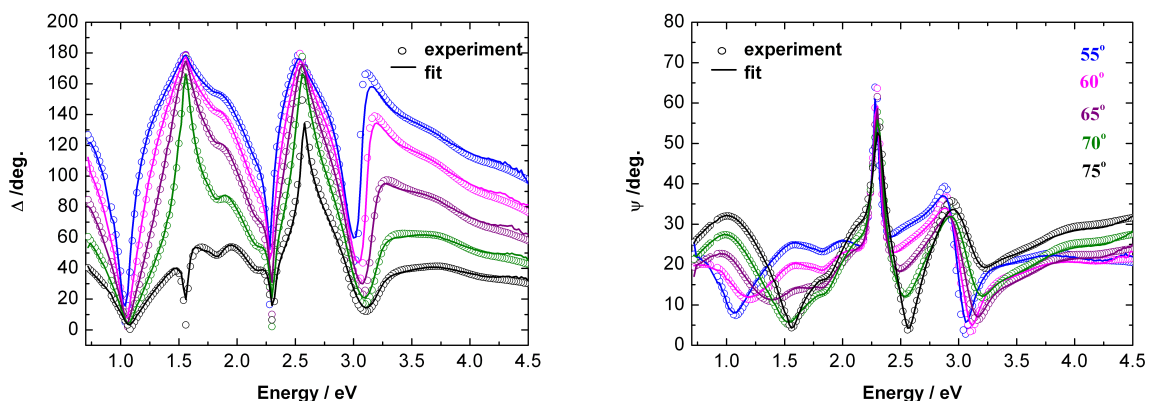
Figure 6.1.4. Ellipsometric Ψ and Δ spectra at different angles of incidence for a H_2Pc film on Si (111) substrate (S3). Open circles are the experimental points and continuous lines the fits.
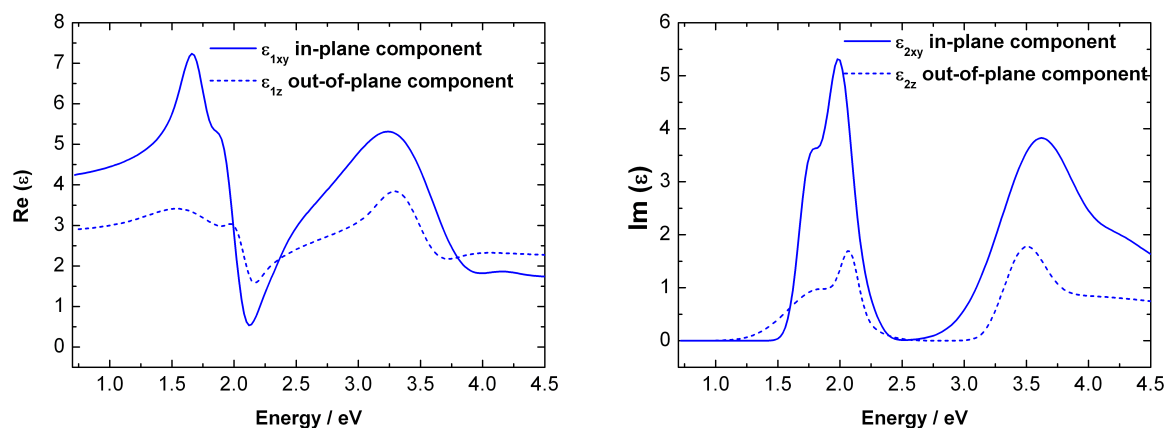
Figure 6.1.5. Anisotropic dielectric function for H_2Pc. left – real part, right – imaginary part. Continuous line represent in-plane components, dashed line out-of-plane component.
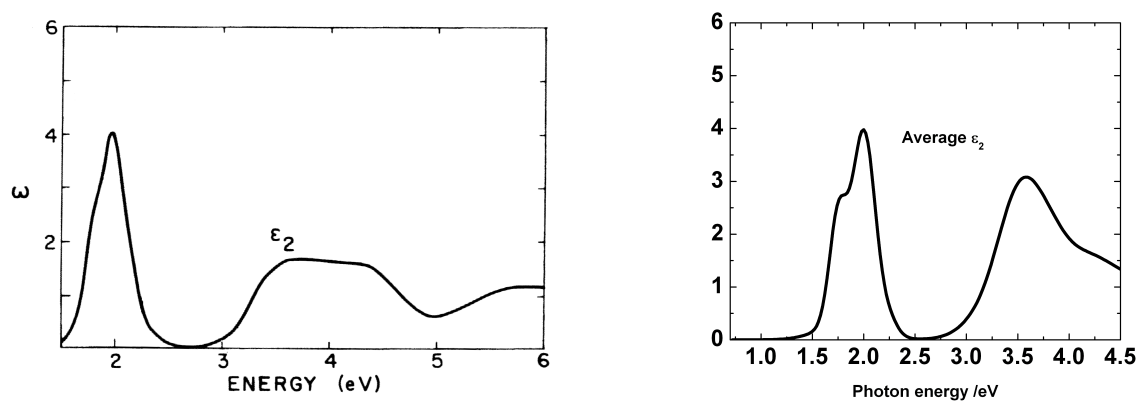
Figure 6.1.6. Comparison between the imaginary part of the H_2Pc dielectric function reported by Arwin and Aspnes [Arw86] and the imaginary part of the H_2Pc dielectric function calculated with the values presented in figure 6.1.5 as if the H_2Pc film would be isotropic.

In order to compare the results with the isotropic case [Arw86] the imaginary part of the dielectric function can be recalculated as if the H_2Pc film would be isotropic.

$$\varepsilon_2 = \frac{2\varepsilon_{2xy} + \varepsilon_{2z}}{3} \qquad (6.1.1.1)$$

The average values calculated with formula 6.1.1.1 are compared with the values reported by Arwin and Aspnes [Arw86] in figure 6.1.6.

In order to understand the correlation between the macroscopic optical constants of the uniaxial films (figure 6.1.5) and the crystalline structure we were the first to propose a coarse model based on molecular and crystal properties [Gor04a].

Since the phthalocyanine π orbitals are antisymmetric with respect to the molecular plane, all allowed $\pi-\pi^*$ transition are in-plane polarized. Considering the H_2Pc molecule (figure 4.1.1a) in molecular coordinates, the x and y direction have the same contribution to absorption. For the α-form, the β angle is 91.1^0 and the a–axis of the crystal is assumed to be in the molecular plane (figure 4.1.3). The angle θ between the normal to the molecular plane and the b–axis is 26.5^0. Denoting the absorption in the molecular plane (xy), e.g. the Q-band, with "molecular-in-plane" then in a simple approximation the portion of absorption intensity in a given configuration is proportional to the cosine squared of the angle (γ) between the electric field vector and the direction (x or y):

$$I \propto \cos^2 \gamma \qquad (6.1.1.2)$$

With the electric field vector parallel to the corresponding crystal axis – see figure 4.1.3 – and $g = \cos^2(\theta) = \cos^2(26.5^0) \approx 0.8$ we can consider the absorption to be proportional to the values given in column 2 of table 6.1.3.

If we consider crystals with one axis perpendicular to the sample plane and the two other axes with a random azimuthal configuration in the film plane the contribution of molecular-in-plane to the film in-plane absorption intensities for 3 potential cases can be evaluated by averaging over the absorption contributions for two axes as in column 4 of table 6.1.3. The corresponding contribution to the out-of-plane film absorption (third axis) is displayed in the column 2.

For the samples studied the imaginary part of the dielectric function in the film plane shown in figure 6.1.5 is much higher then the out-of-plane one. This kind of anisotropy for the Q band is only possible for an uniaxial H_2Pc films if the b-axis is predominately oriented perpendicular to the film plane. In all other cases (a-axis or c-axis perpendicular) we should observe a lower molecular-in-plane contribution in the film plane compared to isotropic material.

Using this simple model, an average orientation angle of 32° was calculated from the integral absorption of the Q-band region using the determined extinction coefficient values. An estimation of the determination errors will be discussed in a later chapter.

Table 6.1.3. Relative absorption intensities of molecular in-plane and out-of-plane modes estimated for uniaxial α-phase H$_2$Pc films with one crystal axis perpendicular to the surface.

perpendicular to the film plane		in the film plane	
crystal axis	molecular-in-plane	crystal axes in plane	molecular-in-plane
a	1	b+c	1/2 = 0.5
b	1-g =0.2	c+a	(1+g)/2 = 0.9
c	g =0.8	a+b	(2-g)/2 = 0.6
isotropic	0.67	isotropic	0.67

6.1.2. Ultra High Vacuum deposition

The samples analyzed in this chapter were prepared by Dr. Sakurai in Tsukuba, Japan as described in the chapter 4.4. The deposition rate was measured using a quartz oscillator close to the substrate and was maintained below 0.1 Å/s.

Ellipsometric measurements were performed using the VASE setup described in chapter 5.1.1. In order to determine the thickness and optical properties of the samples, the measurements were carried out in a large spectral range, from 0.73 to 5 eV, with a 0.02 eV energy step. Measuring the samples at incidence angles around the Brewster angle of the substrate increases the sensitivity of this technique. The samples on glass substrates were measured at several angles of incidence, between 55° and 70° with a step of 5°. The measurements for the SiO$_2$/Si substrates were performed between 65° and 75° with the same step. In addition, the transmittance of the organic layers on glass substrates was also measured.

In order to assess the in-plane anisotropy, all samples were measured at different azimuthal angles. The measurement revealed that the ellipsometric spectra are independent of the azimuthal angle. This indicates that all samples have in-plane isotropy. However, due to their intrinsic molecular anisotropy and their crystalline growth it is known that H$_2$Pc [Lez96, Mck98] form anisotropic layers [Gor04a]. Therefore the out-of-plane optical anisotropy was considered when modelling the optical response of the organic layers. In this case the in-plane contributions are equal, i.e. $\varepsilon_x = \varepsilon_y = \varepsilon_{\parallel}$, while the out-of-plane one, perpendicular to the substrate surface, $\varepsilon_z = \varepsilon_{\perp} \neq \varepsilon_{\parallel}$ is different. As the transmission measurements were performed at normal incidence, $\varepsilon_{\parallel}$ data can be used to simulate the spectra for the films deposited on transparent substrates.

The first step in data evaluation is thickness determination. For an accurate determination of the thickness the optical properties of the substrates have to be taken into account. The optical response of the silicon reference substrate was simulated using the

existent dielectric function in the data base for silicon [Jel92] and for the silicon oxide [Pal85]. The thickness of the silicon oxide was found to be (31±0.02) nm.

The dielectric function of the glass substrate was determined from a reference ellipsometric measurement. The real and imaginary parts of the dielectric function of the glass are presented in figure 6.1.7. During the fit the data from both ellipsometry and transmission measurements are considered. Especially for anisotropic samples this procedure is particularly useful in lowering the correlation factor between the floating parameters used to simulate the in-plane and out-of-plane contributions.
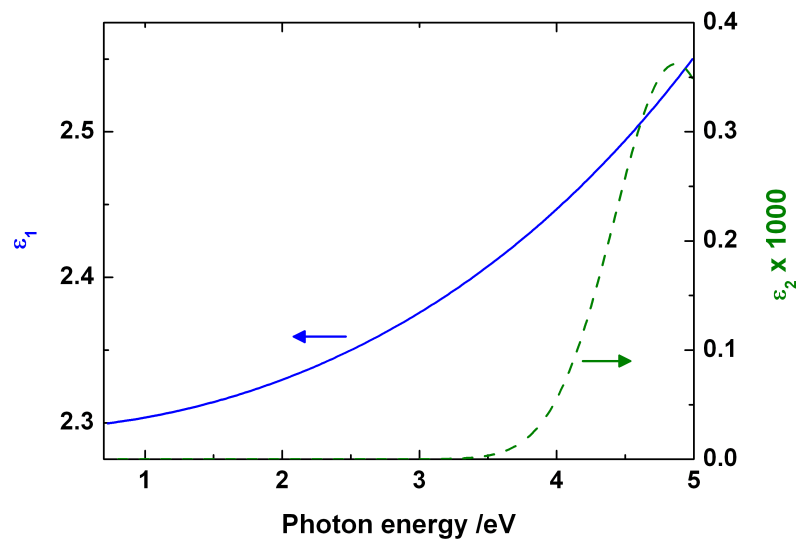
Figure 6.1.7. The complex dielectric function of glass substrates

The film thicknesses of the organic layers were determined in the transparent range of the material using two Cauchy (5.1.2.2) dispersion relations, as described in the previous chapter. Table 6.1.4 presents the thicknesses obtained from the ellipsometric data evaluation. The confidence limits for the thickness determination for H_2Pc on glass are higher due to the lower contrast between the refractive index of H_2Pc and glass substrates.

After the thickness determination transmission spectra can be used to determine $\varepsilon_{\parallel}$. However, the simulation of the ellipsometric spectra using the extinction coefficient determined from the absorption together with the Kramers-Kronig consistent refractive index does not give a satisfactory agreement with the experimental data. Therefore an uniaxial model has to be considered for the ellipsometric data. In this model two sets of dielectric functions are used to model the sample properties in the directions parallel and perpendicular to the sample surface. In order to have a Kramers-Kronig (KK) consistent solution, the imaginary part of the dielectric function is simulated using Gaussian functions while the real part is solved employing the KK relation. In order to reduce the correlation between parameters during the fitting procedure, three samples with different thicknesses

are considered in the model together with their transmission data. The validity of this evaluation holds as long as the organic films have the same optical properties regardless of the film thickness. In figure 6.1.8 the simulated and experimental transmittance data of the H_2Pc films on glass substrates are plotted. The reference glass transmittance is also shown.

Table 6.1.4. Thicknesses of the H_2Pc layers determined from ellipsometry

Substrate	Material	Thickness /nm
Glass	H_2Pc	42.0 ± 6.5
		22.0 ± 3.4
		13.0 ± 2.0
SiO_2/Si	H_2Pc	36.7 ± 3.4
		18.3 ± 1.7
		11.2 ± 1.1
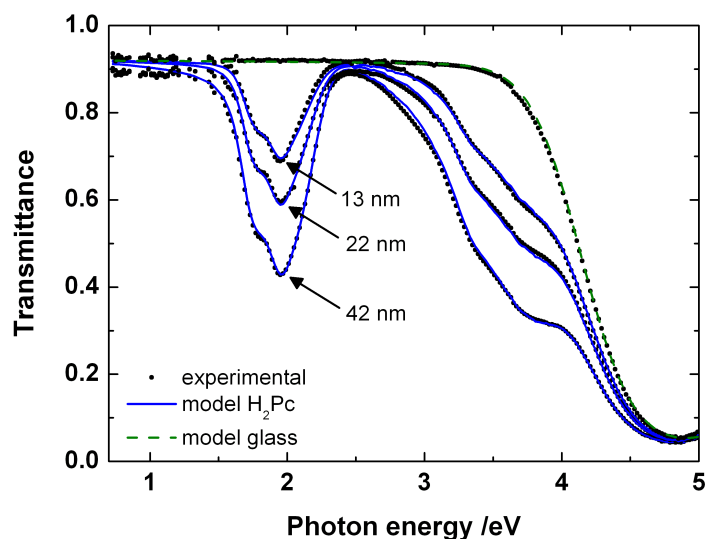
Figure 6.1.8. Transmittance spectra of H_2Pc layers on glass substrates. For comparison the transmittance of the glass substrate is also plotted. The continuous lines represent the model simulation of the transmittance using the in-plane component of the dielectric function.

The anisotropic dielectric function of H_2Pc is presented in figure 6.1.9. As all transmission measurements were performed at normal incidence, the simulation of the transmittance spectra is done using the in-plane components. In contrast to the H_2Pc films grown under HV conditions, in this case the in-plane component of the dielectric function is smaller than the out-of-plane one, indicating a different molecular orientation. However, the shape of the absorption bands is in agreement with previous reports [Arw86,Gor04a] and indicates that the films consist of α-phase H_2Pc with its well known herringbone structure [Lez96, Mck98]. Taking into account that the absorption features in the presented spectral

range are induced by π-π^* transitions, which are polarized in the molecular plane, an average molecular orientation can be deduced from the differences in the extinction coefficient between the xy (in-plane) and the z (perpendicular) directions [Gor04a]. Considering in a first approximation that the H_2Pc is planar and the overall absorption intensity is the result of a scalar product between the electric field vector and the transition dipole, the average orientation of the molecules with respect to the substrate was found to be ~52°. This indicates that the growth mode of H_2Pc is α-phase oriented with the molecular stacking axis parallel to the substrate surface.
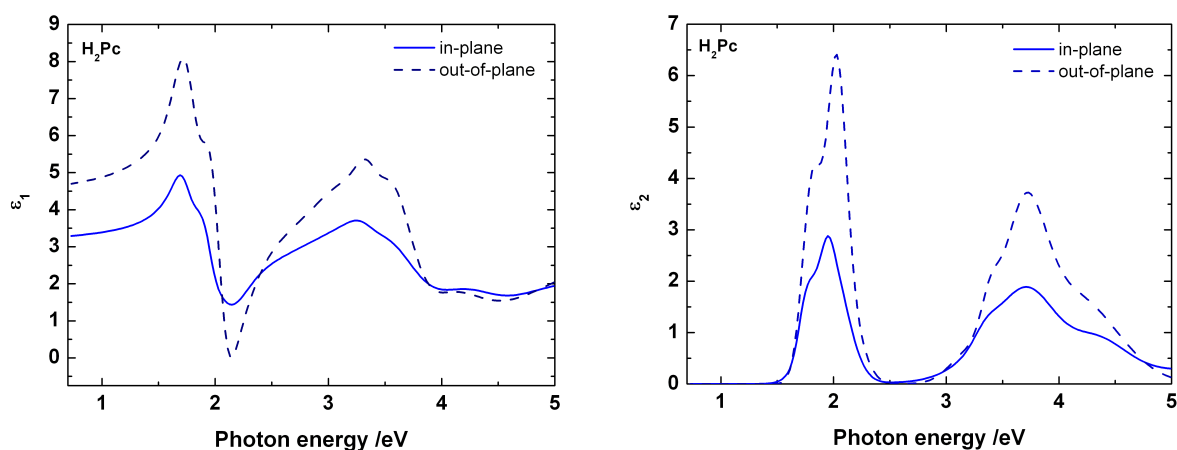
Figure 6.1.9. The real (left) and imaginary (right) part of the dielectric function of the H_2Pc films deposited on glass and SiO_2/Si.

A similar analysis procedure was applied for the H_2Pc films grown on the silicon oxide/silicon substrates. The in-plane dielectric function was found to be identical with the one presented in figure 6.1.9. The out-of-plane component was slightly different leading to a tilt angle of ~53°. As the in-plane component of the dielectric function is identical for the H_2Pc films grown on glass with the one of H_2Pc films grown on silicon substrates and the difference in the out-of-plane component is within the error limits we consider that these films exhibit similar growth modes.

These findings are in agreement with recent studies of H_2Pc orientation studied by infra-red reflection absorption spectroscopy (IRRAS) [Sak05], X-ray diffraction [Sak06] and consistent with previous results derived from ellipsometry for CuPc [Gor04b].

6.2. CuPc

Copper phthalocyanine (CuPc) is one of the most extensively studied Pcs by means of ellipsometry [Deb92, EiN01, Dju02, Yiq03, Bor04], infra-red spectroscopy [Ebe52, Ken53, Sid61, Ass65a] and X-ray diffraction [Rob35, Ass65a, Bro68, Ber00]. Even though the CuPc molecule has an intrinsic optical anisotropy due to its planar structure, in the reported dielectric functions or optical constants derived from ellipsometriy spectra the CuPc layers

were considered as being isotropic [Deb92, EiN01, Dju02, Yiq03, Bor04]. In one previous analysis Debe [Deb92] tried to approximate the anisotropic dielectric function of CuPc by investigating two different types of oriented films – with the b-axis (the molecular stacking axis) perpendicular and respectively parallel to the substrate surface. For each film only the in-plane components of the dielectric function were determined. In other reports [Bar86, Ayu01] the optical anisotropy of the CuPc layer was taken into account but these studies were limited to single wavelength ellipsometry at one angle of incidence. The experimental data in ref. [Bar86] was modelled assuming an isotropic layer for thicknesses below 100 nm and an isotropic inner layer plus an anisotropic outer layer for thicknesses higher than 100 nm. However, the anisotropic dielectric function of CuPc was not reported in the literature so far.

Therefore the aim of this chapter is to present the dielectric function for CuPc films over a wide spectral range (0.73 – 5 eV) obtained from simulating ellipsometry spectra using anisotropic model approaches. As reported previously for metal-free phthalocyanine [Gor04a] and for perfluorinated vanadyl phthalocyanine [Gor04c], the determination of the anisotropic dielectric function from spectroscopic ellipsometry does not only yield physically reliable values, but also allows the orientation of the molecules with respect to the substrate to be determined.

As presented in section 6.1, the molecular orientation of H_2Pc depends on the pressure conditions. In order to study the same dependence, organic thin films of CuPc were grown by OMBD in high vacuum (HV – $8 \cdot 10^{-7}$ mbar) and ultra-high vacuum (UHV – $6 \cdot 10^{-10}$ mbar) on hydrogen passivated Si(111). More details about samples preparations can be found in the chapter 4.4. The thickness of the organic material was monitored by a quartz crystal micro-balance which was located in the vicinity of the samples. The deposition rate was kept constant at approximately 0.3 nm /minute.

Infrared (IR) measurements were performed in reflection at 20^0 and at 60^0 using s- and p- polarized light. KBr pellets containing crystallites with random orientation of the β-phase CuPc were also prepared. These pellets were measured in transmission.

In order to determine the film thicknesses and the energy dependence of the optical constants ellipsometric spectra were recorded at different angles of incidence (65°, 70°, 75°) in the range of 0.73 eV - 5 eV with a 0.02 eV step for each sample.

6.2.1. HV *vs.* UHV

The first assessment of the ellipsometric spectra revealed that all films are in-plane isotropic. This was checked by measuring the ellipsometry spectra for various azimuthal angles. As in the case of H_2Pc [Gor04a], the possibilities are reduced to isotropic or uniaxial anisotropic samples.

In order to decide which model is more appropriate the IR spectra of the samples were analysed. The spectra for the films prepared in the same condition have similar features regardless of the thickness. This leads to the conclusion that the structure of the CuPc films is preserved in this thickness range. Figure 6.2.1 shows the IR spectra of the samples prepared in HV in comparison with the ones prepared in UHV. The spectra were normalised with respect to the reflection of the Si(111) substrate and the 722 cm^{-1} peak. The IR spectrum of the CuPc pellet is also shown.

The peak positions for all samples indicate that the films consist of α-phase CuPc while the CuPc in the pellet exhibits β-form characteristics [Sid61, Ass65a]. According to Debe [Deb92] the 722 cm^{-1} and 770 cm^{-1} peaks correspond to out-of-plane vibrations of the CuPc molecule while the peak at 753 cm^{-1} and all bands above 800 cm^{-1} are due to molecular in-plane vibrations.

Considering s-polarization the relative intensity ratios of the peaks for the samples prepared under HV condition are very different when compared to the ones of the samples prepared in UHV and the ones in the transmission spectrum of the pellet. Especially the peak at 722 cm^{-1} is more intense for samples prepared in UHV. This indicates that the molecular arrangement is different for the two types of films. For the samples prepared in UHV the molecules adopt a standing configuration with respect to the substrate surface, i.e. the molecular plane has a large tilt angle, while for the HV samples the molecules obviously adopt a different orientation.

Considering p-polarization, as can be seen in the figure 6.2.1, the 722 cm^{-1} and 770 cm^{-1} peaks have derivative like shapes, or are pointing downwards for the HV films. This indicates that the displacement of atoms for these oscillations is in the z-direction of the films (perpendicular on the film surface). Consequently the average angle of the molecular plane with respect to the substrate surface is less than 45^0. This can explain the higher coupling of the p-polarization with the out-of-plane vibrations of the molecule, while for s-polarization the IR spectra are similar to that of the bulk. For the UHV films the in-plane vibrations of the molecules exhibit derivative like bands in p-polarization indicating that the average molecular orientation is at a higher angle that 45^0 with respect to the substrate surface.
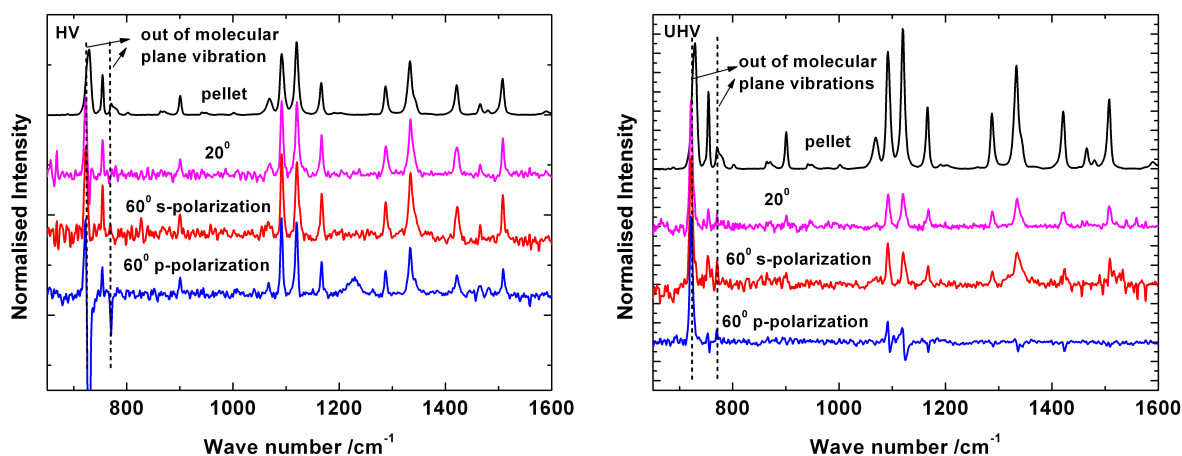
Figure 6.2.1. Left - reflection IR spectra of the CuPc sample HV-1. Right - reflection IR spectra of the CuPc sample UHV-1. The 722 cm^{-1} and 770 cm^{-1} peaks correspond to out-of-plane vibrations of the CuPc molecule while the peak at 753 cm^{-1} and all bands above 800 cm^{-1} are due to molecular in-plane vibrations.

The ellipsometric data evaluation [Gor04a, Gor04b] was performed as presented before for H$_2$Pc. The thicknesses of the CuPc layers were determined by simulating the spectra in the transparent range using two Cauchy functions (5.1.2.2) for the anisotropic refractive index dispersion. Table 6.2.1 summarises the thicknesses and the values for the surface roughness obtained from fitting the experimental ellipsometric spectra with a uniaxial model in the range of 0.73 –1.1 eV. The surface roughness is simulated using an effective medium approximation consisting of 50% film material and 50% voids. The values obtained are in very good agreement with the ones obtained from an atomic force microscopy (AFM) scan. The surface morphology of the samples prepared in HV is different from the ones prepared in UHV as can be seen in figure 6.2.2. This can be related to the different growth modes of the CuPc molecules on Si(111) substrates depending on the pressure conditions.

Like in the case of the H$_2$Pc model [Gor04a], for the uniaxial models of CuPc layers [Gor04b], two sets of functions were used – one in the plane (xy) of the film and one for the out-of-plane (z) direction of the film. Especially for the z component (normal to the surface) it is usually difficult to obtain reliable optical constants for thin uniaxial films [Asp80]. To overcome this problem we used a special multiple-sample analysis procedure [Mcg93]. In the multiple-sample analysis several films with different thicknesses, but the same optical constants can be coupled together in the fit. The films prepared in HV were coupled together in the same model as the IR revealed that the films show similar spectra regardless of the thickness. The same procedure was applied for the UHV films.

Table 6.2.1. Thickness and surface roughness of CuPc films on Si(111) substrates
determined from ellipsometry.

	UHV			HV	
Sample nr.	Thickness /nm	Surface roughness /nm	Sample nr.	Thickness /nm	Surface roughness /nm
UHV 1	49 ±0.6	10 ±0.8	HV 1	46 ±0.5	2 ±0.6
UHV 2	105 ±1	11 ±0.9	HV 2	78 ±0.3	3 ±0.5

HV   UHV
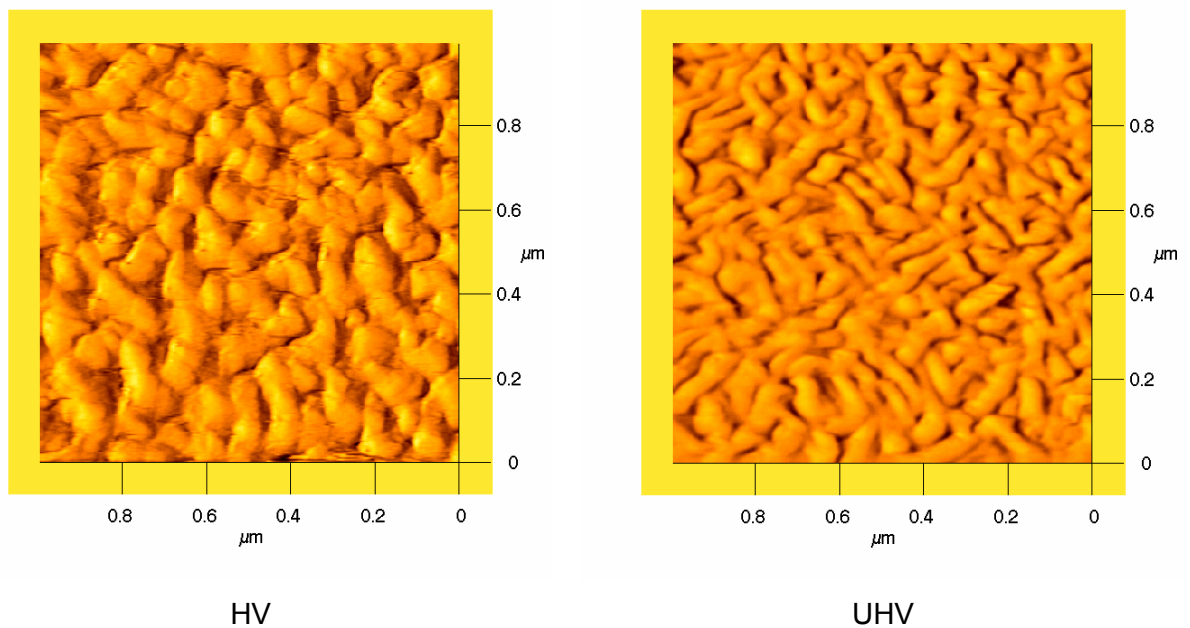
Figure 6.2.2. AFM images of surface morphology for sample HV-1 prepared in HV (left), and
for sample UHV-1 prepared in UHV (right)

Figure 6.2.3 presents the experimental Ψ and Δ values and the anisotropic fit for the HV sample HV-1 and also for the UHV sample UHV-1 as they have almost the same nominal thickness. The corresponding dielectric functions are shown in figure 6.2.4 and 6.2.5. For the samples prepared in HV also an isotopic model was considered. In this case the MSE was 17.9 while using the anisotropic fit the MSE was lowered to 9. However, for the samples prepared in UHV the isotropic fit did not at all yield good agreement with the experimental data. Within the anisotropic fit all samples were coupled together giving a MSE value of 6.4. This indicates that the samples prepared in HV are only slightly anisotropic, while the films prepared in UHV have a more ordered structure with more pronounced anisotropic properties.

a)

b)

c)

d)
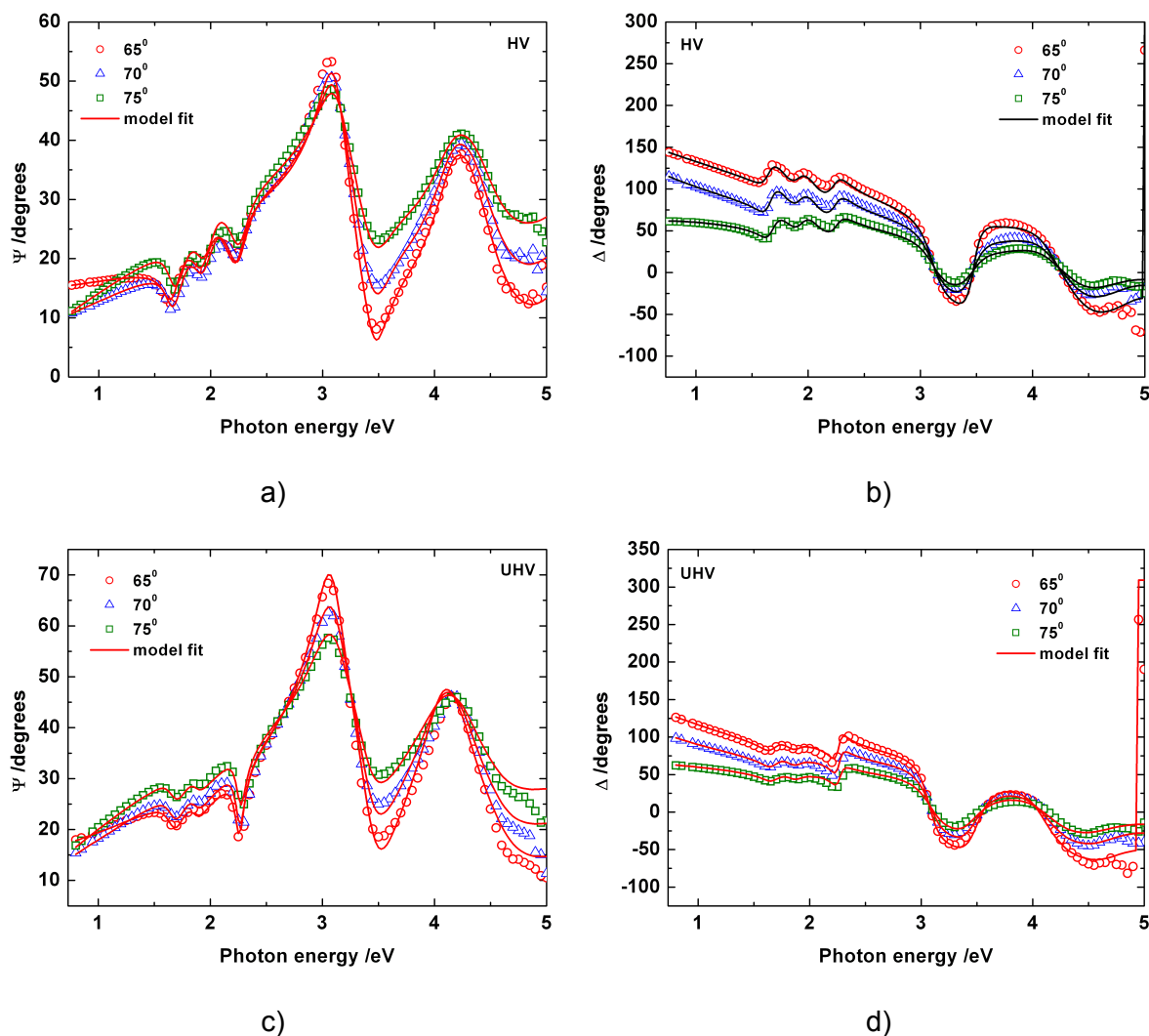
Figure 6.2.3. Ellipsometric Ψ and Δ spectra at different angles of incidence for CuPc samples on Si (111) substrate. Open symbols are the experimental points and continuous lines the fits. a and b - sample HV-1 prepared in HV; c and d - sample UHV-1 prepared in UHV
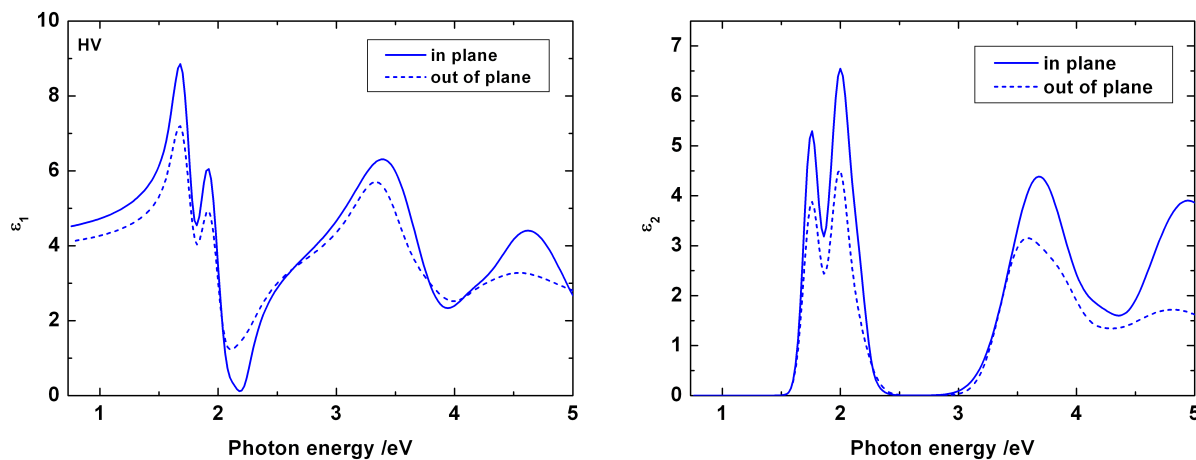
Figure 6.2.4. Anisotropic dielectric function for HV CuPc; left – real part; right – imaginary part.
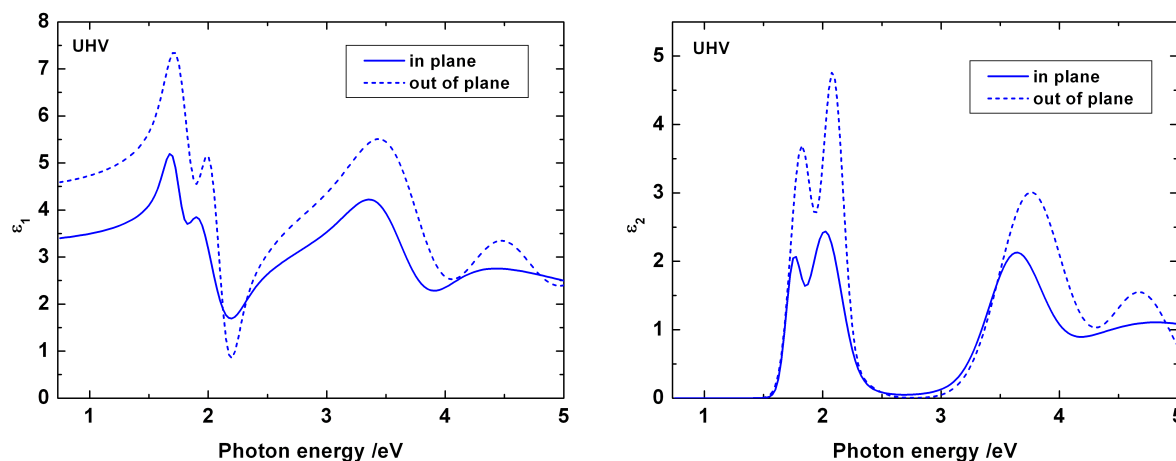
Figure 6.2.5. Anisotropic dielectric function for UHV CuPc; left – real part; right – imaginary part.

The shape of ε_2 is typical for CuPc and is in agreement with previous works [EiN01, Dju02, Yiq03, Bor04]. The absorption band centred at 2 eV with the characteristic splitting (Davidov splitting) for metal phthalocyanine is known as the Q band while the B band is centred around 3.6 eV [Lez96, Mck98]. Similar to H_2Pc, both are π-π^* transitions and are polarised in the molecular plane. For a random molecular orientation the in-plane and out-of-plane component of the dielectric function should be equal. A similar result should be obtained if the CuPc molecules would have an average 45^0 tilt angle with respect to the substrate.

Considering the dipole approximation presented in the previous chapter, an estimate of the average orientation of the molecules with respect to the substrate can be obtained from the differences in the extinction coefficients between the xy and the z directions of the film. For the films prepared in HV the average molecular orientation with respect to the Si substrate is at $\sim 40^0$ while for the sample prepared in UHV the majority of the molecules are at $\sim 53^0$. The differences may be correlated with the markedly different pressure during growth. However, an influence of the purity of the source material cannot entirely be ruled out. Further study of molecular orientation for such anisotropic materials can be of practical interest as the structural order can improve e.g. the charge transport in OFETs and solar cells.

6.3. $F_{16}PcVO$

The properties of the phthalocyanines can be tuned by the choice of the central metal ion and by chemical substitutions at the ligand as presented in chapter 4.1. A special class of Pc, with high electrical conductivity are the perfluorinated phthalocynanies [Sch00a, Sch00b].

Similar to H_2Pc and CuPc, the perfluorinated vanadyl phthalocyanine ($F_{16}PcVO$) exhibits an anisotropic growth mode. Therefore the aim of this chapter is to present the anisotropic optical properties of $F_{16}PcVO$ function of the type of the substrate.

Organic thin films of perfluorinated vanadyl phthalocyanine ($F_{16}PcVO$) were prepared by Dr. Michaelis at University of Oldenburg (Germany) as described in the chapter 4.4. During the deposition the substrate temperature was kept constant at ~42 C for KBr crystals, and at ~85 C for fused silica.

Absorption spectra in the UV-vis (ultraviolet, visible) region were recorded using a double beam spectrometer Specord M 40. In order to determine the film thicknesses and the wavelength dependence of the optical constants ellipsometric spectra were recorded at different angles of incidence (50°, 60°, 70°) in the range of 0.73 eV - 4.5 eV with a 0.02 eV step for each sample. Prior to the ellipsometric measurement all substrates were back roughened in order to avoid back side reflections. Bare substrates were also measured and their optical constants were determined in the same spectral range.

6.3.1. UV-Vis absorption

The phthalocyanines are usually characterized by an intense absorption band in the visible range (Q - band) and another broad absorption band in the near ultraviolet range (B-band) [McK98]. Both bands correspond to π-π* transitions. In figure 6.3.1 the absorption spectra of the $F_{16}PcVO$ films on fused silica and KBr substrates are presented. Additionally the fused silica glass absorption spectrum is plotted. The shape of the B-band for the $F_{16}PcVO$ films on fused silica cannot be very well distinguished as the fused silica glass starts to absorb at ~450 nm. The KBr crystal is absorption free in this range. In the case of an isolated molecule the absorption band at lower energy - Q-band - corresponds to HOMO-LUMO transitions while the broad band of the film can be explained by strong excitonic interactions. Clear differences of the $F_{16}PcVO$ spectra can be observed for different substrates. For the KBr substrate the spectrum is dominated by a strong absorption peak near 1.65 eV (750 nm) while for the fused silica substrate the band centered at about 1.9 eV (650 nm) is the strongest. According to Schlettwein *et al.* [Sch00a] the shape of the Q-band of the $F_{16}PcVO$ on KBr can be explained by a head-to-tail arrangement of the chromophores, while the $F_{16}PcVO$ film on fused silica has a cofacial (face-to-face) arrangement of the molecules.

Considering the model presented before for H_2Pc in the section 6.1 an average orientation of the molecules with respect to the substrate could be obtained from the differences in the absorption intensities for the two different substrates [Sch00a]. The $F_{16}PcVO$ molecules are thus lying on the KBr substrates while for the fused silica substrate the molecules are predominantly vertical to the surface.
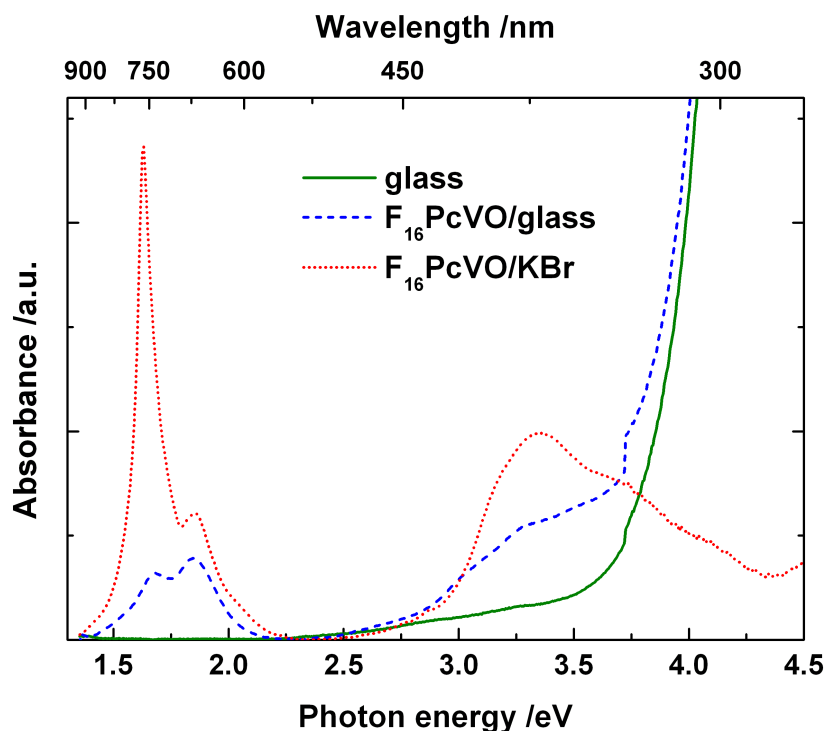
Figure 6.3.1. UV-vis absorption spectra of F_{16}PcVO on fused silica and on KBr substrates. Continuous line – absorption spectrum of fused silica. The KBr crystal is absorption free in this range.

6.3.2. Fused silica substrates

Ellipsometric data evaluation was performed as described in the previous chapters for H_2Pc and CuPc [Gor04a, Gor04b]. Due to the presence of the fluor atoms, IR spectroscopy was not able to reveal extra information about the film anisotropy. Therefore both isotropic and uniaxial anisotropic models were taken into consideration. The film thicknesses for two sets of samples were determined in the absorption free range (below 1.1 eV) as presented in table 6.3.1 for the fused silica substrates.

Table 6.3.1. Thickness and surface roughness for the F_{16}PcVO films on fused silica substrates determined from ellipsometry using isotropic and uniaxial model.

Model	MSE	Sample 1 F_{16}PcVO/fused silica		Sample 2 F_{16}PcVO/fused silica	
		Film thickness/nm	Surface roughness/nm	Film thickness/nm	Surface roughness/nm
isotropic	1.4	81.9±6.0	6.3±1.0	24.1±1.3	0+0.3
anisotropic	1.0	82.0±3.0	19.4±1.8	25.4±0.9	11.6±0.6

Figure 6.3.2 presents the ellipsometric spectra Ψ, Δ and the fit applying the anisotropic model with a MSE=3.9. The isotropic fit does not yield such a good result –

MSE=16.2. Due to the fact that the anisotropic model has more floating parameters during the fit than the isotropic one, a lower MSE value for the first one is expected. Therefore the value of the MSE itself cannot be used to judge which model is the more physically appropriate. However, a comparison of the extinction coefficients -k- obtained from the uniaxial model respectively from the isotropic model with that calculated from the absorption spectrum supports the appropriateness of the anisotropic model, as can be seen in figure 6.3.3. The extinction coefficient was calculated from transmission spectra of the film T_{film} and the bare substrate $T_{substrate}$ as follows:

$$k_{UV-vis} = \frac{-\ln(T_{film} / T_{substrate})}{2\pi\nu d} \qquad (6.3.2.1)$$

where ν is the wavenumber, and d is the total film thickness. The total film thickness is the film thickness calculated from ellipsometry plus the surface roughness divided by 2. Since the absorption measurement was performed in normal transmission the extinction coefficient calculated can be compared only with the in-plane component of the uniaxial model.

The extinction coefficient values from the anisotropic model is in very good agreement with that calculated from UV-vis for the Q-band, whereas the one calculated from the isotropic model is shifted considerably. Also the shoulder of the Q-band is not well resolved, even though the same number of oscillators was used as for the anisotropic model. The anisotropic optical constants for $F_{16}PcVO$ on fused silica are presented in figure 6.3.4. Since the $F_{16}PcVO$ molecule has an intrinsic optical anisotropy due to its structure, the anisotropy of the film can be explained with a preferential orientation of the molecules with respect to the substrate. Taking into account that the transition dipole lies in the molecular plane an average tilt angle of the molecules of 56^0 with respect to the substrate was calculated from the differences between in-plane and out-of-plane absorption.
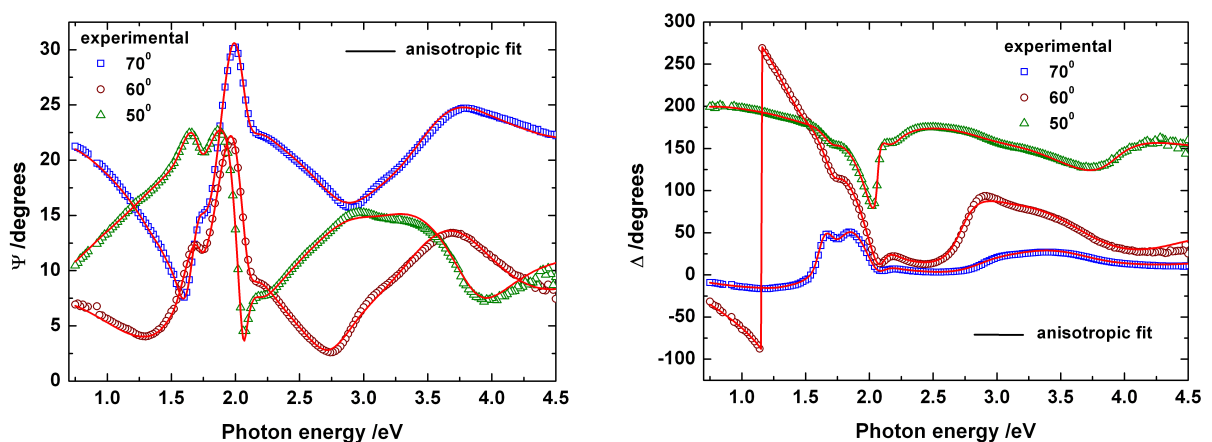
Figure 6.3.2. Ellipsometric Ψ and Δ spectra at different angles of incidence for the 82 nm $F_{16}PcVO$ film on fused silica. Open symbols are the experimental points and continuous lines the fits.
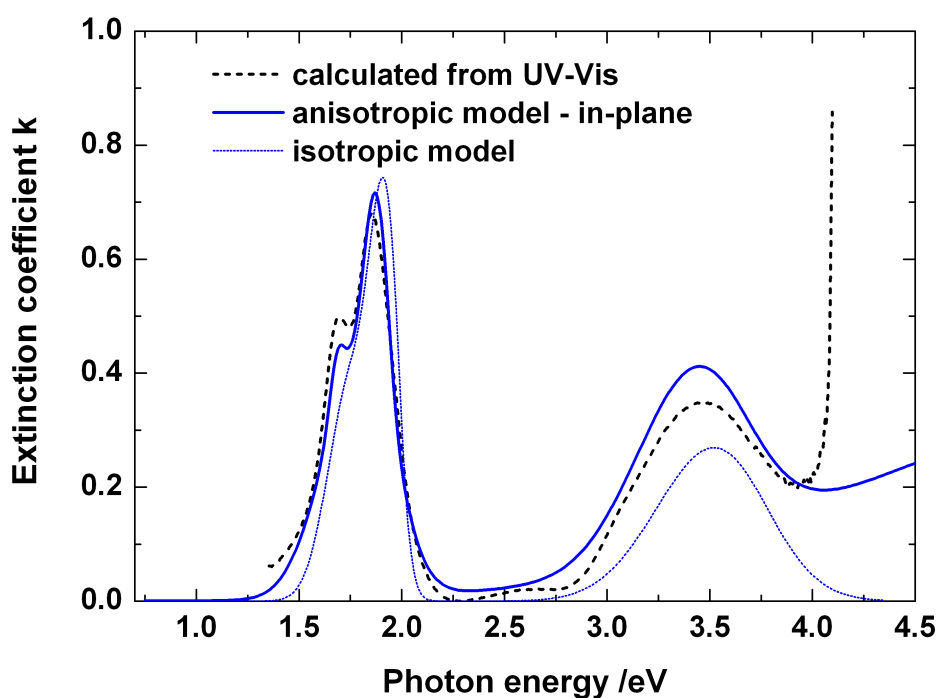
Figure 6.3.3. Extinction coefficient k for the $F_{16}PcVO$ film on fused silica.
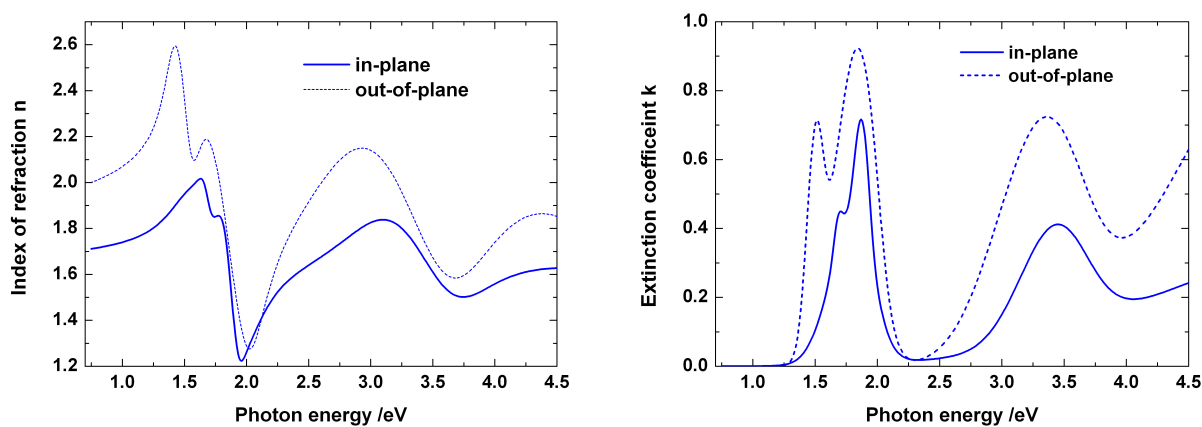
Figure 6.3.4. Anisotropic optical constants for $F_{16}PcVO$ film on fused silica. Left – real refractive index, right – extinction coefficient. Continuous line represents in-plane components, dashed line out-of-plane components.

6.3.3. KBr substrates

In the case of KBr substrates the difference between the $F_{16}PcVO$ film thicknesses determined with isotropic and anisotropic models is bigger than in the case of the glass substrates. The values determined are presented in table 6.3.2. The difference in thickness is related to the difference in the A value from Cauchy formula (5.1.2.2) calculated for isotropic and anisotropic models. This is consistent with a strong in-plane-/out-of-plane

anisotropy for F_{16}PcVO on KBr substrates, while the anisotropy is not so strong for films on fused silica substrates.

Table 6.3.2. Thickness and surface roughness for the F_{16}PcVO films on KBr substrates determined from ellipsometry using isotropic and uniaxial model.

Model	MSE	Sample 3 F_{16}PcVO/KBr	Sample 4 F_{16}PcVO/KBr
		Film thickness /nm	Film thickness /nm
isotropic	1.1	62.6±0.4	21.6±0.1
anisotropic	1.0	76.5±5.8	27.0±0.1

The films on KBr substrates were found to have optical constants varying with thickness. This is most likely related to the growth mode which involves initial island growth. Apparently very thin films have a smaller average density compared to thicker films. This also prohibits the application of the multi-sample analysis. The thinner film was fitted successfully with the isotropic model (MSE=2). Our efforts were, however, concentrated on simulating the optical constants for the thicker film (see table 6.3.2). For this 76.5 nm thick film the isotropic fit yields a large MSE value of 22 while the MSE was lowered to 2 using an anisotropic fit. The ellipsometric spectra Ψ, Δ and the fit applying the anisotropic model are presented in figure 6.3.5. The in-plane values for the extinction coefficient from this model together with the ones from the isotropic model and the one calculated from transmission are plotted in figure 6.3.6. The minor differences between the anisotropic model and transmission can be due to the presence of multiple cleavage planes in the KBr substrates. In order to model the ellipsometric data in a three phase model (ambient-film-substrate) sharp interfaces between these media have to be assumed. If the substrate is rough or the interface between substrate and film is otherwise degraded, then the three phase model is inappropriate and more complex models have to be employed. It is, however, obvious from the comparison in figure 6.3.6 that the isotropic approach leads to stronger deviations from the extinction coefficient derived from absorption. The anisotropic optical constants for F_{16}PcVO on KBr are presented in figure 6.3.7. Since the out-of-plane absorption is very small the optical properties can be modelled with both small absorption and without absorption in the entire spectral range.

From the strong in-plane-/out-of-plane anisotropy the average orientation of the molecules can be calculated using the procedure described above. Neglecting out-of-plane absorption the molecules lie perfectly flat on the KBr substrate, while considering a very small absorption results in an average tilt angle of 3^0. This is in very good agreement with RHEED results obtained by Schlettwein *et al.* [Sch00a].
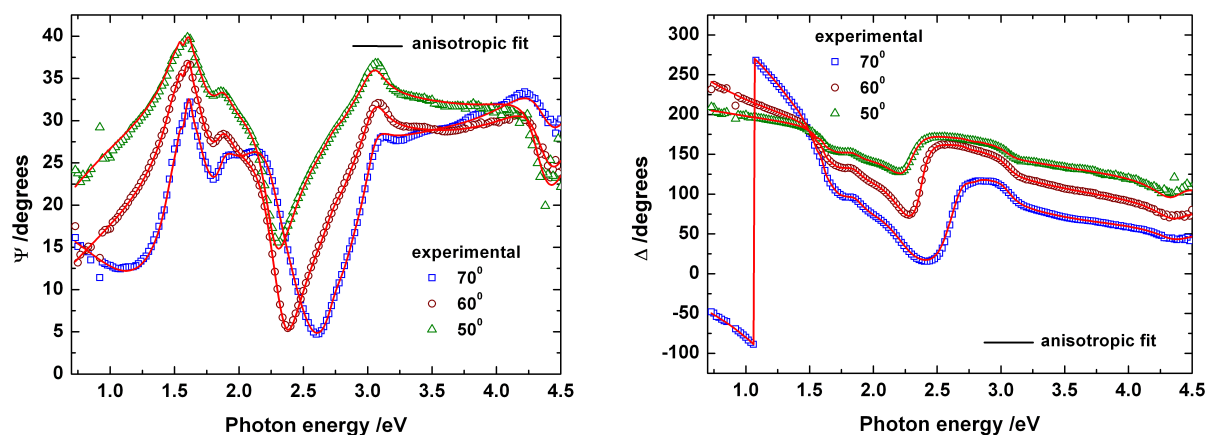
Figure 6.3.5. Ellipsometric Ψ and Δ spectra at different angles of incidence for the 63 nm F$_{16}$PcVO film on KBr substrate. Open symbols are the experimental points and continuous lines the fits.
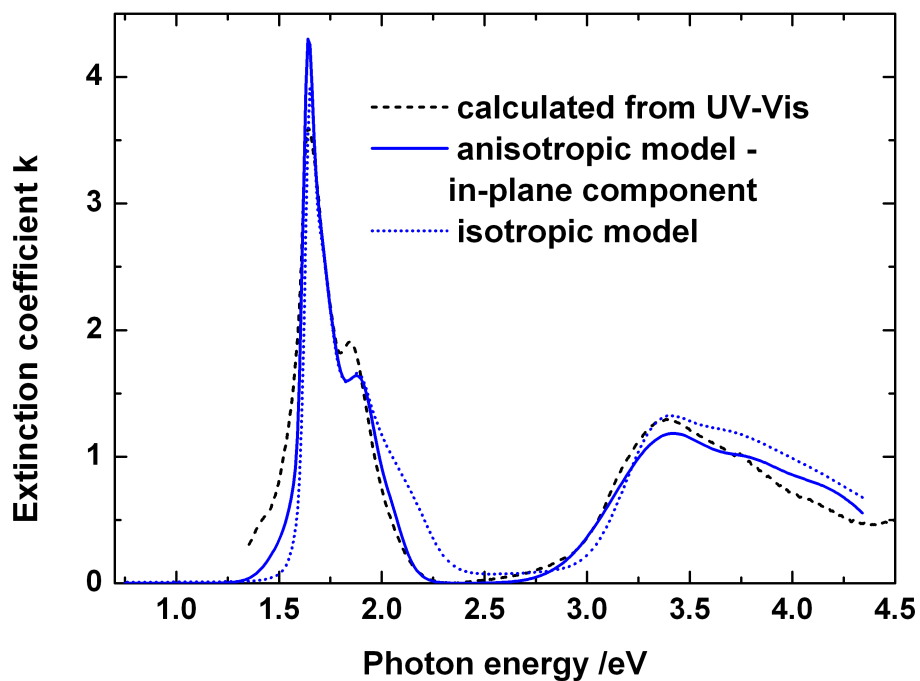
Figure 6.3.6. Extinction coefficient k for the F$_{16}$PcVO film on KBr substrates.
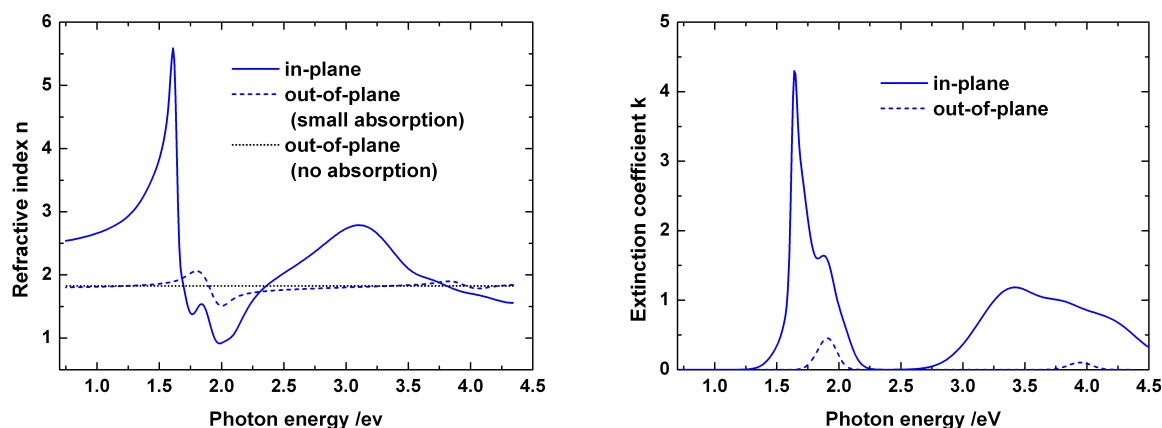
Figure 6.3.7. Anisotropic optical constants for $F_{16}PcVO$ film on KBr substrate. Right – real refractive index, left – extinction coefficient. Continuous line represent in-plane components, dashed line out-of-plane components. The out-of-plane real part, when no absorption is considered is also plotted.

6.4. Summary and Discussion

The studies presented in the previous chapters showed that the growth mode of the Pcs depend on the pressure conditions during deposition, temperature and type of the substrate used. While it is already known that a weak interaction of the Pcs molecules with the substrate will determine a growth mode with b-axis (stacking axis) parallel with the substrate, and a strong interaction will induce a growth mode with the b-axis perpendicular to the substrate [Lez96, McK98], we demonstrated for the first time that the molecular orientation, and therefore the growth mode, can be deduced from anisotropic models using ellipsometry measurements [Gor04a, Gor04b, Gor04c]. The determined anisotropic dielectric function could also be used to optimize the performances of the optoelectronic devices. However, estimating the physical errors of the ellipsometry models remains a difficult task, and many authors refer to the errors as confidence limits (numerical errors). Therefore this chapter will discuss the difference in the molecular orientation of the Pc in the organic films grown in HV and UHV and it will give a rough error estimation.

The standing configuration of the $F_{16}PcVO$ molecules on glass, in comparison with the lying configuration on KBr substrates can be explained by the strong interaction of the $F_{16}PcVO$ molecules with the ionic KBr crystal which induces an epitaxial growth. This was demonstrated by RHEED results obtained by Schlettwein *et al.* [Sch00a]. In a similar way the changes in the Pc molecular orientation on H-Si(111) substrates between UHV and HV samples can be explained by a change in the silicon surface properties due to the impurities for the HV case. The impurities, mainly water, change

the sticking coefficient of the H-Si(111) substrate and therefore the wetting behaviour of the Pc molecules.
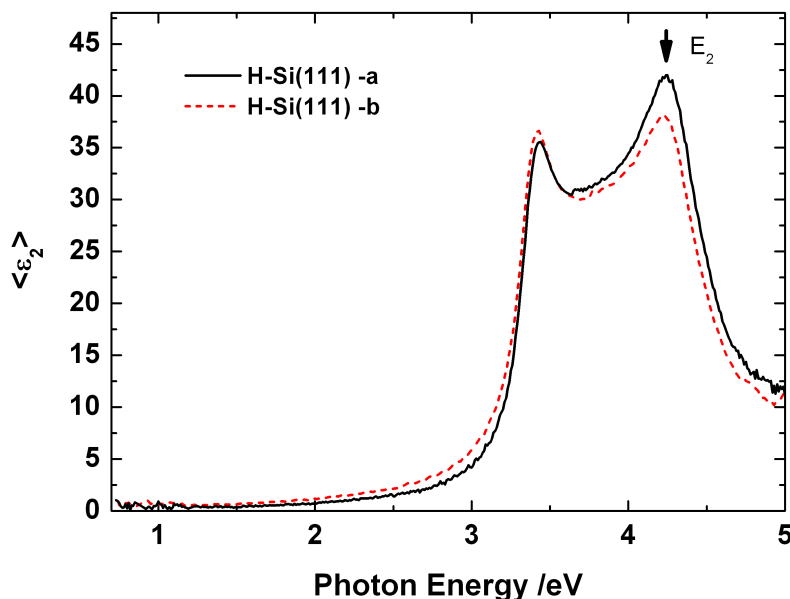
Figure 6.4.1. Continuous line (a) - the imaginary part of the effective dielectric function of a clean H-Si(111) substrate and dashed line (b) - the imaginary part of the effective dielectric function of a H-Si(111) substrate after 6 h in the HV chamber. The decrease of the E_2 features indicate the presence of adsorbates on the H-Si(111) surface.

Figure 6.4.1 shows the effect of the H-Si(111) surface modification on the imaginary part of the effective dielectric function. The measurements were performed *in situ* at a fixed angle of incidence (70°) in a HV chamber ($5.3 \cdot 10^{-7}$ mbar). The continuous line shows the characteristic features for a freshly passivated Si(111). The measurement is identical with the *ex situ* characteristic of H-Si(111) immediately after passivation. The dashed lines shows the imaginary part of the effective dielectric function for a H-Si(111) after several hours in the HV chamber. The decrease of the E_2 feature clearly indicates the presence of an adsorbate layer on the silicon surface [Ros96]. As the HV chamber was not baked prior to the experiment, probably the majority of the impurities are water molecules. A similar decrease in the E_2 peak can be observed for H-Si(111) exposed to the atmosphere more than half hour after passivation.

On the two substrates, with the dielectric functions presented in the figure 6.4.1, zinc Phthalocyanine (ZnPc) was deposited. Figure 6.4.2 shows the imaginary part of the measured effective dielectric function at a fixed angle of incidence (70°) for different thicknesses of the ZnPc layer. The thicknesses were monitored using the equivalent frequency shift registered by a quartz microbalance.

a)   b)
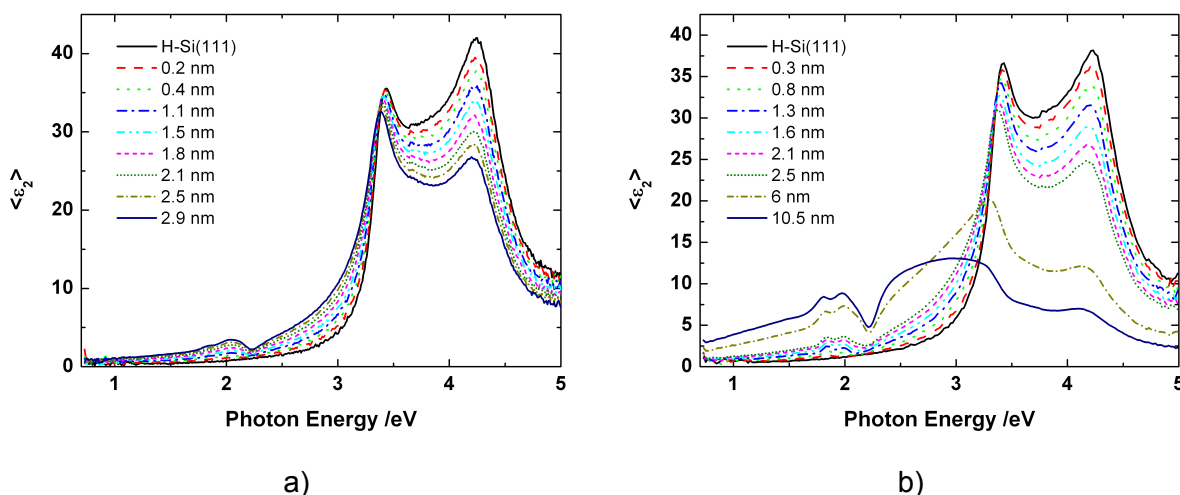
Figure 6.4.2. The changes in the imaginary part of the effective dielectric function with increased ZnPc thickness: a) on clean H-Si(111); b) on H-Si(111) with adsorbates

The thicknesses in figure 6.4.2 were calculated from the quartz microbalance shift, taking into account that a frequency shift of 12 Hz corresponds to a thickness equivalent of 1 nm. As the measured effective dielectric function contains information about the whole system – substrate plus film, a direct interpretation is not all the time obvious (see chapter 3.2). However, in this case the strong decrease of the silicon E_2 features indicates the increasing thickness of the organic layer, and the features that appear around 2 eV, where the $<\varepsilon_2>$ of the silicon is featureless, clearly belong to the Q-band of the phthalocyanine.

A zoom of this region is presented in figure 6.4.3. As can be seen in this figure the shape of the Q-band for the ZnPc layer grown on clean substrate has a markedly different shapes and evolution from the ZnPc layer grown on the H-Si(111) with the surface modified by the adsorbates.

a)   b)
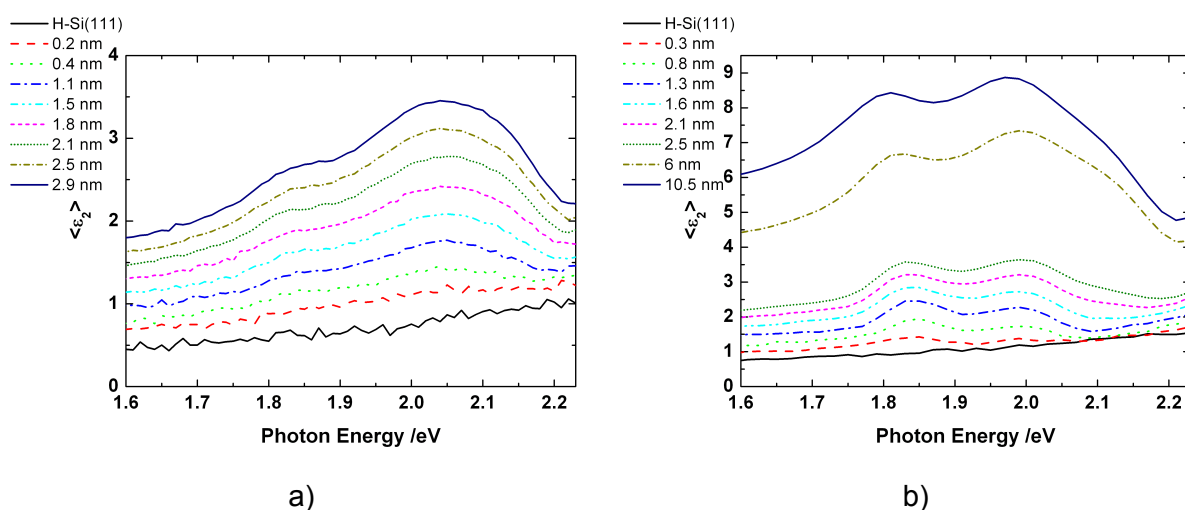
Figure 6.4.3. The changes in the imaginary part of the effective dielectric function with increasing ZnPc thickness: a) on clean H-Si(111); b) on H-Si(111) with adsorbates. Zoom of the Q-band region.

The differences in shape and spectral position of the ZnPc Q-band presented in figure 6.4.3 clearly indicate that the molecules on the clean substrate have a different packing compared with the ZnPc film deposited on the substrate with impurities adsorbates. A more detailed comparison showed that the relative area of the Q-band for the same thickness is bigger for the ZnPc grown on the H-Si(111) with the modified surface. This indicates that the molecules lie flat on the substrate, while the ZnPc molecules grown on clean H-Si(111) do not interact with the passivated surface which will lead to a standing configuration typical for the α-phase with the b axis parallel with the substrate. As in both cases the substrates were at room temperature during the deposition the packing will slowly relax with the increasing film thickness towards the α crystal structure.

The *in situ* experiment proved that the different orientation of the Pc molecules grown in HV on silicon substrates is due to the presence of impurities. This will lead to stronger interactions between the molecules and the substrate, inducing a strained structure which subsequently relaxes to the α structure with the b axis perpendicular to the substrate surface. As the growth mode of the Pc is dependent on the impurities present in the HV chamber and therefore on the time that the substrate remains in the chamber before deposition, in order to have high quality and reproducible films UHV conditions are better suited for Pc sample preparation. While for some potential application *e.g.* solar cells the growth mode of the Pc with the b-axis perpendicular to the substrate is of practical interest, the molecular orientation can be controlled using a PTCDA layer as template as it will be presented in the next chapter.

Estimating the errors in ellipsometric modelling remains difficult, as besides the numerical errors of the fitting procedure, the errors introduced by the simple physical approximations have to be considered. Even the error bars from thickness determination have to be regarded as numerical confidence limits. The error bars of a numerical fitting depend on the shape of the minimum of the minimized function and on the exit condition from the iterative loop. For example a sharp minimum will lead to small error bars as a small change in the parameters of the minimized function will induce a strong deviation from the minimum. In contrast a shallow minimum will lead to larger error bars. In the simple thickness determination using the Cauchy model, the layer is considered to be homogenous. However, the molecular orientation and packing may change with thickness as presented before for ZnPc. In this case an error in thickness determination will appear due to this simple approximation and it is difficult to know if this error falls within the numerical error of the fit. However, due to the fact that the relaxation occurs rather fast, this error will be significant for films thinner than 10 nm. Knowing the precise changes in the structure from complementary techniques or by doing *in situ* ellipsometry measurements more complex models which consider a gradient in the refractive index of the film should be considered.

The errors of the determined molecular orientation from ellipsometry data have two sources – a numerical one as the ellipsometry measurements have a reduced sensitivity for the out-of-plane component and a physical one due to the simple dipole approximation. Understanding from the complex ellipsometry equations why the ellipsometric measurement is less sensitive to the out-of-plane component is difficult, and a simplified view can be found in chapter 3.3. However, this is performed in the first order approximation considering the anisotropic case like a small perturbation from the isotropic one. Figure 6.4.4 shows the experimental spectra for a 42 nm H_2Pc film on glass substrate and the uniaxial model simulation using the dielectric function presented in the figure 6.1.9.
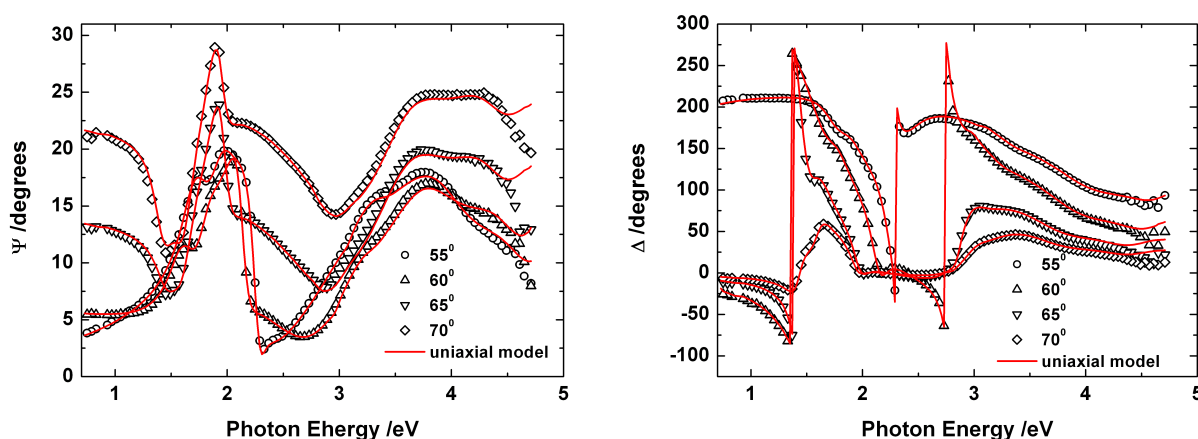
Figure 6.4.4. Open symbols - the experimental ellipsometric spectra of a 42 nm H_2Pc film on glass substrate and the uniaxial model fit in continuous line.

As presented in chapter 6.1.2 transmission data (figure 6.1.8) can be simulated using the in-plane component of the dielectric function. Considering the film as isotropic with the dielectric function the same in all direction and equal with the in-plane one presented in figure 6.1.9 an isotropic simulation can be performed. The result of the simulation is presented in figure 6.4.5.
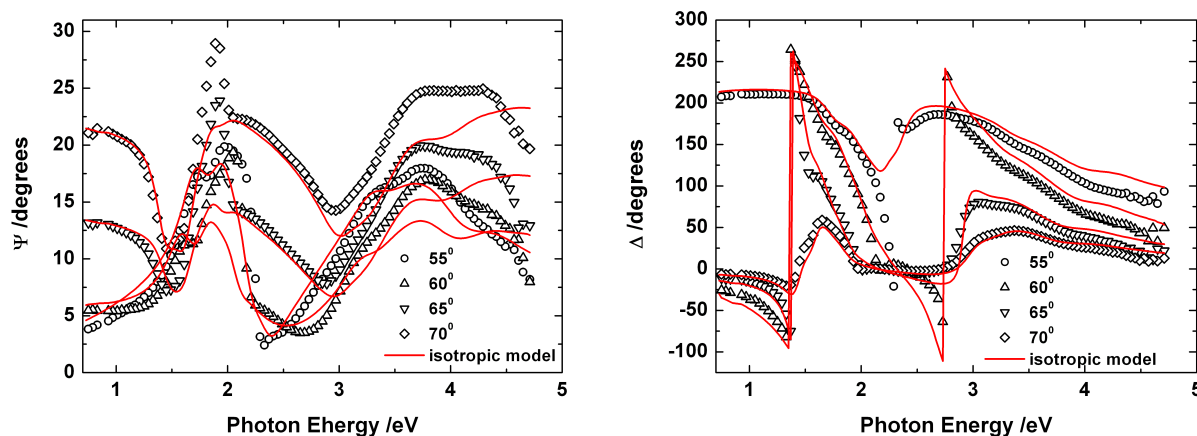
Figure 6.4.5. Open symbols - the experimental ellipsometric spectra of a 42 nm H_2Pc film on glass substrate and the isotropic model fit in continuous line.

Especially in the spectral region where the film has strong absorptions of the Q and B bands deviations between the experimental data and the isotropic model simulation can be noticed. In contrast to the uniaxial model (figure 6.4.4) the isotropic one fails to describe accurately the experimental data. As can be seen comparing these two figures, from the variation of the simulated isotropic and anisotropic spectra the sensitivity to the out-of-plane component of the dielectric function is smaller than to the in-plane one and therefore the shape of the out-of-plane component can have slightly different shapes for the same qualitative simulation. However, a careful evaluation of the different solution for the out-of-plane shape show that the relative area does not change so much and therefore a maximum error in the molecular orientation of ±4° was deduced for the simple dipole approximation.

More difficult to evaluate is the physical error introduced by the dipole approximation. While for single Pc or PTCDA molecules the HOMO-LUMO transition have the dipoles in the molecular plane, in molecular crystals polarization effects and charge transfer transitions (CT) should be taken into account. The optical properties of organic molecular crystals are commonly described in the frame of Frenkel exciton theory [Sil94]. The most basic small radius exciton theory considers only Frenkel excitons, i.e. crystal states are described as superpositions of neutral molecular states [Hof03]. That means, all states in which electrons would be transferred from one molecule to another one are excluded, and the exciton radius defined as the mean separation between the excited electron and the remaining hole is necessarily smaller than one lattice constant. Frenkel exciton theory is now a standard tool described in many reviews and monographs (e.g. [Cra68, Dav71, Agr82]). It was extensively applied in the third quarter of the 20th century to describe optical properties of naphthalene and anthracene crystals [Sil94]. In this case when the pair electron-hole is located on the molecule and taking into account the long wavelength of the optical range, multipole contributions can be neglected. However, besides the intramolecular electronic transitions, in

the organic molecular crystal CT-transitions take place, which correspond to optical electron transfer to the nearest neighbouring molecule. Using electroabsorption spectroscopy which makes it possible to determine the nature of optical excitation (intramolecular excitation or CT transition) it was shown that in the case of anthracene the CT transitions lies between 8% and 3% of the total absorption [Sil94]. Similar studies were performed on CuPc films by Blinov *et al*. [Bli70, Bli72]. While the authors revealed the presence of CT-transitions using the electroabsorption spectroscopy they mention that the Pc crystal has a very pronounced excitonic spectrum (Frenkel) and the CT-transitions are not visible in the wide background of the absorption spectrum. Therefore due to the small intensity of the CT-transitions the error introduced in determining the orientation angle should be small. However, a precise calculation of this error cannot be done without a theoretical computation of the oscillator strength for the transitions which have the dipole moment perpendicular to the molecular plane. Such calculations are at present underway in the Chemnitz Theoretical Physics Department for PTCDA crystals.

7. Molecular Interaction in Heterostructures

For many practical applications the organic materials are used in different combinations in complex heterostructures. Unlike bulk materials low dimensional multilayered structures exhibit unusual optical and physical properties. In recent years organic semiconductors were used as active layers in devices, and they proved to be a viable alternative for light emitting diodes (OLEDs), solar cells, photodetectors and gas sensors [Cha86, Lez96, Yon96, Bao00, Hoh00]. Compared to simple heterostructures, multilayered OLED structures showed increased light emission efficiency [Hai98]. However, the intermolecular interaction at the interface is less studied and understood.

Therefore the aim of this chapter is to present the investigations of interface effects in multilayered organic structures by means of spectroscopic ellipsometry. Among novel research subjects for improving photovoltaic cell efficiencies, such as the development of low band-gap materials and device structures, especially controlling the molecular orientation has a great potential for improving the electrical and optical properties of organic films due to the anisotropic molecular orbitals which contribute to carrier transport and visible light absorption [Pop99]. Nevertheless, only few attempts to control the molecular orientation have been made for the application of photovoltaic cells because most organic semiconductors are difficult to be controlled in their molecular orientation on substrate surfaces of glass and metal oxides due to a weak adsorbate-substrate interaction [Tok95, Lez96, McK98].

It was recently reported that 3,4,9,10-perylene tetracarboxylic dianhydride (PTCDA) template layers can control the stacking direction of H_2Pc and phthalocyanine derivative films parallel to the surface of a glass substrate [Heu00,Sak05]. Such a molecular templating technique is one of the easiest methods for fabricating device structures. Moreover, the orientation of the H_2Pc molecular plane formed on PTCDA is beneficial for photovoltaic cell applications because the stacking direction of the π orbitals predominantly contributes to carrier transport and optical absorption [Pop99]. However, there is no report in literature on the optical properties of orientation controlled molecular films deduced from an anisotropic model. The first part of this chapter will present the dielectric function for H_2Pc films formed on PTCDA over the wide spectral range (0.73 – 5 eV) obtained from the simulation of ellipsometry spectra using anisotropic model approaches [Gor06a].

In the second part two different material system types were chosen as representative for a compared investigation. The first one is composed of planar molecules PTCDA and CuPc which leads to anisotropic layers [Gor05a, Gor06b], while the second is composed of more complex molecules like α-NPD and Alq_3 which form isotropic layers [Him05, Her05]. The crystalline growth of CuPc and PTCDA results in anisotropic layers with a relative high surface roughness while the planar structure of the molecules leads to a high degree of

overlap of the π orbitals. As the optical properties of these materials are attributed to π-π^* transitions [McK98] the molecular interaction at the interfaces will affect the optical properties of the multilayer. In contrast α-NPD and Alq$_3$ form isotropic layers with low surface roughness providing sharp interfaces.

7.1. Ellipsometric Study of an Organic Template Effect: H$_2$Pc/PTCDA

After the first report using X-ray studies of the template effect of PTCDA on H$_2$Pc [Heu00], the effect was explained by theoretical calculation of the van der Waals energy interaction [Yim03]. According to Yim *et al.* the growth of H$_2$Pc molecules with the molecular plane parallel to the one of PTCDA is indeed a more stable configuration from the energetic point of view, as presented in figure 7.1.1.[Yim03]
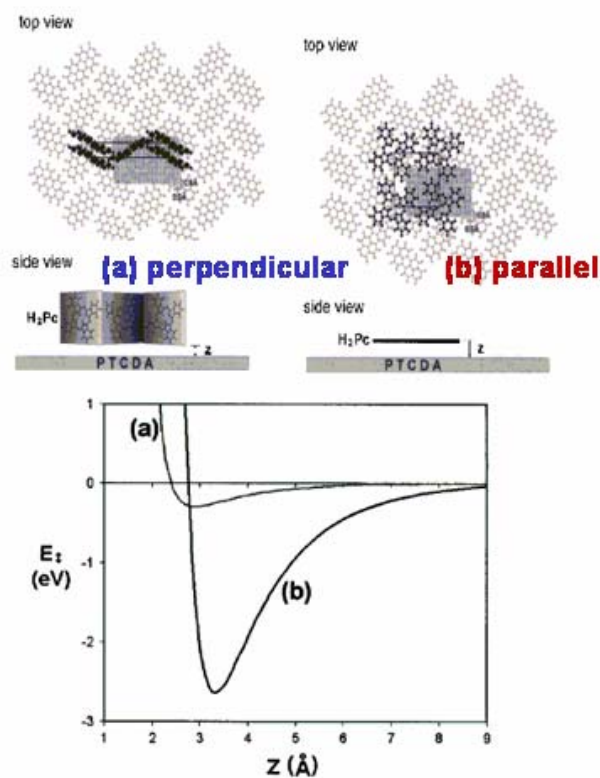
Figure 7.1.1. Molecular arrangement and intermolecular interaction energy curves between the PTCDA layer and a) the α-herringbone H$_2$Pc unit cell and with the staking axis parallel to the PTCDA molecular planes; b) the planar layered H$_2$Pc unit cell as a function of the stacking distance z. [Yim03]

While X-ray studies probe the periodicity of the crystal structure in a direction parallel or perpendicular to the substrate plane, the ellipsometry can also reveal the crystal structure from the shape of the Pc Q-band and the molecular orientation from the anisotropy. Especially for optoelectronic applications like organic solar cells, knowing the complex dielectric function (or optical constants) is thus very important.

PTCDA samples and H_2Pc/PCTDA were prepared by Dr. Sakurai as described in chapter 4.4. In order to simulate the optical response of the heterostructures the dielectric function of the PTCDA layer has to be determined. A similar coupled analysis, like the one described in the section 6.1.2 was performed for PTCDA layers grown on glass and silicon oxide/silicon substrates. The thicknesses and the numerical confidence limits of the PTCDA layers deduced from the ellipsometric data evaluation are presented in table 7.1.1.

Table 7.1.1. The thicknesses of the PTCDA layers from the ellipsometric evaluation

Substrate	Material	Thickness /nm
Glass	PTCDA	10.5 ± 1.6
		2.0 ± 0.4
SiO_2/Si	PTCDA	10 ± 1
		0.5 ± 0.4

Figure 7.1.2 shows the anisotropic dielectric function of PTCDA. In figure 7.1.3 the experimental transmittance spectra of PTCDA on glass and the corresponding model simulation are presented. The difference in the imaginary part of the dielectric function between the in-plane component and the out-of-plane one indicates that the molecules lie flat on these substrates [Sak05, Gor06a]. The shape of the in-plane dielectric function is in agreement with previous reports [Fri02, Gor05b].
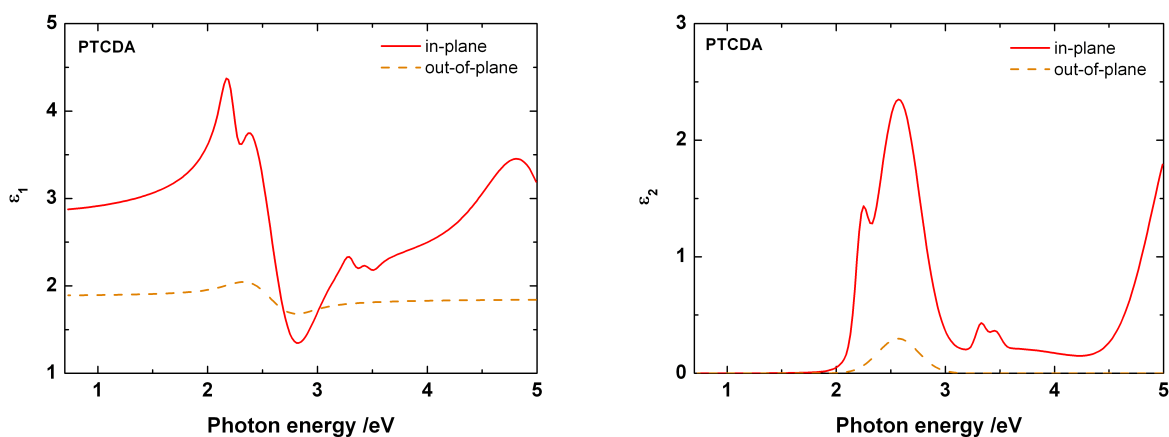
Figure 7.1.2. The complex dielectric function of the PTCDA films deposited on glass and SiO_2/Si substrates.
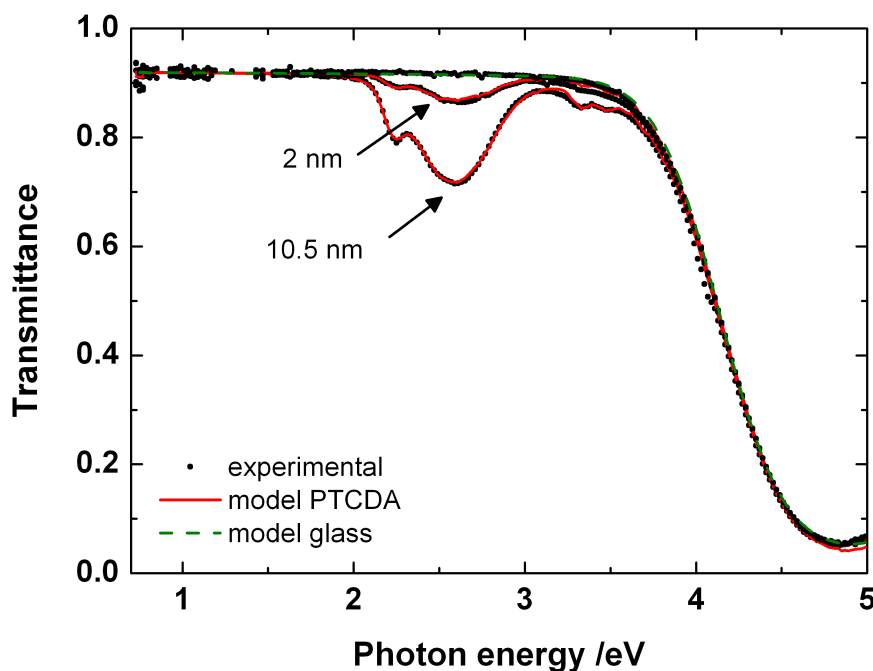
Figure 7.1.3. Transmittance spectra of PTCDA layers on glass substrates. For comparison the transmittance of the glass substrate is also plotted. The continuous lines represent the model simulation of the transmittance using the in-plane component of the dielectric function.

In the ellipsometric data evaluation of the H_2Pc/PTCDA /substrate heterostructures, the previously determined dielectric function was used for the PTCDA layer. The thicknesses of the PTCDA layers beneath H_2Pc were estimated from transmission measurements, in the range where PTCDA has its strong absorption feature and H_2Pc has a very low absorption. With the PTCDA thickness fixed, the previously described ellipsometric procedure (section 6.1.2) was applied to find the H_2Pc thickness. Compared to H_2Pc single layers a good data simulation was obtained only if surface roughness was considered in the model. Table 7.1.2 summarizes the values obtained. While for the first set of samples the thicknesses and the surface roughness of the H_2Pc layers were determined in the transparent range as described in chapter 6.1.2, for the rest of the samples the determined optical constants were used to calculate the thickness. As in the first case both the thickness and the parameters of the Cauchy dispersion relation are fitted at once, the values of the confidence limits are like presented in table 7.1.2. In the second case when only the thicknesses of the layers were floating parameter during the numerical fit, the values of the confidence limits were less than 0.03 nm and they were not listed in table 7.1.2.

Figure 7.1.4 shows the anisotropic dielectric function of the H_2Pc layer deposited on PTCDA. As can be seen the in-plane component now is stronger than the out-of-plane one suggesting that the H_2Pc molecules have a considerably lower tilt angle with respect to the substrate. This is most likely due to the strong interaction of the PTCDA π orbitals with the π orbitals of the first monolayer of H_2Pc, which leads to a templating effect [Heu00, Sak05,

Sak06]. Applying the procedure described for the H_2Pc in the section 6.1.2, a ~25° average tilt angle was calculated for the molecular orientation. This value is very close to the 27° value deduced from IRRAS [Sak05] and in agreement with a crystalline growth of H_2Pc with the stacking axis perpendicular with the substrate surface.

Table 7.1.2. Thicknesses of individual layers in the H_2Pc/PTCDA/substrate heterostructures

Substrate	PTCDA Thickness /nm	H_2Pc	
		Thickness /nm	Surface roughness /nm
Glass	6.7 ± 0.4	20 ± 3.2	8 ± 2.2
	14.5 ± 0.4	16.6 ± 2.2	3.3 ± 1.9
	12 ± 0.4	5.6 ± 0.8	2.9 ± 0.6
SiO_2/Si	7.5	19.6	7.9
	13.3	16.5	2.5
	10.4	5.0	1.2
Glass	1.4	29.1	10.2
	0.4	11.6	7.5
	0.3 ?	7.6	6.2
SiO_2/Si	5.1	25.3	12.5
	5.9	9.5	8.3
	3.8	5.5	7.8
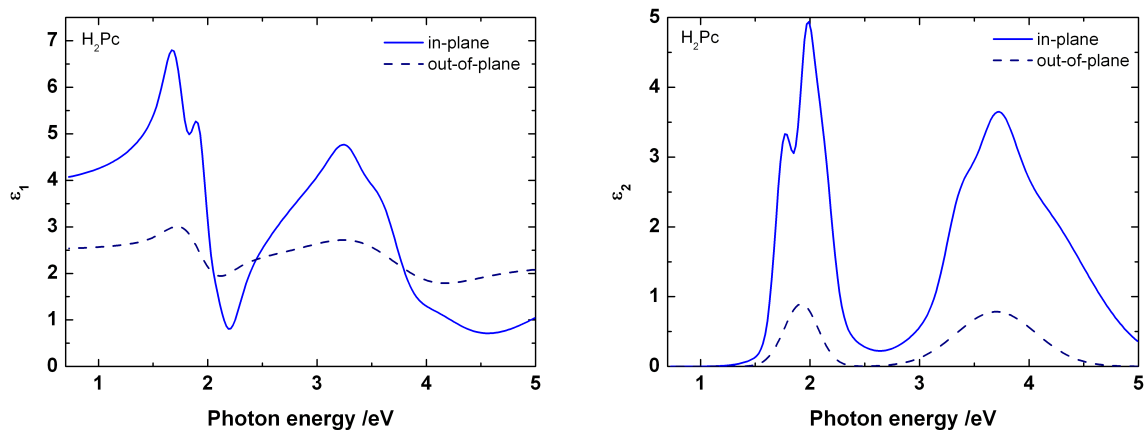
Figure 7.1.4. The complex dielectric function of the H_2Pc films deposited on PTCDA.
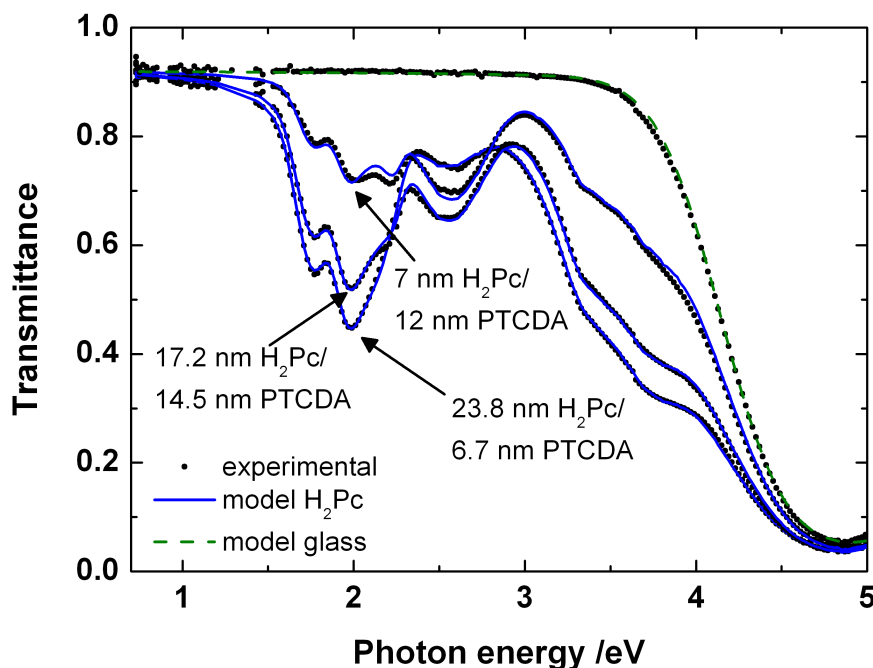
Figure 7.1.5. Transmittance spectra of H_2Pc layers on PTCDA/glass substrates with PTCDA thickness higher than 6 nm. For comparison the transmittance of the glass substrate is also plotted. The continuous lines represent the model simulation of the transmittance using the in-plane component of the dielectric function.
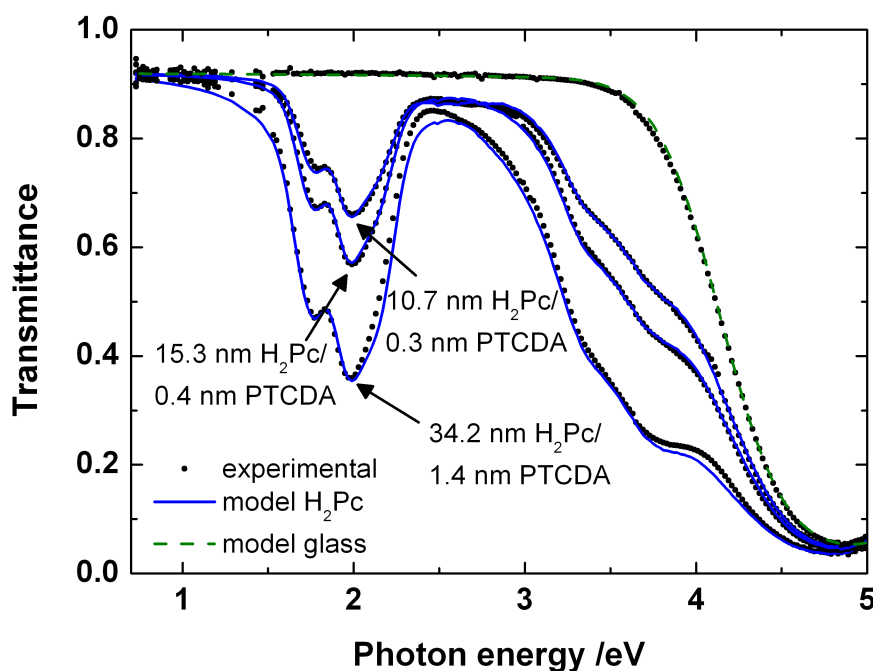
Figure 7.1.6. Transmittance spectra of H_2Pc layers on PTCDA/glass substrates with PTCDA thickness less than 2 nm. For comparison the transmittance of the glass substrate is also plotted. The continuous lines represent the model simulation of the transmittance using the in-plane component of the dielectric function.

Figure 7.1.5 shows the transmittance data of the H_2Pc films on PTCDA layers thicker than 6 nm and the model simulation. The total thickness of the H_2Pc layers is indicated. In ellipsometry the surface roughness is modelled using an effective medium approximation with 50% voids. The total thickness thus is calculated by adding the surface roughness divided by 2. As can be seen in figure 7.1.5 the model simulation matches perfectly for the thick H_2Pc layers, but a small deviation in the transmission data can be noticed for the 7 nm H_2Pc layer. This deviation was also observed in the ellipsometric spectra. This is an indication that the thin H_2Pc layer has a small deviation in the optical constants, when compared to thicker layers. The difference is probably due to a small difference in the molecular packing [Sak06], as the structure of the first H_2Pc monolayers has a deviation from the α-phase H_2Pc due to the templating effect of the PTCDA.

The same model was applied successfully to H_2Pc layers grown on PTCDA layers with thicknesses lower than 1.4 nm. This proves that even a very small thickness starting with a monolayer of PTCDA is sufficient to induce the template effect. Figure 7.1.6 shows the transmittance data for these layers grown on the glass substrate. Also in this case a small deviation from the experimental data was noticed for the 34 nm H_2Pc layer. As this layer is the thickest, it seems to support a small molecular reorientation with increasing thickness. However, for this layer a higher uncertainty in calculating the PTCDA layer thickness, probably less than 0.3 nm, was noticed due to the small value.

The data evaluation for the SiO_2/Si substrate was more difficult because it was hard to estimate the thickness of the PTCDA layer beneath H_2Pc. The previous determined dielectric functions of H_2Pc on PTCDA and of PTCDA on glass were used to determine the thickness. This evaluation gave a very good simulation of the ellipsometric spectra in the measured spectral range, indicating that the films on SiO_2/Si substrates have the same optical properties like the ones on glass substrates.

Figure 7.1.7 shows the imaginary part of the in-plane dielectric function for the H_2Pc layers grown on glass and SiO_2/Si substrates, compared with the one of the films grown on PTCDA. Besides the higher values for H_2Pc grown on PTCDA due to the lower tilt angle with respect to the substrate, which demonstrate the template effect induced by PTCDA, a splitting of the Q-band can be observed. The splitting is also visible in the transmission measurements. While the difference can be attributed to the observation of the optical properties of α-phase H_2Pc in different crystal direction, the splitting can also be a sign of a small deviation from the perfect H_2Pc α-phase crystal [Heu03, Sak06].
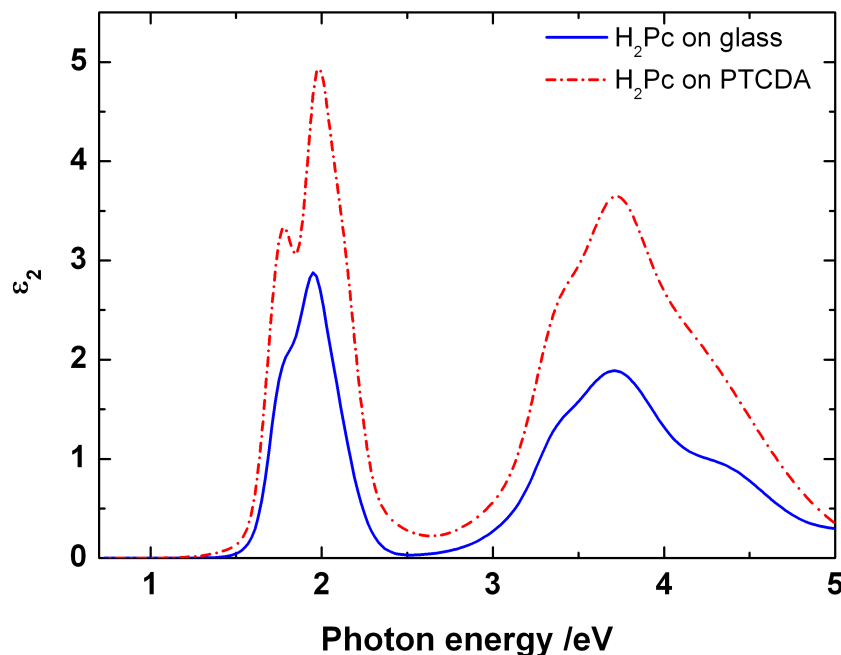
Figure 7.1.7. Comparison between the in-plane imaginary dielectric function of H_2Pc on glass and SiO_2/Si and the in-plane imaginary dielectric function of H_2Pc on PTCDA.

Using X-ray investigations [Sak05] and IRRAS [Sak05] Sakurai *et al.* proposed a model in which the first layers of H_2Pc lie on PTCDA and the structure will gradually relax towards the α-crystal structure. As in ellipsometry we see the average response of the whole structure this model could explain the changes in the refractive index with the thickness as well as the splitting of the Q-band. Also the observed molecular tilt angle of 25° would be smaller than the one in the crystal (26.5°) as it is averaged over the whole structure.
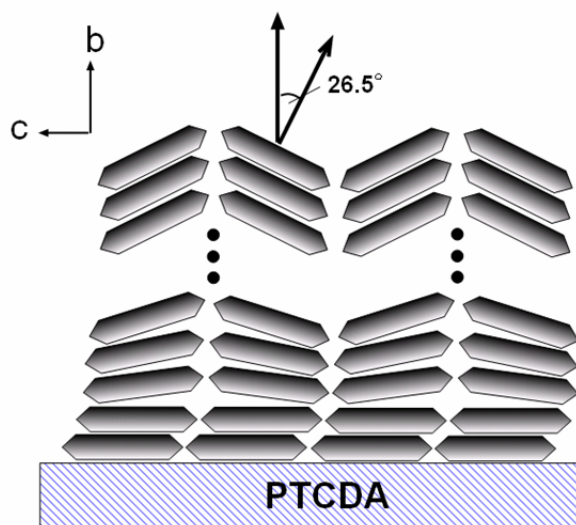
Figure 7.1.8. Schematic model of the H_2Pc growth on PTCDA

7.2. Comparative study of the interfaces in organic/organic multilayered heterostructures

In this second part of chapter 7 the investigation by means of spectroscopic ellipsometry of the interface effect in multilayered organic structures [Gor05a, Gor05b, Her05, Gor06b] will be presented on two different material systems – 1) α-NPD and Alq$_3$ which are known to give isotropic layers with low surface roughness [Him05], 2) PTCDA and CuPc which from anisotropic layers [Gor05a].

Organic multilayered heterostructures consisting of alternating layers of Alq$_3$/α-NPD and PTCDA/CuPc were prepared by OMBD in high vacuum (HV – $8 \cdot 10^{-7}$ mbar) on hydrogen passivated Si(111) (for preparation details see chapter 4.4). The substrates were kept at room temperature during the deposition. The deposition rate was kept constant at approximately 0.5 nm /minute for Alq$_3$ /α-NPD and at 0.3 nm /minute for PTCDA /CuPc. Using the same deposition conditions mixed layers Alq$_3$ /α-NPD and PTCDA /CuPc were prepared by codeposition.

7.2.1. Single layers

The ellipsometric data evaluation of the individual layers revealed that the optical response of Alq$_3$ and α-NPD can be simulated using isotropic models. The thickness was determined in the transparent range up to 2.5 eV. The dielectric functions of the layers were determined in a multi-sample analysis procedure as described in section 5.1.2. The determined optical constants are similar to those of ref. [Him05]. The complex dielectric functions are presented in figure 7.2.1. The Kramers-Kronig (KK) consistency of the solution was verified by simulating the imaginary part of the dielectric function using Gaussian functions and solving the real part according to the KK relation.
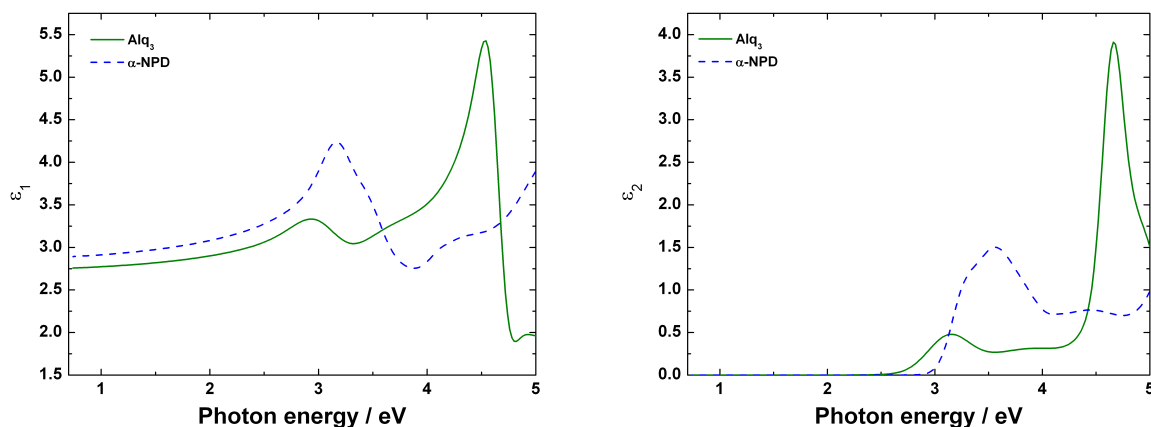
Figure 7.2.1. Complex dielectric function of Alq$_3$ and α-NPD. Left – real part, right – imaginary part.

Even if the *in situ* ellipsometric studies revealed that the Alq_3 films prepared by OMBD are not stable in atmospheric conditions [Him05a] in comparison with the Organic Vapour Phase Deposition (OVPD) films, the fresh prepared films in HV exhibit the same optical characteristics like the one prepared in UHV and by OVPD. This indicates that the isotropic amorphous Alq_3 and α-NPD films are less sensitive to the preparation conditions than the planar molecules which give crystalline films.

The PTCDA films were evaluated using reflection IR spectroscopy and ellipsometry. The complete description of the measurement conditions and evaluation procedures can be found in subsection 5.1.2 and in the references [Gor05a, Gor06b]. The complex dielectric function of the PTCDA layers is presented in figure 7.2.2.
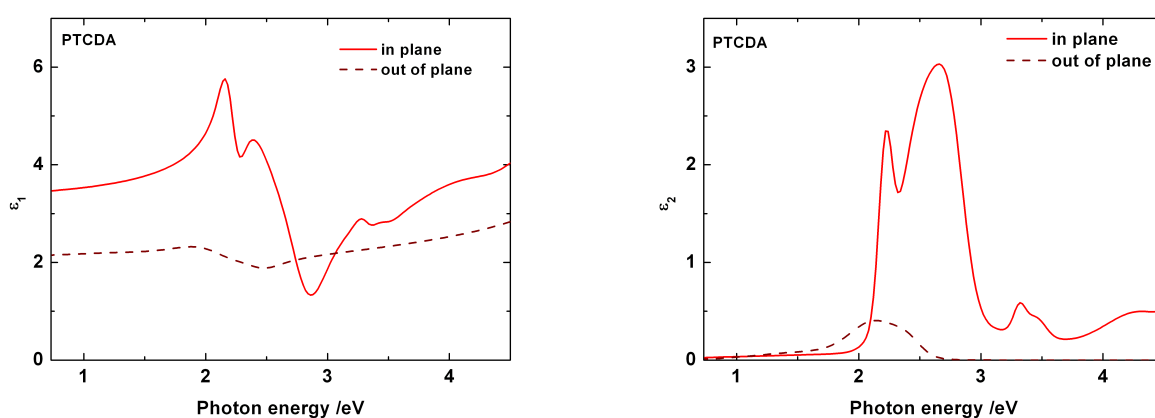
Figure 7.2.2. Complex dielectric function PTCDA. Left – real part, right – imaginary part. Continuous lines represent the in-plane component and dashed lines the out-of-plane one.

Even if the optical anisotropy and the shape of the absorption for PTCDA are similar to the ones reported in ref. [Fri02, Fri03] and in section 7.1 in figure 7.1.2, the values are slightly different. This is probably due to the different growth conditions of the HV films compared to the UHV ones. However, taking into account that the transition dipole lies in the molecular plane, the strong in-plane absorption of PTCDA compared to the out-of-plane one indicates that the molecules are lying on the substrate in a similar way like for the UHV films.

The evaluation of the IR spectra confirmed the molecular orientation deduced from ellipsometry. The PTCDA molecule exhibits out-of-plane vibrations below 900 cm^{-1}. As it can be seen in figure 7.2.3 these bands appear just for the pellet spectra and for p-polarisation while they disappear completely for the s-polarization. This indicates that the PTCDA molecules lie flat with respect to the Si(111) substrate surface.
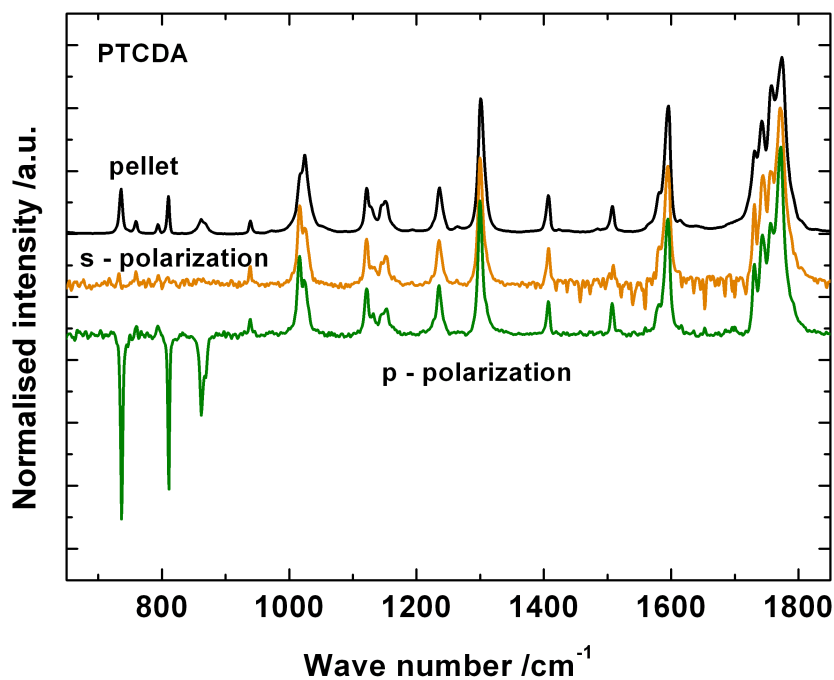
Figure 7.2.3. The reflection IR spectra of s- and p- polarization of the HV PTCDA films at 60°
angle of incidence in comparison with the IR transmission spectra of randomly oriented
PTCDA crystals in KBr pellet.

The dielectric function and IR spectra of CuPc layers are presented in figures 6.2.4
and 6.2.1, respectively. The complete description of the measurements and data evaluation
can be found in the section 6.2.

7.2.2. Multilayered Heterostructures

Using the previously determined dielectric functions a fit was performed in order to
obtain the thicknesses. The results are summarised in table 7.2.1. In a first model sharp
interfaces between PTCDA and CuPc were assumed. The MSE (see eq. 5.1.2.1) value was
35.4, while taking into account an additional intermixed interface layer the MSE was lowered
in a second model to 19.4. The intermixed layer is simulated using an effective medium
approximation consisting of 64% PTCDA and 46% CuPc. The percentage is also a fit
parameter. The results are again summarised in table 7.2.1. The atomic force microscopy
(AFM) investigation on single layers of PTCDA and respectively CuPc revealed a surface
roughness between 2.5 to 3.5 nm for PTCDA and between 2 to 3 nm for the CuPc. This
indicates that the mixing of the materials at interfaces has to be taken into consideration.

Table 7.2.1. Thickness of the PTCDA and CuPc layers in the multilayered heterostructure determined from ellipsometry.

Model 1	Thickness /nm	Model 2	Thickness /nm
PTCDA	9.5 ±0.1	PTCDA	5 ±0.2
-	-	Intermix	2.9 ±0.2
CuPc	3.7 ±0.1	CuPc	2.2 ±0.4

Figure 7.2.4 shows the experimental ellipsometric spectra and the simulated data with the two models. As can be seen in this figure the second model provides an almost perfect match with the experimental data in the range from 0.73 to 1.5 eV. The corresponding MSE value is 2, while in the same region the first model gives 8.7 MSE value. In this range the PTCDA layer has a very small absorption and the CuPc is transparent. Consequently the experimental spectra are dominated by the real part of the refractive index. The small MSE value for the second model proves that the optical constants of PTCDA and CuPc for this range are similar to the previously determined ones (figures 7.2.2 and 6.2.4). However, in the 1.5 - 4.5 eV range the same model reveals small deviations when compared to the experimental data thus giving a higher value for the MSE. In this range both materials exhibit strong absorption bands due to their corresponding π-π^* transitions [Lez96, McK98]. The interaction of the π orbitals of PTCDA with the π orbitals of CuPc at the interfaces obviously seems to affect the absorption shape. This explains the higher deviation for the model which considers sharp interfaces.

Figure 7.2.5 shows the imaginary part of the in-plane dielectric function for CuPc and PTCDA compared with the imaginary part of the effective dielectric function $\langle\varepsilon\rangle$ of the multilayer. The effective dielectric function is calculated from the ellipsometric experimental data as if the sample would be an isotropic bulk (see section 3.2). The optical response a multilayered structure is given by the optical properties of each individual layer and also by the optical interferences. As a result the optical properties of the layered multilayer can be tuned within a large range using different layer thicknesses and different number of periods. For example the imaginary part of the effective dielectric function $\langle\varepsilon_2\rangle$ is presented in figure 7.2.6 from a simulation using model 2 with different periods for the multilayer. For clarity only $\langle\varepsilon_2\rangle$ for the 55° angle of incidence is presented.
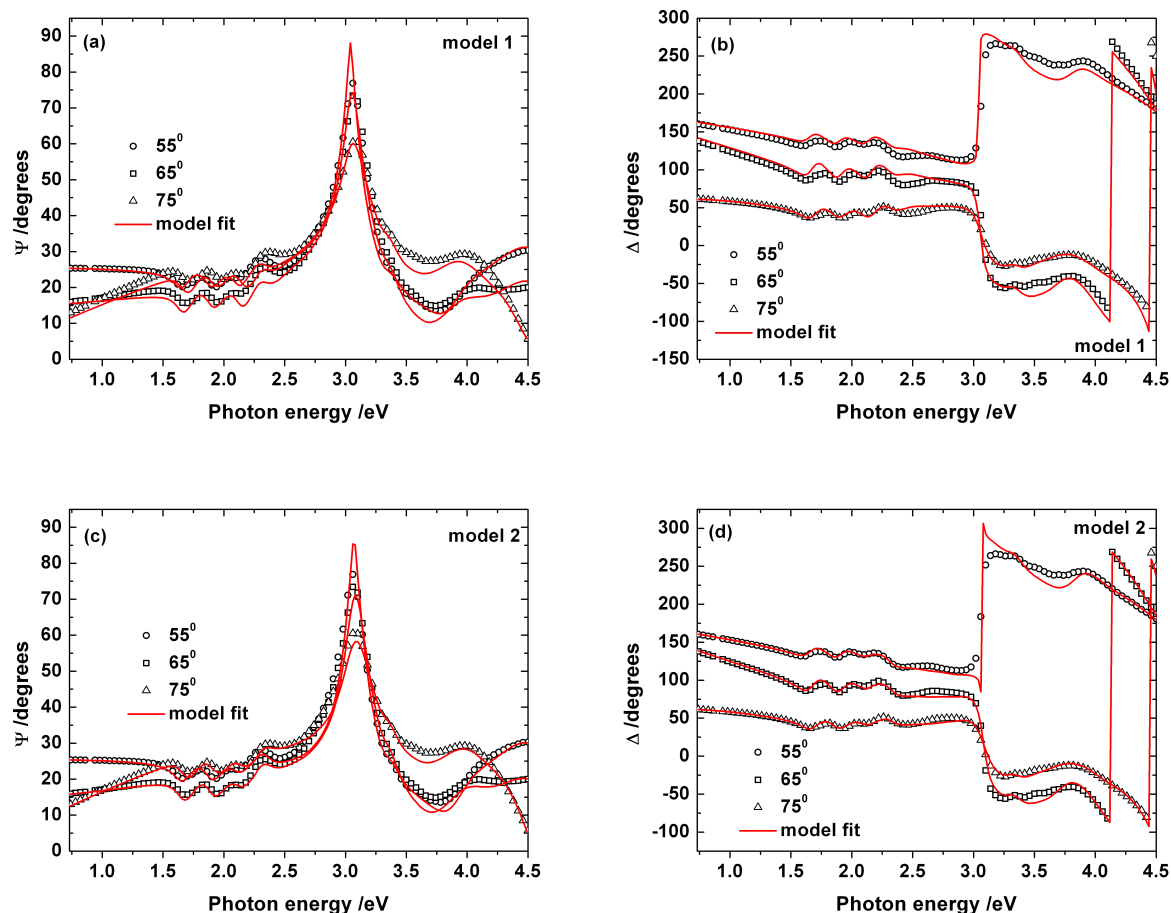
Figure 7.2.4. Ellipsometric Ψ and Δ spectra at 55°, 65°, 75° angles of incidence for a multilayer with 5 alternating layers of PTCDA and 5 alternating layers of CuPc on Si (111) substrates. Open circles are the experimental points and continuous lines the fits. Model 1 considers sharp interfaces and in the model 2 interfacial mixing was taken into account.

Figure 7.2.7 shows the IR spectra of the multilayer compared with the ones of single layers of PTCDA and CuPc. As can be seen in the figure the IR spectra of the multilayer can be reconstructed using a linear superposition of the IR spectra of PTCDA and CuPc. As the IR peak positions in the multilayer are identical to the ones in the single layers we can conclude that no chemical interaction occurs between PTCDA and CuPc. Moreover, the relative peak intensities show that the molecular orientation remains the same for PTCDA in the multilayer. For CuPc the analysis is more complex as the refraction index in the IR region also has to be taken into account. We cannot exclude the possibility that the CuPc molecules have a slightly different orientation in the multilayer compared to the CuPc in the single layers. However, from the IR peak positions we can conclude that the crystal structure of the CuPc is the same as the one in the CuPc single layers. As CuPc exhibits small differences in the effective values of the in-plane respectively out-of-plane dielectric functions just small deviations in the values of the dielectric function for the CuPc in the multilayer are expected.
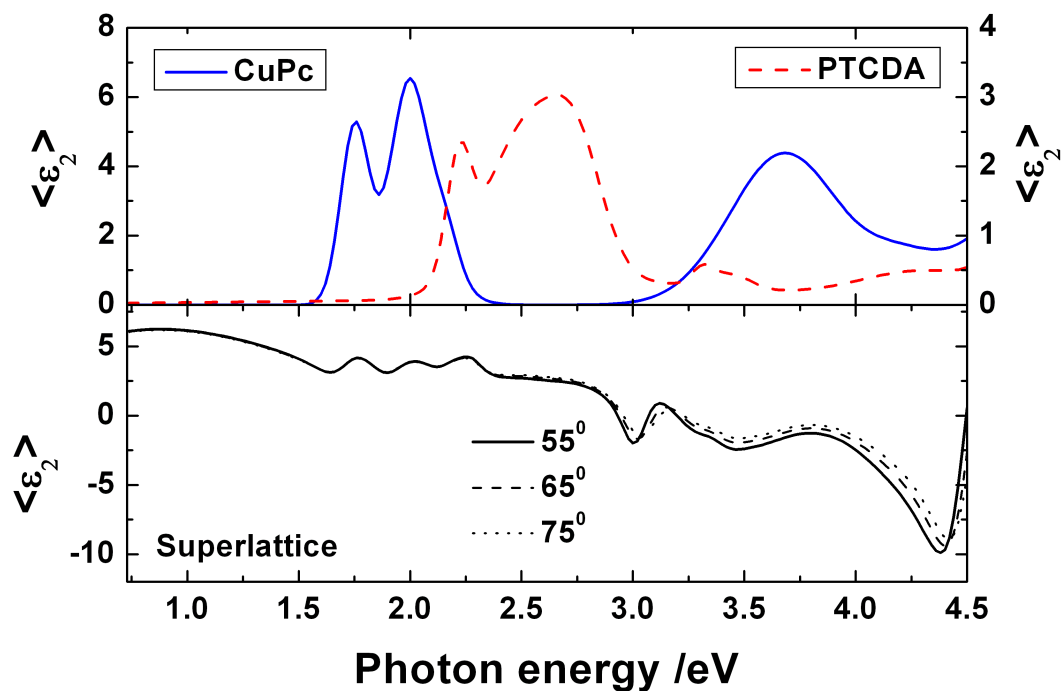
Figure 7.2.5. The in-plane imaginary part of the dielectric function of CuPc and PTCDA compared with the optical response of the layered structure.
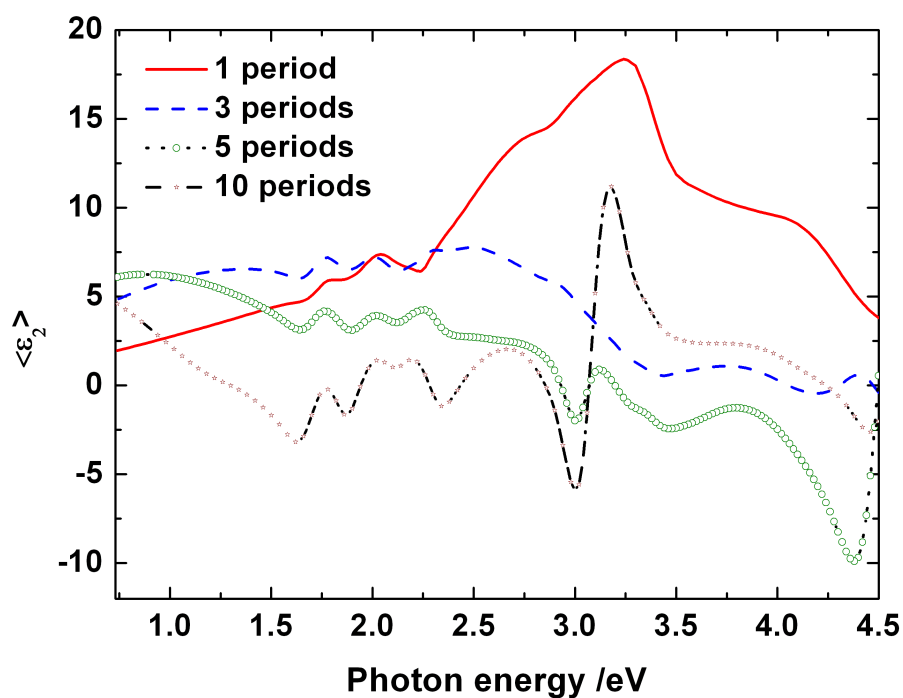
Figure 7.2.6. Simulation of the imaginary part of the effective dielectric function for different multilayer periods. For clarity only $<\varepsilon_2>$ for the 55° angle of incidence is presented.
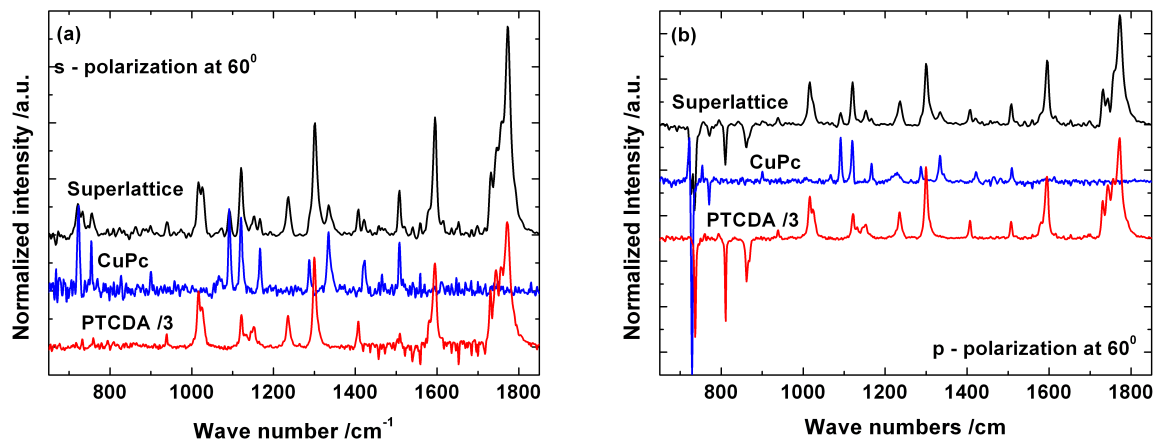
Figure 7.2.7. The IR spectrum of the multilayered structure measured in s-polarization (a) and p-polarization (b) at 60^0 angle of incidence compared with the IR spectra of CuPc and PTCDA.

The optical response of Alq_3/α-NPD multilayered structures with 8 periods and total thicknesses ranging from 160 nm to 16 nm, on the other hand, was successfully simulated using sharp interfaces. During the fit the only floating parameter was the thicknesses of the individual layers in the superstructure. The results are summarised in table 7.2.2. The targeted thickness monitored with the quartz microbalance is also shown in table 7.2.2. Even the multilayer with 1 nm nominal layer thicknesses can be described with sharp interfaces. These results confirm that high quality multilayered structures with constant thicknesses of the individual layers and a very low interface roughness were produced.

Table 7.2.2. Targeted thicknesses in the Alq_3/α-NPD multilayered structures with 8 periods and the determined ones from ellipsometric data evaluation

Alq$_3$		α-NPD		MSE
Expected thickness /nm	Measured thickness /nm	Expected thickness /nm	Measured thickness /nm	
10.0 ±0.2	9.9 ±0.05	10.0 ±0.2	10.73 ±0.05	4.5
8.0 ±0.2	8.16 ±0.04	8.0 ±0.2	8.07 ±0.04	3.8
6.0 ±0.2	6.76 ±0.03	6.0 ±0.2	5.49 ±0.02	3.4
4.0 ±0.2	3.17 ±0.03	4.0 ±0.2	3.96 ±0.03	5.9
2.0 ±0.2	2.19 ±0.01	2.0 ±0.2	2.21 ±0.01	2.2
1.0 ±0.2	1.24 ±0.02	1.0 ±0.2	0.99 ±0.02	2.9

Figure 7.2.8 shows the measured effective dielectric functions of the multilayered structures with individual layer thickness in the range from 1 to 10 nm. For clarity only the values for 65° angle of incidence is plotted. As can be seen in the figure 7.2.8 the optical

response of the multilayered structure can be tuned by appropriate choice of periods and thicknesses of individual layers.

Figure 7.2.9 shows the differences between simulated and experimental data for the structures with MSE values higher than 3. All Alq$_3$/α-NPD samples have a characteristic deviation between experimental and simulated data around 4.5 eV. This corresponds to the strongest absorption peak of Alq$_3$ (fig. 7.2.1). Therefore the deviation can be attributed to a small change of the dielectric function of Alq$_3$ in the multilayer compared to the bulk.
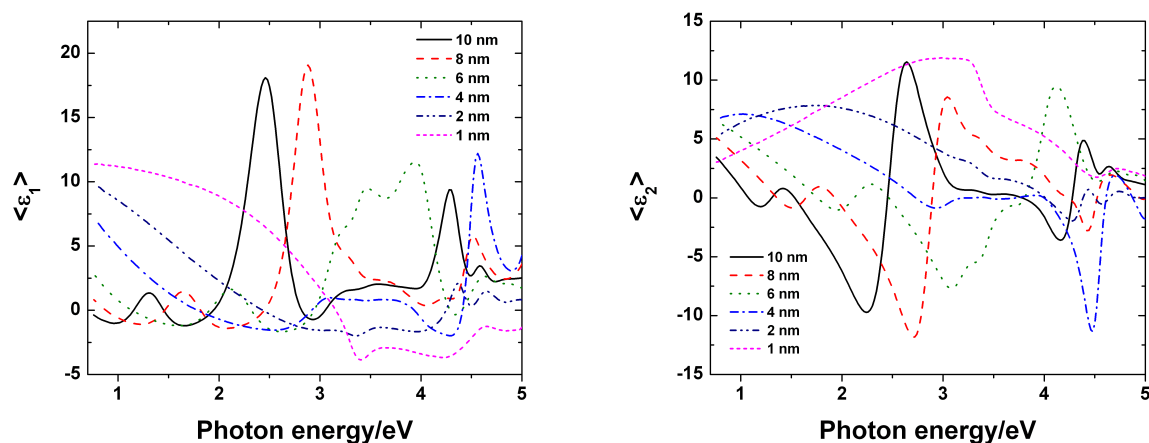
Figure 7.2.8. The measured effective dielectric functions of the multilayered structures with individual layer thickness in the range from 1 to 10 nm. For clarity only the values for 65° angle of incidence is plotted.
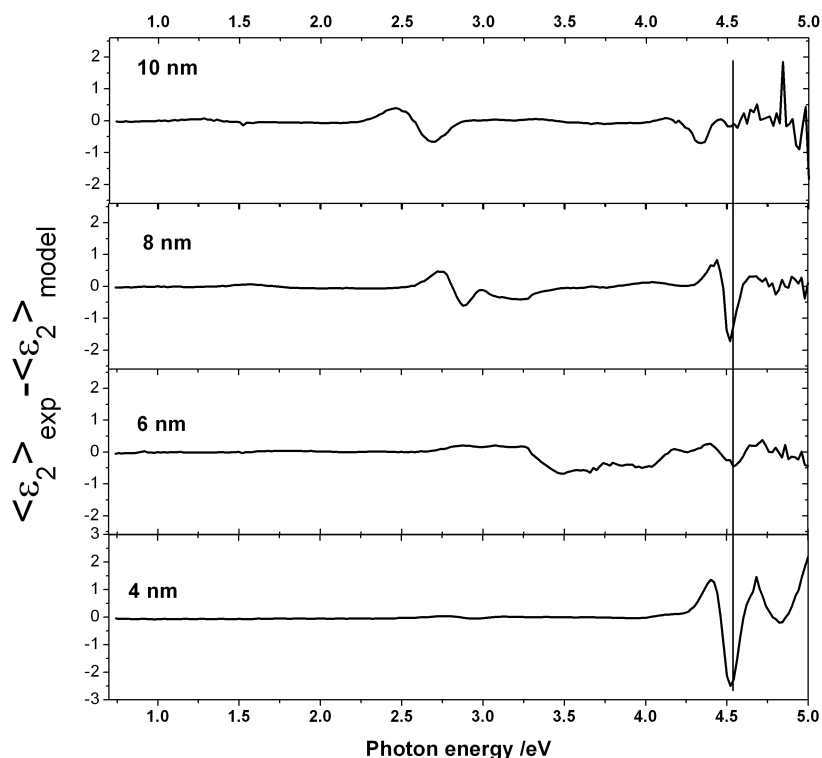
Figure 7.2.9. The difference between the experimental and simulated effective dielectric function of the multilayered structures.

7.2.3. Mixed layers

In the previous part of this chapter we assumed that the differences between the simulated and experimental data are due to the electronic interaction at the interfaces between the constituents, which will affect the electronic transitions and therefore the optical properties. One way to maximize the interaction between the constituents is to mix the two constituents. In order to compare the optical response of the multilayered heterostructures, mixed layers with different thicknesses were prepared. The thicknesses of the mixed α-NPD-Alq$_3$ layers were evaluated using two different multi-sample analysis procedures. In the first one a linear EMA [Ohw97] was used. In this case a linear combination of the previous determined dielectric functions is used to give the dielectric function of the mixed layer like described in section 5.1.2.

In this case the materials a and b from the equation 5.1.2.3 are α-NPD and Alq$_3$, respectively. The mixing ratio is also a fit parameter. The result is shown in figure 7.2.10. The determined ratio of 54.5% α-NPD is in the targeted range of 52%-56%. The final MSE of 4 indicates that this model simulates the experimental data very well. In the second approach the mixed layers were treated like homogenous isotropic ones. The thickness is determined in the transparent range were the refractive index (n) of the layers can be approximated with the Cauchy formula (see section 5.1.2).
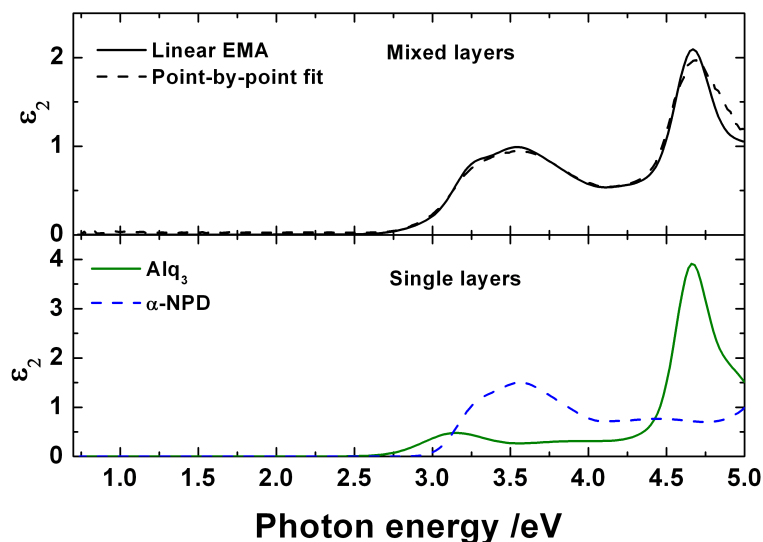
Figure 7.2.10. Mixed layer: α-NPD-Alq$_3$. Comparison between EMA model and fit. In the lower part the imaginary part of the dielectric functions used in the EMA model are plotted.

The determined thicknesses were identical with the ones from the EMA model. However, these thicknesses were lower than the expected ones calculated from the quartz microbalance calibration. This can indicate that the mixed layers may have higher densities compared to the single ones.

Keeping the thicknesses fixed the dielectric function was determined with the procedure described in section 5.1.2, as the layer would be homogenous and isotropic. The simple point by point fit is plotted in figure 7.2.10. The result is almost identical with the one obtained with the EMA model. Some deviation can be seen beyond 4.5 eV, in the region were Alq_3 has the strongest absorption peak. This result is consistent with the one obtained for the multilayered structure.

The mixed layers of PTCDA-CuPc are more difficult to model. In this case the dielectric function along the x,y directions and z direction have to be treated separately. Figure 7.2.11 shows the imaginary part of the in-plane dielectric function from a multi-sample analysis which assumes that the mixed layers are anisotropic. Along the z direction the absorption was found to be very weak. This indicates that the PTCDA molecules as well as CuPc molecules have the molecular planes parallel with respect to the substrate. The MSE of the fit for two coupled mixed layers was 4. The dielectric function is compared with the ones obtained using a linear EMA model and the Bruggeman EMA model. For the effective medium approximation models the out-of-plane component was kept fixed to the values found before for single layers. Considering the in-plane (xy) dielectric function given by a linear EMA the MSE is 18, while for a Bruggeman EMA [Bru35] the MSE goes down to 8. Considering in equation 5.1.2.4 a=PTCDA and b=CuPc the volume fraction of PTCDA is 47%, which is very close to the targeted one.

The differences between the Bruggeman EMA and the model fit in the energy range where CuPc has the Q-band [Lez96, McK98] indicate that the overlap of the CuPc π orbitals is different than in single layers. The change of the peak ratio is a clear indication that the α-phase structure is not preserved in the mixed layers. As the CuPc molecules are lying the herringbone structure of the α-phase cannot be formed. Small changes in the shape and symmetry of the PTCDA absorption peak can also be noticed.

Figure 7.2.12 shows the IR spectra of the single layers, multilayered structure and mixed CuPc-PTCDA layers in the relevant range where the out-of-molecular-plane modes are present. In contrast to single CuPc layers and heterostructures, the peak around 722 cm^{-1} is not present in the mixed layers. As this is attributed [Deb92] to an out of plane molecular vibration the peak absence in the mixed layer indicate that the molecules are parallel with the substrate surface. This mode appears strongly in p-polarization spectra.

For PTCDA the peaks below 900 cm^{-1} in fig. 7.2.12 correspond to out-of-molecular-plane modes. They are not visible for s-polarisation, while they appear in p-polarization indicating that in all structures the PTCDA molecules prefer to adopt a parallel orientation with respect to the substrates. The IR peak positions in the mixed layer are slightly shifted compared to single layers and heterostructure indicating that the molecules have a different packing. These findings are in agreement with the ellipsometry data evaluation.
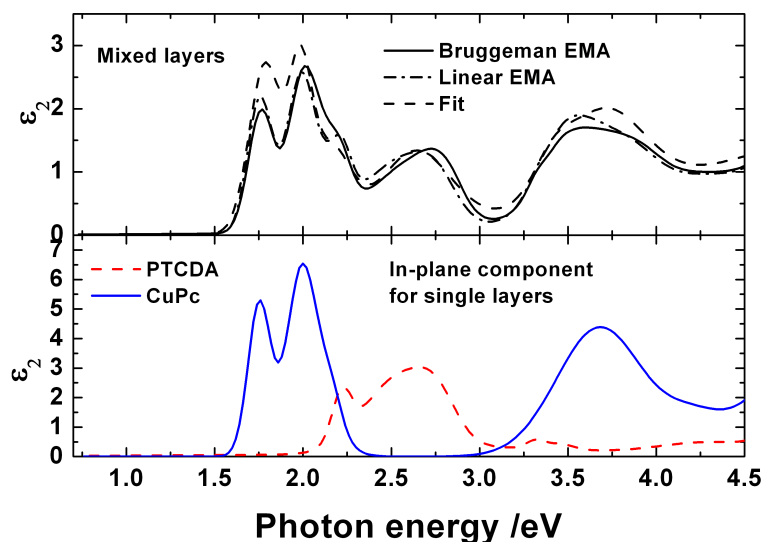
Figure 7.2.11. Mixed layer: PTCDA-CuPc. Comparison between EMA models and fit. In the lower part the imaginary part of the dielectric functions used in the EMA models are plotted.
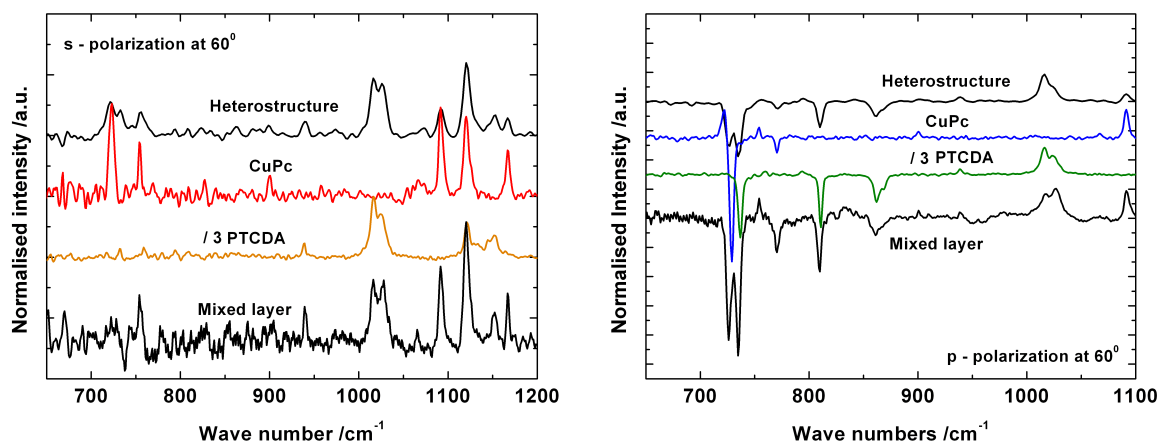
Figure 7.2.12. The IR spectrum of the single layers, multilayered structure and mixed layers measured in s and p polarization at 60° angle of incidence compared with the IR spectra of CuPc and PTCDA.

7.3.   Summary

Different PTCDA/H_2Pc, Alq$_3$/α-NPD, PTCDA/CuPc systems were investigated by means of spectroscopic ellipsometry and IR spectroscopy. Alq$_3$ and α-NPD form isotropic layers and the multilayered heterostructures can be modelled with sharp interfaces using the dielectric functions of single layers. The optical response of mixed layer can be simulated using effective medium approximations. Only small deviations can be noticed in the region where Alq$_3$ has the strongest absorption feature.

For the combination PTCDA - Pc, data evaluation needs a more complex approach due to the anisotropic growth of the layers. The interaction between the PTCDA and H_2Pc leads to a template effect of the PTCDA on the growth mode of the Pc. In the multilayered heterostructures of PTCDA and CuPc the surface roughness and interfacial mixing has to be considered. The differences between experimental and simulated data indicate that a reorientation of CuPc molecules grown on PTCDA cannot be neglected when compared to the HV CuPc layers. In the mixed layers the PTCDA influence is very strong, forcing CuPc molecules to adopt a parallel orientation with respect to the substrate. In this case the herringbone structure of the α-phase CuPc is not preserved. The change in the CuPc and PTCDA π-π^* orbital coupling is reflected in a different shape of the dielectric function of the mixed layers compared to the one calculated using an effective medium approximation.

8. VUV Ellipsometry with Submonolayer Resolution

8.1. Introduction

The optical response and the dielectric function of the organic materials used in devices are influenced by electronic interactions and differ from gas phase and solution. When determining the optical properties of thick layers, bulk properties are used to simulate the optical response. However, when addressing the sub-monolayer regime changes in the intermolecular interaction and other effects are expected, and therefore changes in the optical response. The result may become even more important when dimensions of organic electronic devices shrink to the molecular level. The detailed understanding of nano-scale materials is a key prerequisite for future molecular devices. With the reduced size of future electronics these effects of dimensionality become more and more important. Ellipsometry is a non-destructive and very sensitive surface and thin film measurement technique which can detect the changes in the optical response produced by an overlayer on a smooth surface. However, interpreting the ellipsometry spectra for very low coverages (below few nanometers) down to a monolayer or even submonolayer regime remains a challenging task as the optical path of the light through the material is much smaller than the wavelength [Asp76, Azz92, Ros96]. In this case it is difficult to separate the refractive index of the film and the film thickness. Consequently only the product of these parameters can be uniquely determined [Asp76, Azz92]. A graphical representation of this experimental limit is presented in figure 8.1.1. As can be seen in this figure the changes in Ψ and Δ for different thicknesses and different refractive indexes films are plotted at 2 eV as if the films would grow on a clean silicon surface. While for thicknesses higher than 20 nm the same film thickness will give different pairs of Ψ and Δ, for thicknesses lower than 10 nm the same difference in the refractive index will give almost the same values for Ψ and Δ.

Nevertheless, optical spectroscopies like differential reflection and ellipsometry are sensitive enough to yield information on monolayers. This holds in particular if a spectral range is accessed in which optical absorption bands of the overlayer occur. In previous work McIntyre and Aspnes [Mcl71] proved that differential reflection spectroscopy can be a powerful tool in investigating the optical properties of ultra-thin films. Using spectral ellipsometry the optical response of monolayers was successfully investigated as well [Rit83, Ros93, Ess95, San95]. Rossow *et al*. [Ros93] presented the effective dielectric function of an As-terminated Si(111) surface compared to the one of a clean Si(111) surface. The dielectric function of the As monolayer evaluated from a three phase model was determined. In a study by Ritz [Rit83] the electronic structure of GaP(110) and copper phthalocyanine (CuPc) overlayers was investigated. Esser *et al.* [Ess95, San95] used the combined information from

ellipsometry, reflectance anisotropy spectroscopy (RAS) and Raman spectroscopy to characterize the modification of the surface properties induced by hydrogen exposure to GaAs(100) and Sb-monolayer terminated GaAs(110). In this study the surface and monolayer electronic properties were evaluated from ellipsometry data. In a more recent work Proehl *et al.* [Pro04] studied the intermolecular interaction between PTCDA molecules with monolayer resolution by means of differential reflection revealing shifts in molecular transition energies related to intermolecular coupling.
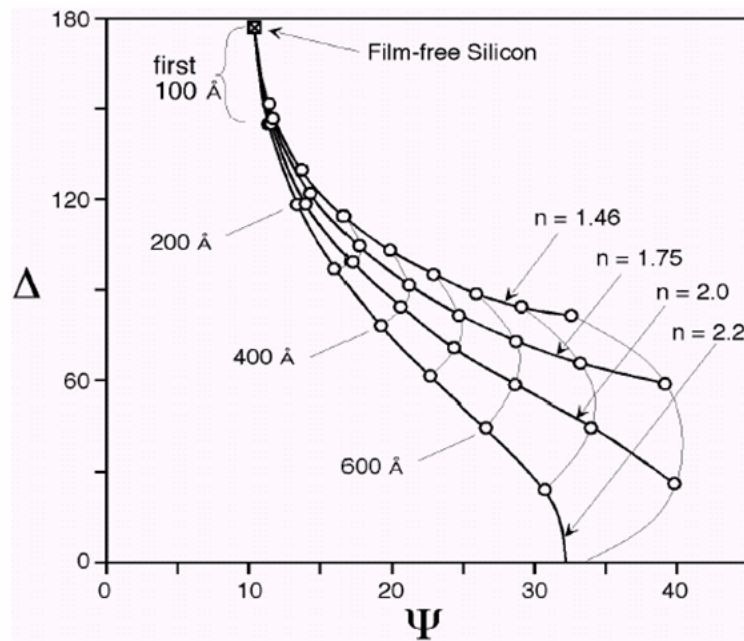
Figure 8.1.1. Graphical representation of the experimental limit at 550 nm wavelength.

While the direct inspection of the measured effective dielectric function can provide useful information about the layer growth (e.g. section 6.4 figure 6.4.3) and complementary methods of measurement and evaluation can be applied [Rit83, Ros93, Ess95, San95, Pro04], the determination of the dielectric function (or optical constants) in the visible range for layers below 1 nm remains an almost impossible task to achieve. This becomes clear by looking at the simulation presented in figure 8.1.2. A silicon substrate with the dielectric function like in the ref. Jel92 was considered in the model, and then the simulation for 0.2, 0.6 and 1 nm layer thicknesses with refractive indexes from 1.45 to 2 was performed. The data in figure 8.1.2 is valid for an angle of incidence of 70°, which is close to the Brewster angle of silicon. Due to this reason at this angle the higher sensitivity to changes of the refractive index of the silicon surface is achieved. At 1 eV energy (or 1239.8 nm wavelength) there is basically no change in the Ψ value, and less than half of a degree change in the Δ value. However, the spread in the Δ values becomes larger for lower wavelengths, and at 4 eV one can distinguish between the different refractive indexes even for 0.6 nm of coverage, as the variation in Δ is one degree from a refractive index of 1.45 to a refractive index of 2.2.

This indicates that higher sensitivity to the refractive index and thickness is achieved in the Ultra Violet range.
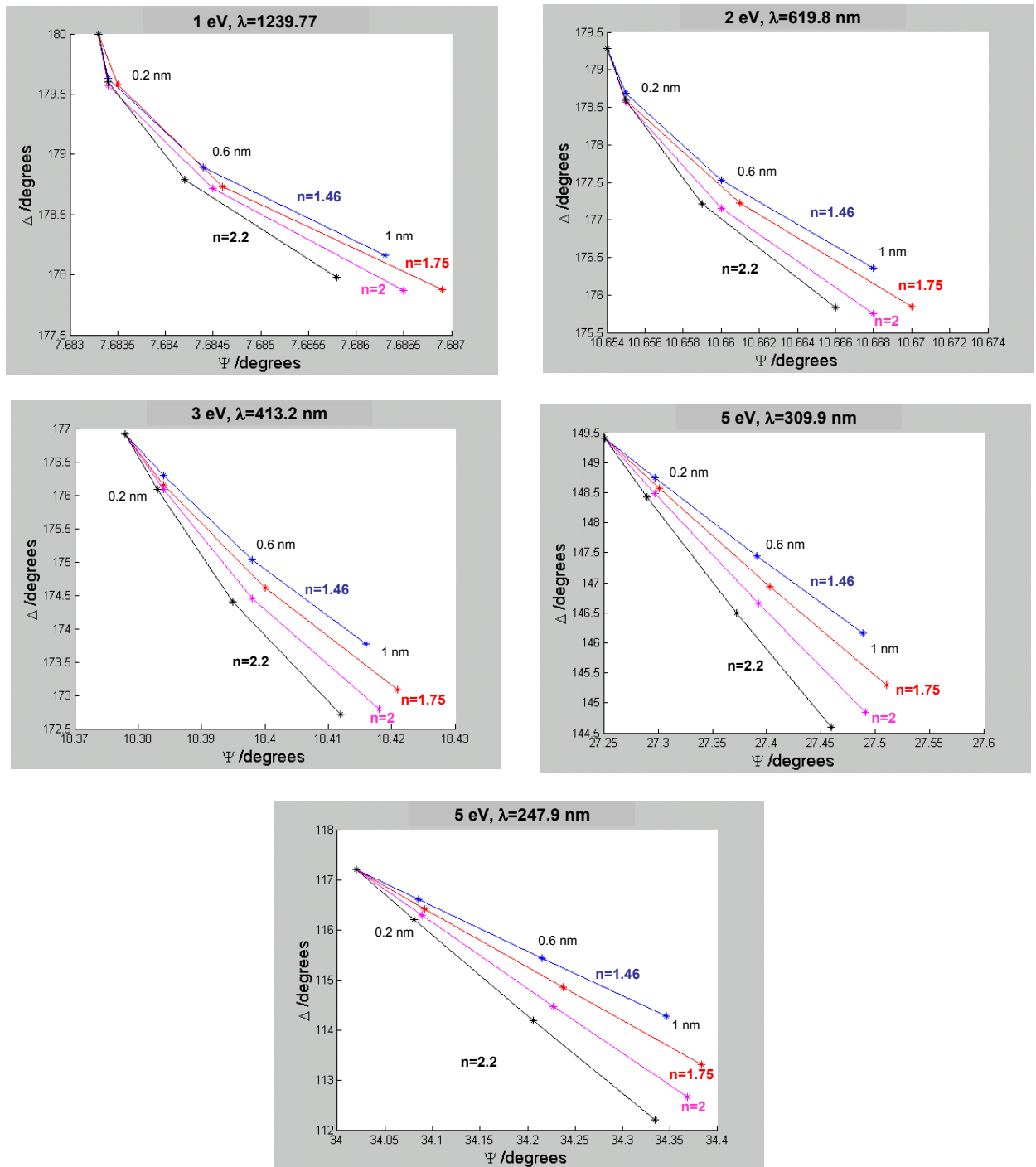
Figure 8.1.2. Graphical representation of the experimental limit for layer thicknesses lower than 1 nm. The stars represent the thicknesses of 0.2, 0.6 and 1 nm.

Another way to visualize the sensitivity of the ellipsometric measurement is to plot the difference $\delta\Delta$ between the Δ value of the bare substrate and the Δ value of the covered substrate. In order to have an idea about the sensitivity that can be achieved in the UV range using the BESSY ellipsometer (see section 5.1.1 and figure 5.1.4 for the schematics) a

simulation was performed for 68° angle of incidence. In the simulation the dielectric function of silicon in the extended UV range [Joh99] was used. The values are presented in figure 8.1.3.
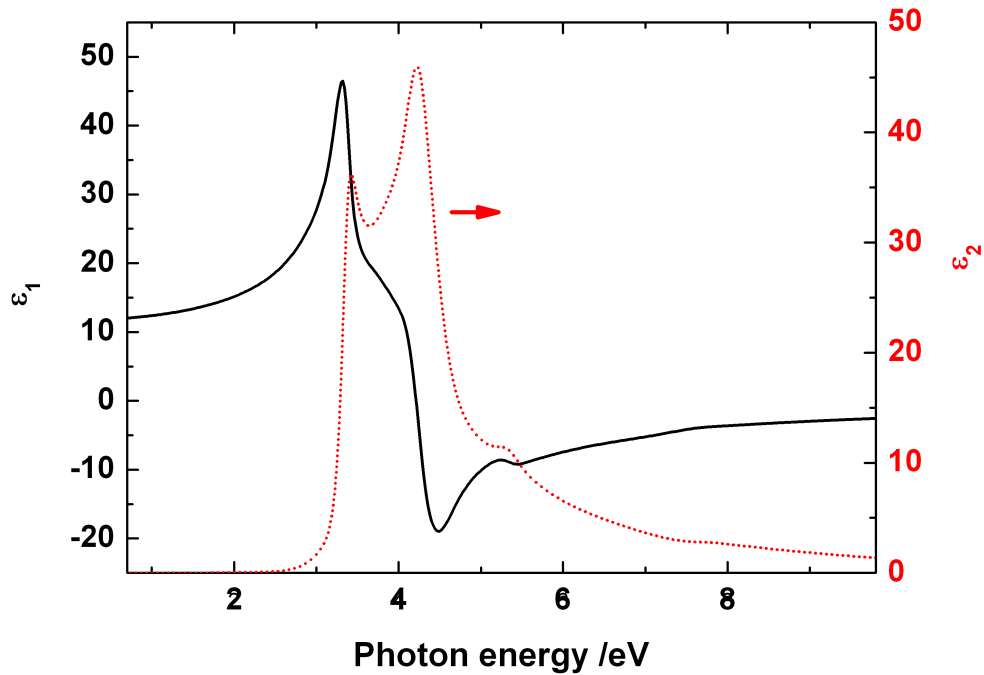
Figure 8.1.3. The complex dielectric function of silicon in an extended energy range [Joh99]
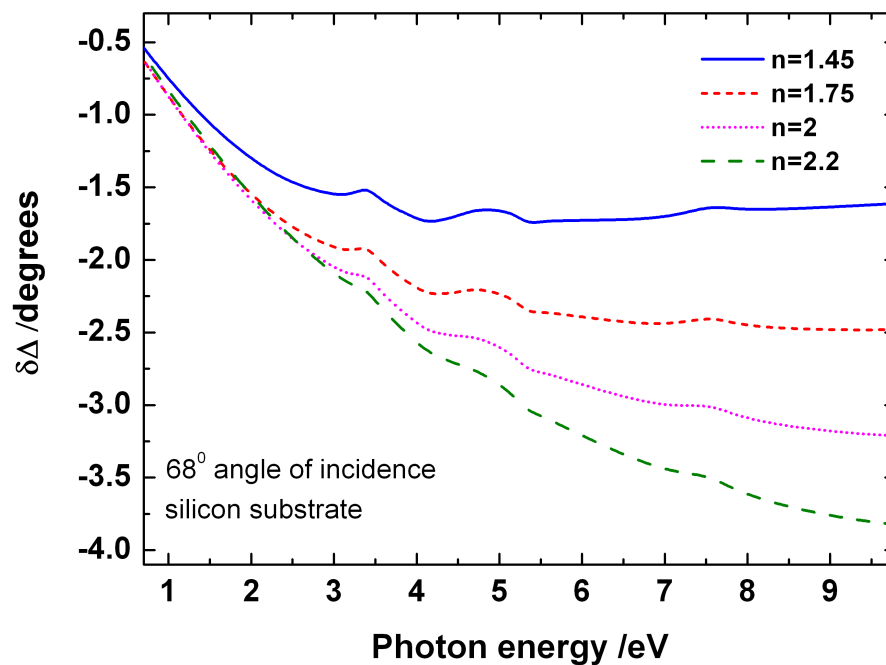
Figure 8.1.4. The difference $\delta\Delta$ between 0.6 nm thick films with different refractive index, at 68° angle of incidence.

The difference $\delta\Delta$ between the Δ value of the silicon substrate and the Δ value of the covered substrate with 0.6 nm film with a refractive index from 1.45 to 2.2 is presented in

figure 8.1.4. It is clear that up to energies of 3 eV it is very hard to distinguish the refractive index for the films with this thickness. However, in the higher energy range the refractive index of the film can be determined if the ellipsometer has a measurement accuracy in Δ better than 0.5°.

While the changes in the measured Δ values depend also on the refractive index of the substrate, in figure 8.1.5 the simplest case of a substrate with constant refractive index of 1.5 is shown.
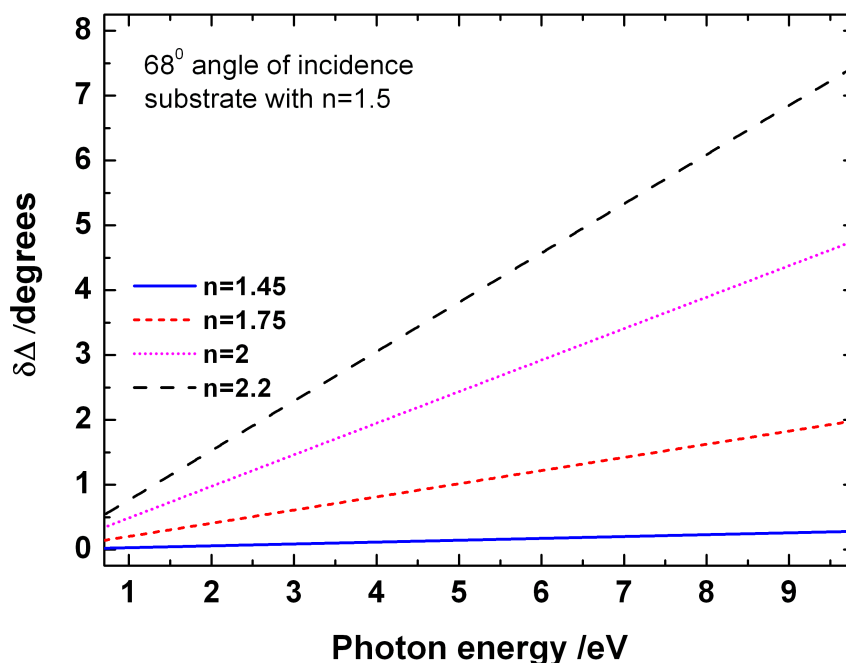
Figure 8.1.5. The difference $\delta\Delta$ between 0.6 nm films with different refractive index, at 68° angle of incidence on a substrate with n=1.5

Due to these difficulties in detecting and determining the optical response of very small amount of adsorbates on surfaces, the majority of the reported studies compare the absorption and photoluminescence of diluted solutions of molecules in organic solvents with those of thick films. Even if the lower wavelength of the UV light should be more sensitive for ultra-thin films to our knowledge there is no investigation yet of organic monolayers using VUV ellipsometry.

Therefore the aim of this chapter is to present the optical response of small organic molecules in the vacuum ultra-violet (VUV) range starting from sub-monolayer coverage to thick layers with bulk-like optical properties. More specifically, as it will be shown, absorption bands of these molecules fall within the VUV spectral range [Gor06c].

8.2. Alq$_3$

Alq$_3$ is an organic electron transporting and green light emitting material and one of the most successful organic material used in OLEDs. More information about the molecular structure and applications can be found in the section 4.3.

Several ultra-thin films of Alq$_3$ were prepared by OMBD on hydrogen passivated Si (111) substrates in the UHV preparation chamber in BESSY, as described in the chapter 4.4. In order to obtain the optical constants of Alq$_3$ several thick films which exhibit bulk like features were also prepared. At a crucible temperature of 211 C the frequency change was constant around 8 Hz/min. The calibration using the thickness of a thick Alq$_3$ film determined from ellipsometry provided a deposition rate of (1.36 ±0.17) nm /min.

Immediately after deposition the samples were transferred under UHV into the ellipsometry analysis chamber (base pressure ~4·10^{-9} mbar). The measurements were performed at BESSY in the range from 4 eV to 9.5 eV (energy steps of 0.025 eV) using the setup described in section 5.1.1, figure 5.1.4.

The first assessment of the ellipsometric spectra revealed that Alq$_3$ exhibits remarkable absorption bands in the VUV region. Figure 8.2.1 shows the complex dielectric function of a 1.5 μm thick Alq$_3$ film.

The thickness calibration was performed in the absorption free range of Alq$_3$ from 0.8 to 2.5 eV using a variable angle spectrometric ellipsometer (Woollam VASE) (see section 5.1.2, figure 5.1.6). Table 8.2.1 presents the thicknesses obtained from the ellipsometry evaluation compared with the frequency shift of the quartz microbalance. The graphical representation can be seen in figure 8.2.2.

Table 8.2.1. Thickness of the ultra-thin Alq$_3$ layers on Si(111) substrates determined from ellipsometry.

Sample	Thickness /nm	Frequency shift /Hz
1	5.6	36
2	3	18
3	1.8	9
4	0.64	4

The dielectric function of the Alq$_3$ layer in the VUV range was evaluated using a three phase model [Gor06c]. The dielectric function of the Si(111) substrate was determined from a reference H-passivated Si(111) sample. The Alq$_3$ layer was treated as isotropic [Bri00, Him05a]. After an initial point-by-point fit, in which the data at each wavelength are fitted separately, a more complex model was used. In this model a sum of Gaussian oscillators was used for the simulation of the line shape of the imaginary part of the dielectric function ε_2, while the real part of the dielectric function ε_1 is generated according to Kramers-Kronig

(KK) relation. As seen in fig. 8.2.1 the simulated dielectric function coincides with the experimentally measured effective dielectric function. This indicates that the film can be treated as a semi-infinite medium (the light does not "see" the substrate).
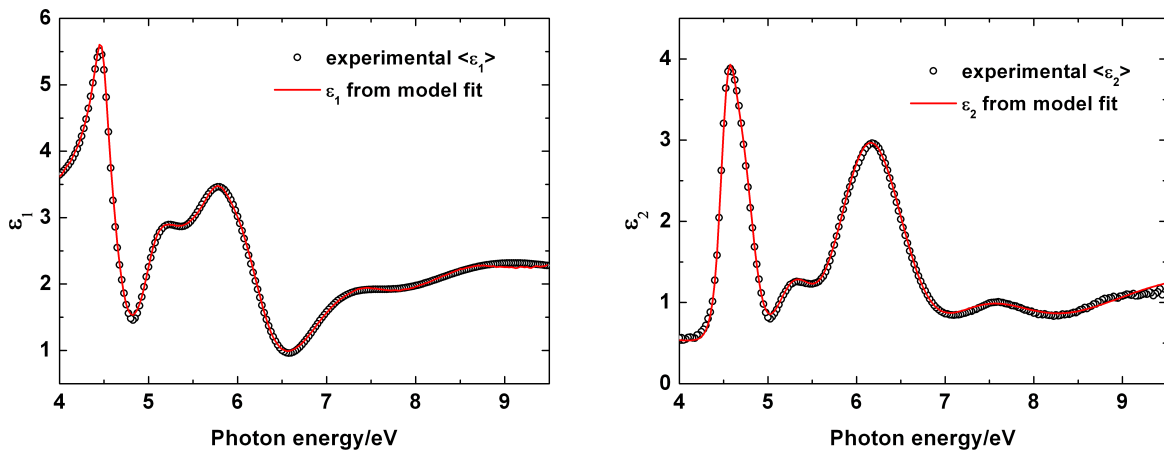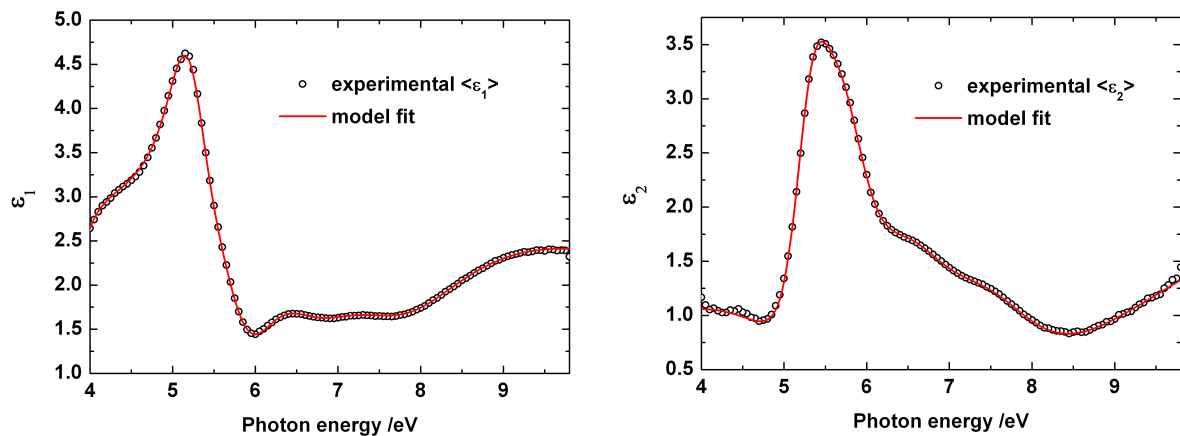

Figure 8.2.1. Dielectric function of Alq_3 – continuous line, in comparison with the experimental effective dielectric function – open circles . Left - real part, right - imaginary part.
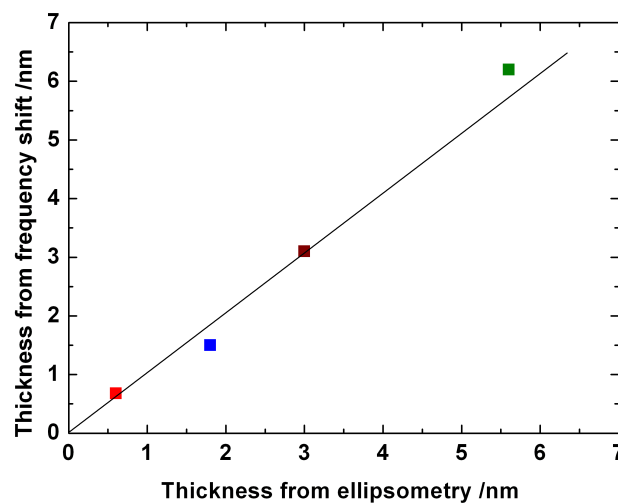
Figure 8.2.2. The thicknesses of the ultra-thin Alq_3 layers on Si(111) substrates determined from ellipsometry *vs.* the thicknesses determined from the frequency shift of the quartz microbalance.

The lowest investigated nominal thickness of 0.6 nm is below the monolayer thickness of Alq_3 which is approximately 1.1 nm, according to the size of the molecule. As seen in figure 8.2.3 the optical response differs significantly from that of the H-passivated Si(111), even for sub-monolayer coverage. A reduction of the E_2 peak of silicon is known to occur even for transparent overlayers on Si [Ros96]. Apart from the decrease of Si related structures, however, the effective dielectric function shows additional well defined structures between 4.6-5 eV, (marked by dashed lines), which we attribute to molecular optical

transitions. To emphasize the features of the experimental spectra the inset of fig. 8.2.3 shows the second derivative of the effective dielectric function in the relevant spectral range. Two optical transitions around 4.6 eV and 4.9 eV are resolved, clearly separated from Si related structures at 4.4 eV and 5.3 eV. These features increase with the film thickness and can thus be unambiguously attributed to Alq_3.
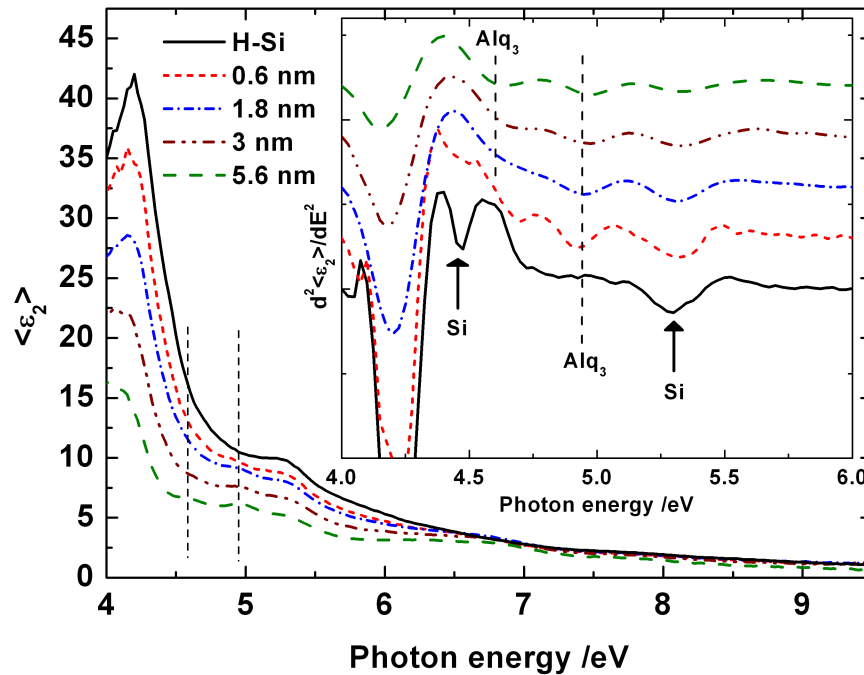
Figure 8.2.3. The effective $<\varepsilon_2>$ of the samples 1-4 compared with the $<\varepsilon_2>$ of the H-Si(111) substrate; vertical dashed lines mark the positions of strong Alq_3 induced features. In the insert - second derivative of $<\varepsilon_2>$.

The occurrence of the additional features in the effective dielectric function of the Si substrate coated with thin Alq_3 layers is a sign of strong optical absorption by the overlayer. In order to separate overlayer and substrate dielectric functions we use two different methods: (1) analysis in terms of a conventional three phase model [Azz92] and (2) a parameter-free approximation valid for ultra-thin films, proposed by Aspnes [Asp76]. In the second approach the effective dielectric function $<\varepsilon>$ can be approximated by equation 3.4.2. This formula is valid for $\frac{d\sqrt{\varepsilon}}{\lambda} \ll 1$, which holds for thicknesses below 1 nm [Ros96]. The quadratic equation can be easily solved to find ε_L. More details about this approximation can be found in section 3.4. Figure 8.2.4 shows the result of the ultra-thin layer approximation together with the three-layer model fit and ε_2 of the Alq_3. While in the three layer model Kramers-Kronig consistency is imposed to achieve the solution, in the ultra-thin layer approximation the only input parameter is the layer thickness. The approximation is dependent on two measurements, namely that of clean and adsorbate covered silicon, and

therefore the solution is affected by the noise of two different measurements. Figure 8.2.4 shows that the absorption features of the ultra-thin film corresponding to molecular transitions of the Alq_3 are sharper and spectrally blue-shifted with respect to those of the bulk-like layers. Further inspection of the experimental data revealed that the optical transitions of the 1.8 nm Alq_3 film appear at the same energies as for bulk-like samples.
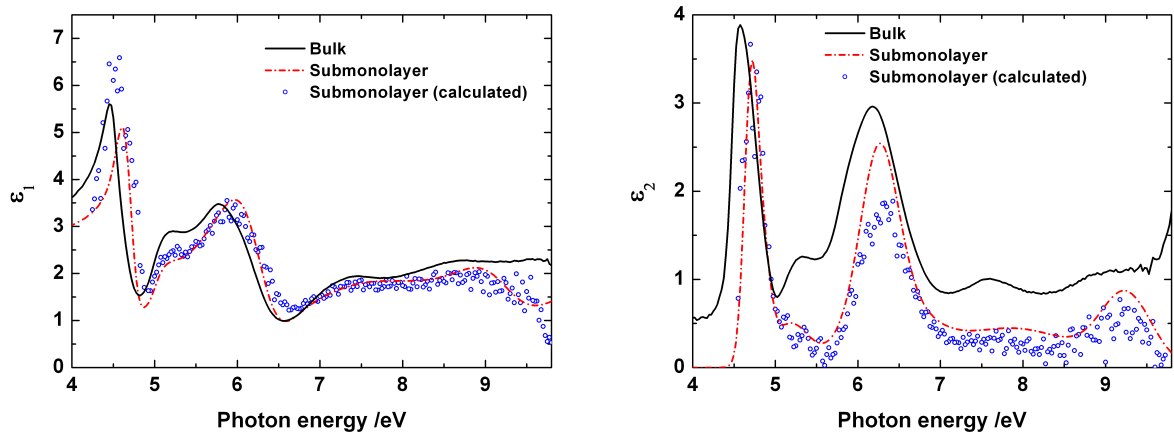
Figure 8.2.4. Comparison between the dielectric function for a sub-monolayer of Alq_3 obtained from a model fit and calculated using equation 3.4.2. The dielectric function for bulk Alq_3 is also plotted. The calculated ε_2 from equation 3.4.2 is affected by the experimental noise of two different measurements, namely that of the H-Si(111) substrate (ε_s) and of the ultra-thin Alq_3 layer ($<\varepsilon_L>$).

A quite similar blue-shift of the optical absorption bands was also reported for low molar concentration of Alq_3 in solution [Bri00]. The lower part of figure 8.2.5 shows the absorption of an Alq_3 film on quartz compared to that of Alq_3 in solution as reported by Brinkmann *et al* [Bri00]. In the upper part the extinction coefficient of the Alq_3 films and sub-monolayer on Si(111) is presented as derived from ellipsometry data. The extinction coefficient k is calculated from the complex dielectric function according to $(n + ik)^2 = \varepsilon_1 + i\varepsilon_2$, where n is the refractive index of the material. There is a striking resemblance of the absorption data with our ultra-thin film ellipsometric result.
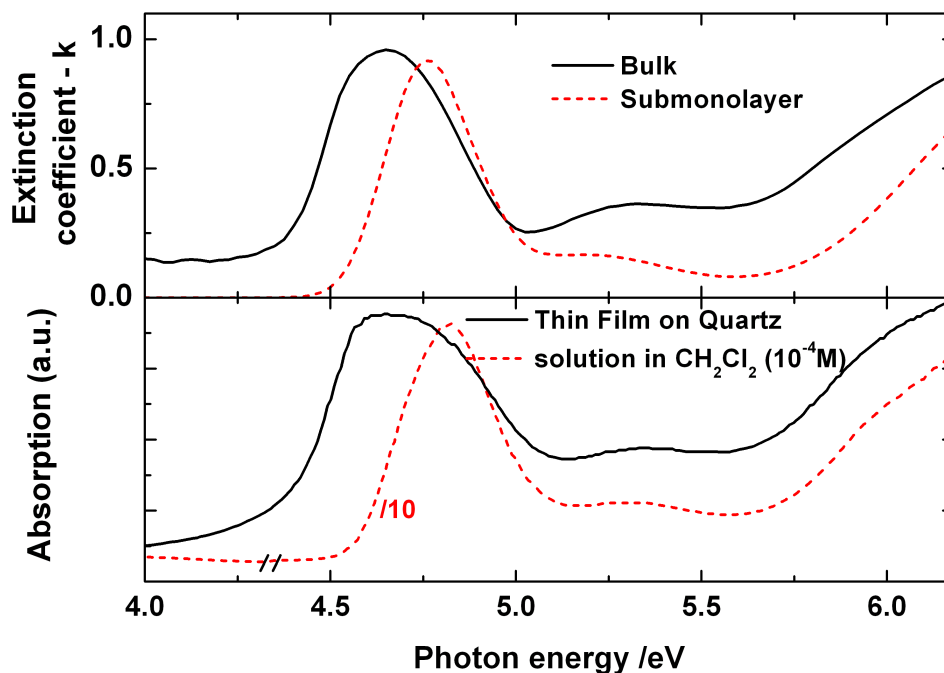
Figure 8.2.5. Comparison between the absorption spectra of a thin Alq$_3$ film on quartz and Alq$_3$ in solution as reported in ref. [Bri00]. In the upper part the extinction coefficient of a thick Alq$_3$ and sub-monolayer on H-Si(111) is plotted.

Additionally the dominant features of the extinction coefficient were assigned by comparison with the singlet-singlet transitions calculated using the Gaussian 03 software [Fri01]. The molecular geometry of the *meridional*-isomer [Cöl04] was optimised using the Kohn-Sham density functional theory (DFT) with the 3-21G basis set and the Becke three-parameter hybrid exchange correlation functional (B3LYP). The time-dependent density functional theory (TD-DFT) was subsequently employed to calculate the excitation energies, oscillator strengths, and excited-state compositions in terms of excitations between occupied and unoccupied orbitals.
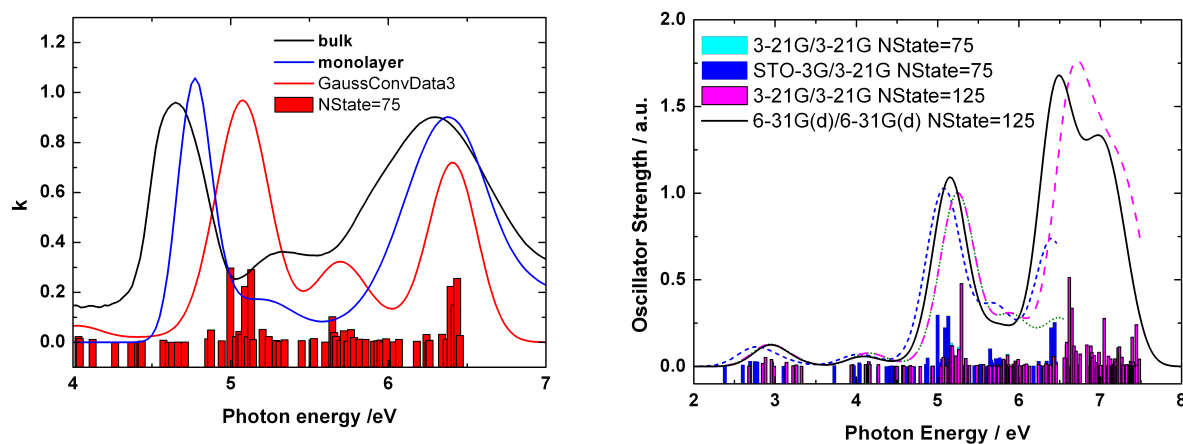
Figure 8.2.6. Experimental and calculated Alq$_3$ extinction coefficient

Figure 8.2.6 shows the extinction coefficient of the bulk Alq_3 and of the ultra-thin layer in comparison with Gaussian convolution of the excited states. Using higher basis sets for calculation of the excited states leads to a further shift towards higher energies of the convoluted features.

Taking into account the blue-shift of the absorption features reported for low molar concentration of Alq_3 in solution [Bri00] and the result of the theoretical calculation, the observed shift could be attributed to the molecular interaction between the Alq_3 molecules. However, the different dipolar character of the solvents can lead to changes in the absorption maxima of up to 1000 cm^{-1} and due to the high polarizability of the silicon the influence of the H-Si(111) substrate on the Alq_3 ultra-thin film could not be excluded. In order to clarify if the silicon substrate has an influence on the observed shift, zinc oxide (ZnO) substrates with Zn and O terminated surfaces were used. While the Zn side and O side have similar dielectric functions, the different terminations can help to investigate the stability of the Alq_3 molecules on these surfaces. The AFM topography images of these two ZnO surfaces are presented in figure 8.2.7.

a) Zn side

b) Zn Side
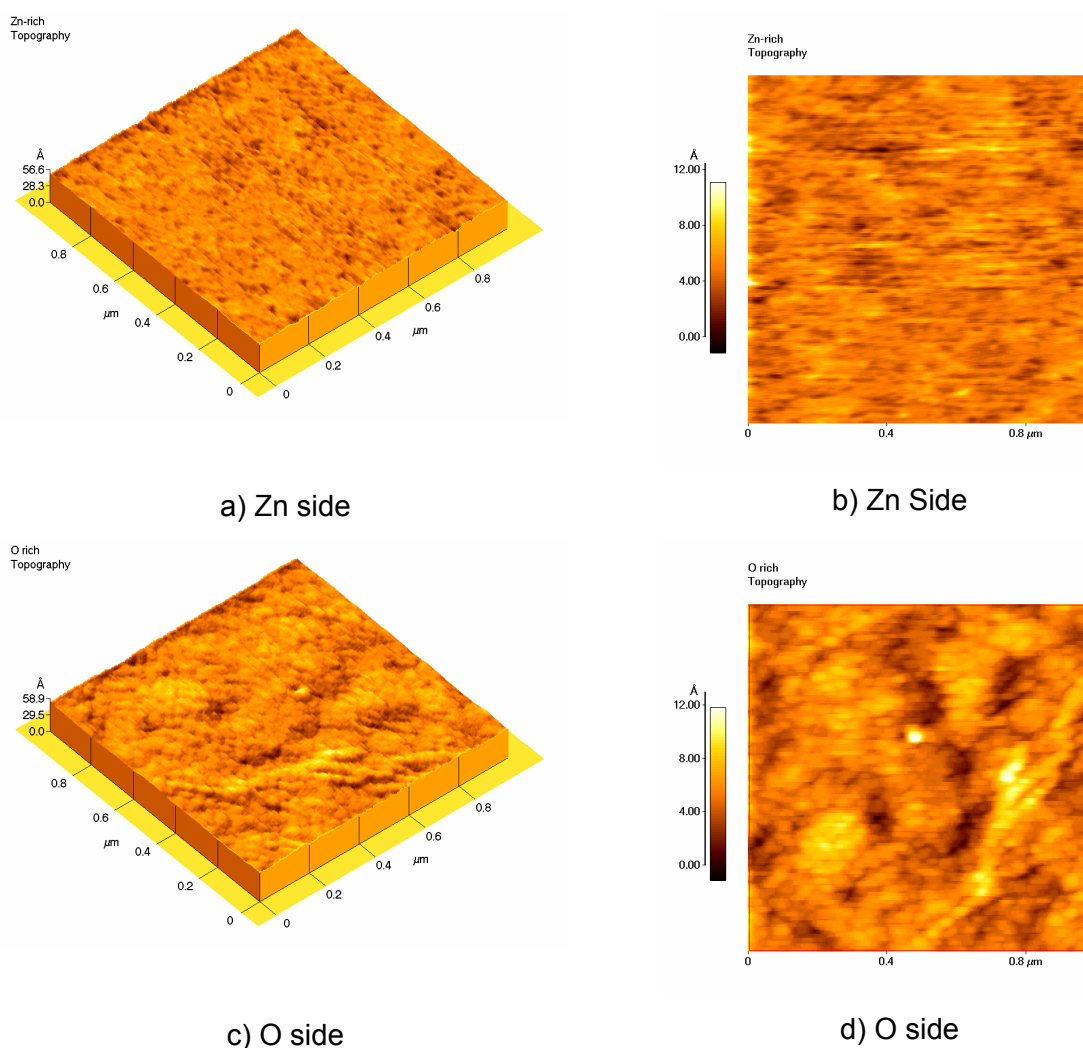
c) O side

d) O side

Figure 8.2.7. AFM topography images of ZnO substrates: a, b – Zn side; c, d – O side.
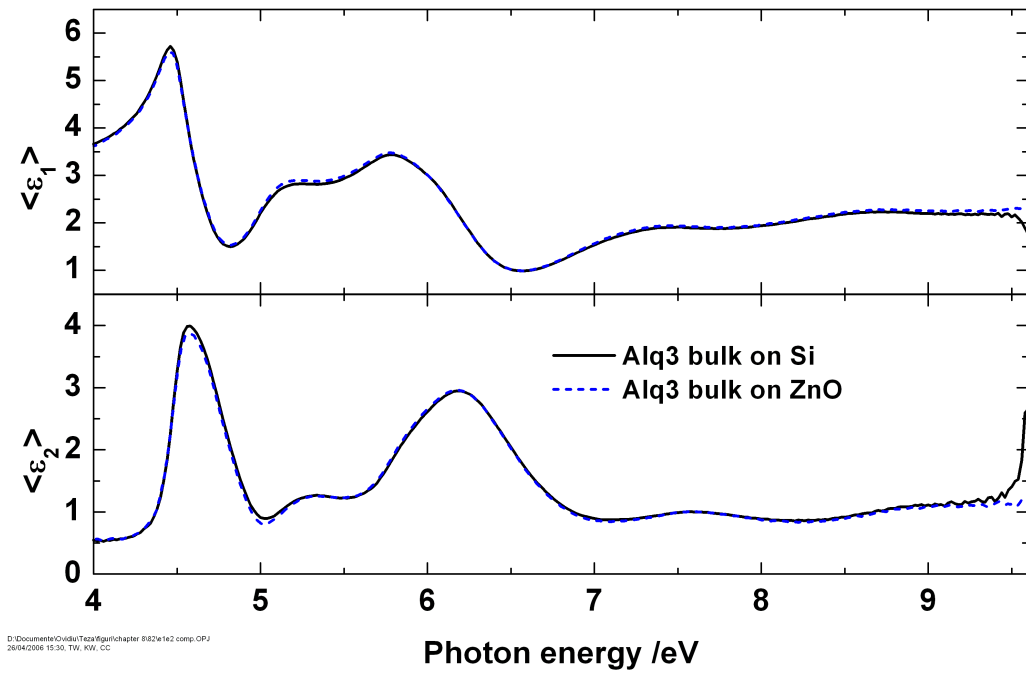
Figure 8.2.8. The measured effective dielectric function of bulk like Alq₃: continuous line – on silicon substrate, dashed line on ZnO substrate.
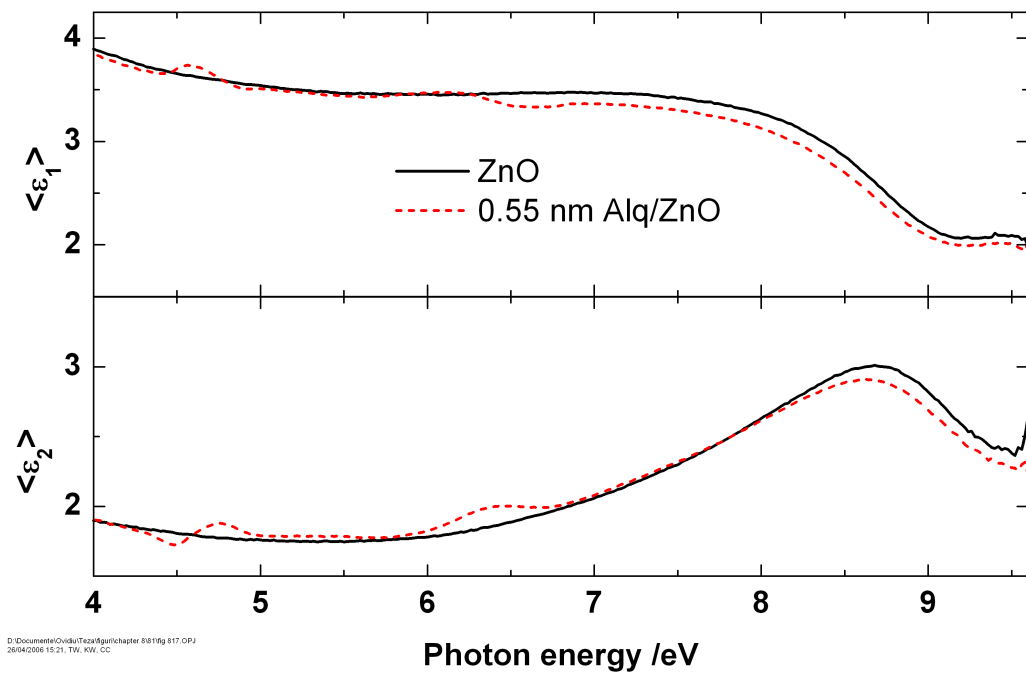
Figure 8.2.9. Continuous line – the complex dielectric function of ZnO; dashed line – the measured effective dielectric function of ZnO covered with 0.55 nm of Alq₃

In order to assess if the ZnO substrates induce a different growth mode and a different packing of Alq₃ molecules when compared to the growth mode of Alq₃ on H-Si(111), thick films were also prepared. The measured effective dielectric function for Alq₃ bulk like layers on ZnO was compared with the previous determined one on H-Si(111). As can be

seen in figure 8.2.8 the measurements are identical, indicating that the Alq_3 layers grown on ZnO have identical optical properties with the ones grown on H-Si(111).

The analysis of the Alq_3 ultra-thin films on ZnO substrates was performed as described before using the Aspnes approximation [Asp76]. Figure 8.2.9 presents the dielectric function of the ZnO substrates and the measured effective dielectric function of the substrate covered with 0.55 nm of Alq_3. In contrast to the H-Si(111), ZnO is practically featureless in the range where Alq_3 exhibits its absorption features, and the changes in the measured values are a clear indication of the Alq_3 presence on the surface. The analysis results of these values using equation 3.4.2 are presented in the figure 8.2.10.
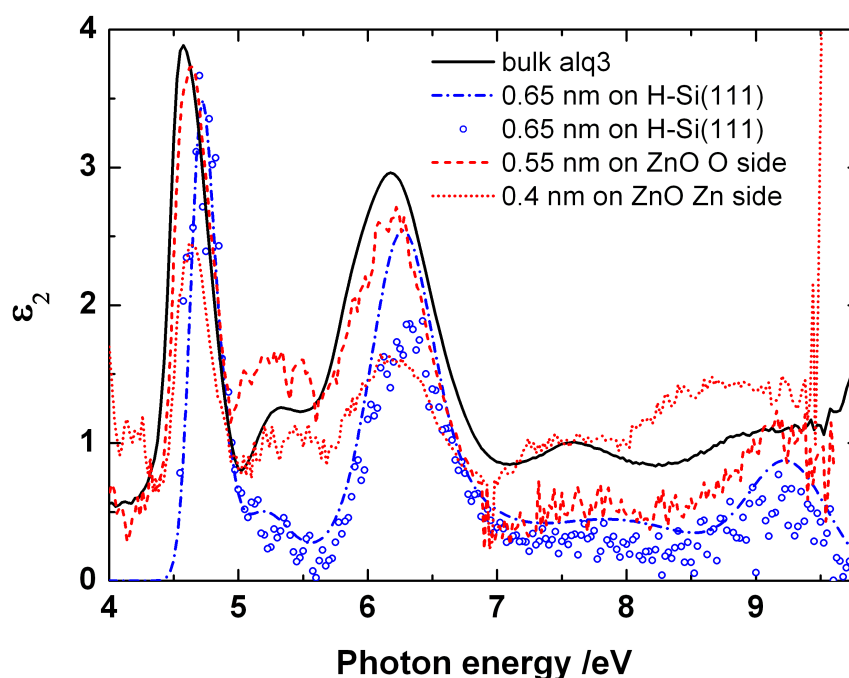
Figure 8.2.10. Comparison between the dielectric functions for a sub-monolayer of Alq_3 on H-Si(111) and on ZnO obtained from a model fit and calculated using equation 3.4.2. The dielectric function for bulk Alq_3 is also plotted. The calculated ε_2 from equation 3.4.2 is affected by the experimental noise of two different measurements.

As can be seen in the figure 8.2.10 the determined dielectric functions of the Alq_3 submonolayers on the ZnO substrate with Zn terminated surface as well as for the O terminated side, are almost identical with the bulk one. The differences in the amplitudes of the spectral features of Alq_3 are probably related to a small measurement calibration error. This indicates that both ZnO surfaces are inert and there is no chemical reaction with the Alq_3 molecules. A more closer look in the region from 4.3 eV to 5.2 eV (see figure 8.2.11) reveals that the shift of the strongest spectral feature of the Alq_3 submonolayers is smaller than for the Alq_3/H-Si(111) case. While it is hard to speculate about the reason for this shift, probably the high polarizability of the silicon substrate induces in the Alq_3 submonolayer a similar effect like the polarity of the solvent for Alq_3 in solution (see figure 8.2.5). However,

besides the high silicon polarizability other effects like inter-molecular interactions, deformation of the Alq$_3$ molecule on the silicon surface and the effective field induced by the arrangement of the Alq$_3$ molecules on the surface should not be neglected.
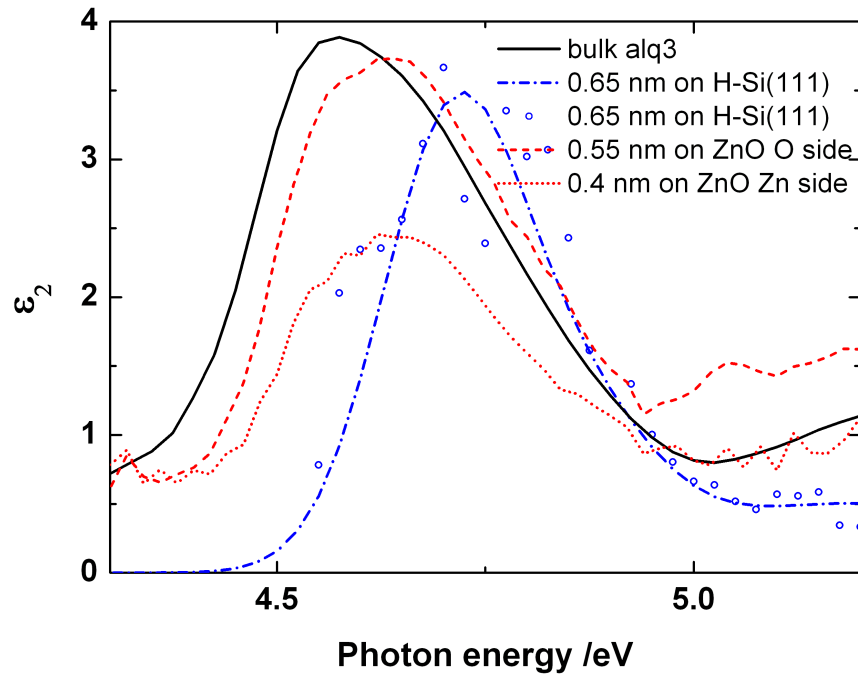
Figure 8.2.11. Comparison between the dielectric functions for a sub-monolayer of Alq$_3$ on H-Si(111) and on ZnO obtained from a model fit and calculated using equation 3.4.2. The dielectric function for bulk Alq$_3$ is also plotted. The calculated ε_2 from equation 3.4.2 is affected by the experimental noise of two different measurements. Zoom in the 4.3-5.2 eV spectral range.

8.3. α-NPD

A similar study was performed for α-NPD on H-Si(111) substrates. α-NPD is a blue light emitter and hole transporting material which is often used in combination with Alq$_3$ in OLEDs. Like Alq$_3$, α-NPD forms homogenous isotropic layers (see section 4.3). Figure 8.3.1 shows the measured effective dielectric function for several α-NPD layers with different thicknesses grown on H-Si(111) substrates in similar experimental conditions like the ones described at the beginning of the section 8.2. The optical response of the α-NPD can be simulated using the isotropic dielectric function presented in figure 8.3.2.

After determining the bulk dielectric function of α-NPD, ultra-thin layers were also prepared. The analysis of the measured data was performed like described in the section 8.2, namely using the three phase model and Aspnes approximation [Asp76]. The results are presented in figure 8.3.3.
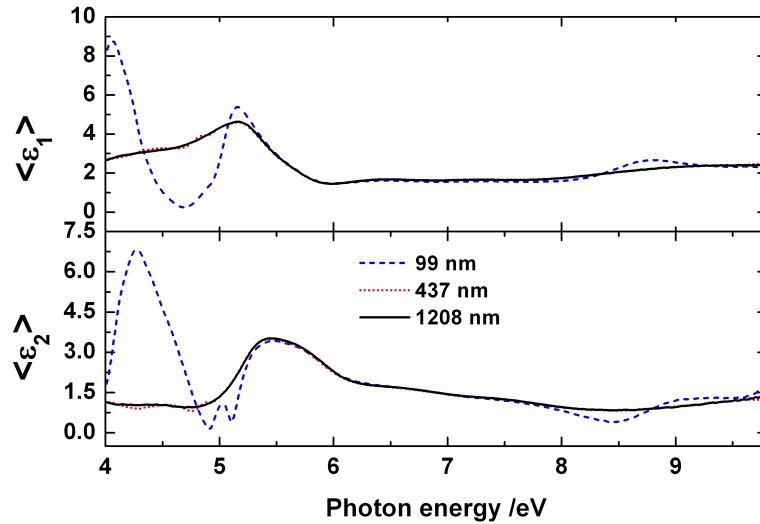
Figure 8.3.1. The measured effective dielectric function for different thicknesses of α-NPD layers on H-Si(111) substrates.

Figure 8.3.2. Dielectric function of α-NPD – continuous line, in comparison with the experimental effective dielectric function – open circles . Left - real part, right - imaginary part.

The result calculated using equation 3.4.2 is affected by the experimental noise of two different measurements, namely that of the H-Si(111) substrate (ε_s) and of the ultra-thin α-NPD layer ($<\varepsilon_L>$). In this case we had bigger noise in the low energy region of the recorded spectra, than for Alq_3 measurements. Due to this reason the calculated result is not plotted in this region. However, figure 8.3.3 clearly shows that in this case also there is a spectral shift of the dielectric function features, which probably can be attributed to two different contributions: inter-molecular interaction and the effect of the silicon substrate.
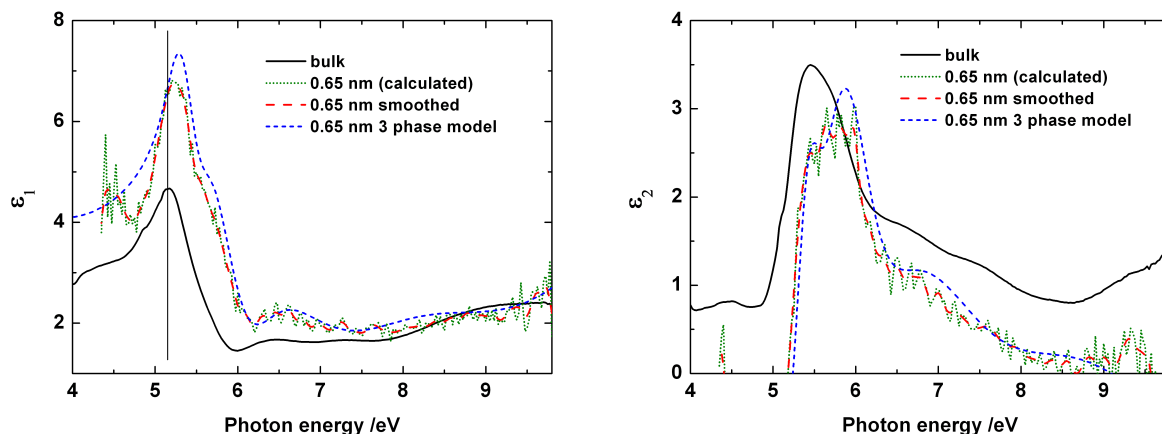
Figure 8.3.3. Comparison between the dielectric function for a sub-monolayer of α-NPD obtained from a model fit and calculated using equation 3.4.2. The dielectric function for bulk α-NPD is also plotted. The calculated ε_2 from equation 3.4.2 is affected by the experimental noise of two different measurements, namely that of the H-Si(111) substrate (ε_s) and of the ultra-thin α-NPD layer ($<\varepsilon_L>$).

8.4. Summary

As the low dimensional systems exhibit different optical properties compared to bulk it is vitally important to know the optical properties of very small aggregates in solid phase. We proved for the first time that sub-monolayer sensitivity can be achieved in the VUV range using spectroscopic ellipsometry and moreover the dielectric function of these very low coverages can be determined. While in the explanation of the spectral shifts still remain some open questions, we proposed several hypotheses. The strong shift observed for the silicon substrates is probably due to two contributions: inter-molecular interactions and the effect of the high polarizability of the silicon substrate. The changes induced by the inter-molecular interactions should be on the same magnitude as observed for the ZnO oxide substrates. This idea is also supported by the results obtained for the multilayered structure of Alq_3 and α-NPD and the mixed layers. Only small changes were noticed in the dielectric function of Alq_3 in these structures when compared to the bulk.

The amazing experimental resolution that can be achieved with ellipsometry in the VUV range is again demonstrated in figure 8.4.1. In the left side the measured Δ spectrum of the bulk Alq_3 is compared with the difference $\delta\Delta$ between the measured Δ spectrum of the H-Si(111) substrate and the measured Δ spectrum of the H-Si(111) + Alq_3. As can be seen in the right side of the figure 8.4.1 even a 0.65 nm of Alq_3 induced more than 2° changes in Δ values making it possible to determine the dielectric response. While the equation 3.4.2 was deduced 30 years ago by Aspnes [Asp76] and is valid for layer thicknesses much

smaller than the wavelength, we proved for the first time that this approximation is valid in the VUV range and gives similar result with the 3 phase model.
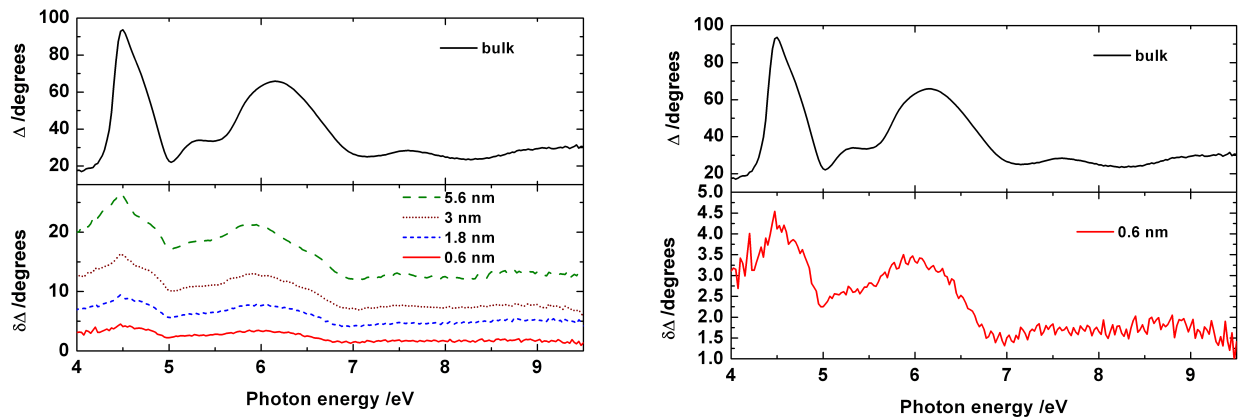
Figure 8.4.1. Comparison between the measured Δ of the bulk Alq_3 with the difference $\delta\Delta$ between the measured Δ value of the H-Si(111) substrate and the measured Δ value of the H-Si(111) + Alq_3

With the development of very stable Photo-Elastic Modulators (PEM) it is possible today to replace the mechanical rotating elements of the ellipsometer, used to analyze the polarization, with PEMs. There are companies which claim that the sensitivity of such ellipsometers is usually shot noise limited, and typically is equivalent to an ellipticity of about 10^{-5}, or to a polarisation angle of 10^{-3} degrees at a time constant of 1 s. This is equivalent to a detection limit of less than 10^{-12} m (1 pm) of oxide on the silicon surface (about 1/100 of a monolayer). This kind of accuracy in determining the Δ values would theoretically allow to determine the dielectric function of very thin layers even for photon energies lower than 4 eV.

9. Conclusions

Several organic systems were investigated using spectroscopic ellipsometry and IR spectroscopy. While the versatility of the variable angle measurements allows to determine the optical anisotropy, the measurements in the VUV range accessible in BESSY enabled us to obtain the dielectric function for ultra-thin films.

The growth of several Phthalocyanine molecules was investigated, and from the strong in-plane/out-of-plane anisotropy the average molecular orientation angle was determined. The knowledge of the molecular orientation combined with the information accessible from the shape of the Q-band of the Pc can provide an insightful picture of the molecular growth. While the Pc layers grown on HV condition grow with the b-axis (stacking axis) perpendicular to the substrate and $F_{16}PcVO$ lies on the KBr substrates, the Pc samples prepared in UHV adopt a parallel to the substrate b-axis configuration.

The ellipsometric studies on Pc / PTCDA heterostructures proved that PTCDA has a template effect on the Pc growth and the interaction between these two molecules affects the optical response at the interfaces. In contrast to this system where rough interfaces were assumed in the model, the combination Alq_3 / α-NPD gives sharp optical interfaces.

The *in situ* measurements performed at BESSY proved that sub-monolayer sensitivity can be achieved in the VUV range using spectroscopic ellipsometry and moreover the dielectric function of these ultra-thin films can be determined. A spectral shift towards higher energies of the Alq_3 and α-NPD features was observed for sub-monolayers on silicon substrate when compared with the bulk reference. The smaller shift observed for the Alq_3 sub-monolayers on ZnO substrate indicate that the effect of the silicon substrate has to be taken into account when explaining the spectral behaviour of the sub-monolayers.

While ellipsometry was extensively used in the last decades for fundamental research as well in industry for controlling and optimizing device performances, the advances in the numerical computation methods made it possible to simulate the optical response with anisotropic models only in recent years. This can be seen in the continuous increase of the scientific reports of anisotropic studies in the last two-three years. In contrast the surface sensitivity of this technique is well known for many years, but the interpretation of the experimental spectra still remains a challenge due to the reasons mentioned in this work. While the strong optical anisotropy of the highly oriented organic layers can be used to determine the molecular orientation, the access to the VUV range made possible to univocally determine the dielectric function of organic sub-monolayers.

References

[Agr82]   V. M. Agranovich and M. D. Galanin, Electronic Excitation Energy Transfer in Condensed Matter, North-Holland, Amsterdam (1982)

[Arw86]   H. Arwin and D.E. Aspnes, Thin Solid Films 138(1986) 195

[Ash66]   M. Assida – Bull. Chem. Soc. Jpn. 39 (1966) 2632

[Asp76]   D.E. Aspnes – Spectroscopic Ellipsometry of Solids, Chapter 15, Optical Properties of Solids-New Developments, ed B.Seraphin, North Holland (1976)

[Asp80]   D.E. Aspnes – J. Opt. Soc. Am, 70 (1980) 1275

[Asp83]   D.E. Aspnes, A.A. Studna – Phys. Rev. B 27 (1983) 985

[Ass65]   J. M. Assour and S. E. Harrison, J. Am. Chem. Soc. 87 (1965) 652

[Ass65a]   J. M. Assour, J. Phys. Chem. 69 (1965) 2295

[Ayu01]   B. M. Ayupov, S. A. Prokhorova, Optics and Spectroscopy 90 (2001) 446

[Azz92]   R.M.A. Azzam, N.M. Bashara – Ellipsometry and Polarized Light, Elsevier, Amsterdam (1992)

[Bao00]   Z. Bao – Adv.Mater.,12 (2000) 227-230

[Bar86]   M. A. Barret, Z. Borkowska, M. W. Humphreys and R. Parson, Thin Solid Films, 28 (1986) 137

[Bar91]   J. Barth, R. L. Johnson, and M. Cardona, - Handbook of Optical Constants of Solids II, edited by E. Palik, Academic Press, New York, (1991)

[Bay99]   S. M. Bayliss, S. Heutz, G. Rumbles, and T. S. Jones – Phys. Chem.1 (1999) 3673

[Ber00]   O. Berger, W. J. Fischer, B. Adolphi, S. Tierbach, V. Melev, J. Schreiber, J. Mater. Sci. 11 (2000) 331

[Ber72]   Berreman – J. Opt. Soc. Am. 62 (1972) 502

[Bli70]   L.M. Blinov and N. A. Kirichenko – Soviet Solid State Physics 12 (1970) 1574

[Bli72]   L.M. Blinov and N. A. Kirichenko – Soviet Solid State Physics 14 (1972) 2490

[Bor04]   E. G. Bortchagovsky, Z. I. Kazantseva, I. A. Koshets, S. Nespurek, L. Jastrabik, Thin Solid Films, 460 (2004) 269

[Bri00]   M. Brinkmann, G. Gadret, M. Muccini, C. Taliani, N. Masciocchi, A. Sironi – J. Am. Chem. Soc. 122 (2000) 5147

[Bro68]   C. J. Brown, J. Chem. Soc. A (1968) 2488

[Bru35]   D. A. G. Bruggeman, Ann. Phys. (Leipzig) 24 (1935) 636

[Bur64]   D.K. Burge and H.E. Bennett – J. Opt. Soc. Am, 54 (1964) 1428

[Cha86]   A. V. Chadwick, P. B. M. Dunning and J. D. Wright – Mol. Cryst. Liq. Cryst., 134 (1986) 137

[Che98]   C.H. Chen, J. Shi – Coord. Chem. ReV. 171 (1998) 161

[Cöl04]   M. Cölle, and W. Brütting, phys. Stat. sol. (a) 201 (2004) 1095

[Cra68]   D. P. Craig and S. H. Walmsley, Excitons in Molecular Crystals, W. A. Benjamin, Inc., New York (1968).

[Cur98]   A. Curioni, M. Boreo, W. Andreoni – Chem. Phys. Lett. 294 (1998) 263.

[Dav71]   A. S. Davydov, Theory of Molecular Excitons, Plenum Press, New York (1971)

[Deb91]   M.K. Debe and D.R. Field, J. Vac. Sci. Technol. A 9 (1991) 1265

[Deb92]   M.K. Debe, J. Vac. Sci. Technol. A 10 (1992) 2816

[Dju02]   A.B. Djurisic, C.Y. Kwong, T.W. Lau, W.L. Guo, E.H. Li, Z.T. Liu, H.S. Kwok, L.S.M. Lam, W.K. Chan, Optics Communications 205 (2002) 155–162

[Dog92]   S. Dogo, J. P. Germain, C. Maleysson, and A. Pauly – Thin Solid Films 219 (1992) 244

[Dow91]   J. Dowdy, J. J. Hoagland, and K. W. Hipps – J. Phys. Chem. 95 (1991) 3751

[Ebe52]   A. A. Ebert, H. B. Gottlieb, J. Am. Chem. Soc. 74 (1952) 2806

[ElN01]   M. M. El-Nahass, F.S. Bahabri, R.Al-Harbi, Egypt. J. Sol., 24 (2001) 11

[Ess95]   N. Esser, P. V. Santos, M. Kuball, M. Cardona. M. Arens, D. Pahlke, W. Richter, F. Stietz, J. A. Schaefer, B. O. Fimland – J. Vac. Sci. Technol. B 13 (1995) 1666

[For97]   S.R. Forrest – Chem. Rev. 97 (1997) 1793

[Fri01]   M. J. Frisch *et al. - Gaussian 03*, Gaussian, Inc.: Pittsburgh, PA, (2001)

[Fri02]   M. Friedrich, Th. Wagner, G. Salvan, S. Park, T. U. Kampen, D. R. T. Zahn, Appl. Phys. A. 75 (2002) 501.

[Fri03]   M. Friedrich, G. Gavrila, C. Himcinschi, T. U. Kampen, A. Yu. Kobitski, H. Mendez, G. Salvan, I. Cerrillo, J. Mendez, N. Nicoara, A. M. Baro, D. R. T. Zahn – J. Phys. Condens. Matter 15 (2003) 2699

[Gor04a]   O. Gordan, M. Friedrich, D. R. T. Zahn - Thin Solid Fims 455-456 (2004) 551-556

[Gor04b]   O. Gordan, M. Friedrich, D. R. T. Zahn, Organic Electronics 5 (2004) 291

[Gor04c]   O. Gordan, M. Friedrich, W. Michaelis, R. Kröger, T. Kampen, D. Schlettwein and D.R.T. Zahn – JMR 19, 7 (2004) 2008-2013

[Gor05a]   O.D. Gordan, S. Hermann, M. Friedrich, D.R.T. Zahn – J. Appl. Phys., 97 (2005) 063518

[Gor05b]   O.D. Gordan, S. Hermann, M. Friedrich, D.R.T. Zahn – Phys. stat. sol. (b), 242 (13) (2005) 2688

[Gor06a]   O.D. Gordan, T. Sakurai, M. Friedrich, K. Akimoto, and D.R.T. Zahn – submitted to Organic Electronics

[Gor06b]   O.D. Gordan, S. Hermann, M. Friedrich and D.R.T. Zahn – Journal de Physique

IV (Proceedings ICFSI-10), Vol. 132 (March 2006), 73

[Gor06c] O.D. Gordan, C. Himcinschi, D.R.T. Zahn, C. Cobet, N. Esser, W. Braun – Appl. Phys. Lett., 88 (2006) 141913

[Gri86] P.R. Griffiths, and J.A. de Haseth – Fourier transform infrared spectrometry, Wiley, (1986)

[Gu96] G. Gu, V. Bulovic, P. E. Burrows, S. R. Forrest, and M. E. Thompson, Appl. Phys. Lett. 68 (1996) 2606

[Hai98] Haiyan An, Baijun Chen, Jingying Hou, Jiacong Shen, Shiyong Liu, Appl. Phys. 31 (1998) 1144

[Hal01] M.D. Halls and H.B. Schlegel – Chem. Mater. 13 (2001) 2632

[Has92] A. K. Hassan and R. D. Gould – Physica Status Solidi A, Applied Research (1992) 132

[Her05] S. Hermann, O.D. Gordan, M. Friedrich, D.R.T. Zahn – Phys. stat. sol. (c) 2, 12 (2005) 4037

[Heu00] S. Heutz, R. Cloots, T. S. Jones: Appl. Phys. Lett. 77 (2000) 3938

[Heu03] S. Heutz, G. Salvan, S. D. Silaghi, T. S. Jones, D. R. T. Zahn, J. Phys. Chem. B. 107 (2003) 3782

[Him05] C.Himcinschi, N.Meyer, S.Hartmann, M.Gersdorff, M.Friedrich, W.Kowalsky, H.-H.Johannes, M.Schwambera, G.Srauch, M.Heuke, D.R.T.Zahn, Appl.Phys. A80 (2005) 551

[Him05a] C. Himcinschi, O. Gordan, G. Salvan, C. Cobet, N. Esser, W. Braun, F. Müller, N. Meyer, M. Heuken, and D.R.T. Zahn – Appl. Phys. Lett. – 86 (2005) 111907

[Hof00] M. Hoffmann, Ph.D. Thesis, Dresden (2000)

[Hof03] M. Hofmann – Mixing of Frenkel and Charge-Transfer Excitons and Their Quantum Confinement in Thin Films, in: V. M. Agranovich and G. F. Bassani (Eds.), Electronic Excitations in Organic Multilayers and Organic Based Heterostructures, Elsevier, Amsterdam (2003), Chapter 5, (Thin Films and Nanostructures, Vol. 31)

[Hoh00] D. Hohnholz, S. Steinbrecher, M. Hanack – J. Mol. Structure, 521 (2000) 231-238

[Hun02] L.S. Hung and C.H. Chen, Mat. Sci. Eng. R39 (2002) 143

[Jel92] G.E. Jellison – Opt. Mater. 1 (1992) 41

[Joh89] R. L. Johnson, J. Barth, M. Cardona, D. Fuchs, and A. M. Bradshaw – Rev. Sci. Instrum. 60 (1989) 2209

[Joh99] B. Johs, J. A. Woollam, C. M. Herzinger, J. Hilfiker, R. Synowicky, and C. L. Bungay – SPIE Crit. Rev. Opt. Sci. Technol. CR72 (1999) 29

[Ken53] D. N. Kendall, Anal. Chem. 25 (1953) 382

[Kol97]   B. A. Kolesov, T. V. Basova, and I. K. Igumenov – Thin Solid Films 304 (1997) 166

[Lez96]   C. C. Leznoff and A. B. P. Lever – Phthalocyanines: Properties and applications, ed. VCH, New York, 1996 vol. 4

[Lin34]   R.P. Linstead – J. Chem. Soc., (1934) 1016

[Mcg93]   W. A. Mcgahn, B. Johs, J. A. Wollam, Thin Solid Films 234, (1993) 443

[McI71]   J. D. E. McIntyre and D. E. Aspnes – Surface Science 24 (1971) 417

[McK98]   N. B. McKeown,– Phthalocyanine materials, Cambrige University Press (1998)

[Mön93]   W. Mönch – Semiconductor Surfaces and Interfaces, Springer, Berlin (1993)

[Nes94]   S. Nespurek, H. Podlesak, and C. Hamann – Thin Solid Films 249 (1994) 230

[Oga99]   T. Ogawa, K. Kuwamoto, S. Isoda, T. Kobayashi, N. Karl, Acta Cryst. B 55 (1999) 123

[Ohw97]   T. Ohwaki, M. Takeda, Y. Takai – Jpn. J. Appl. Phys. 36 (1997) 5507

[Pal85]   E. Palik (ed) Handbook of Optical Constants of Solids. Acad. Press. 1985, Vol. 1, p. 759

[Pop99]   M. Pope and C. Swenberg – Electronic Processes in Organic Crystals and Polymers (Oxford Univ. Press, New York, 1999) 2nd ed.

[Pro04]   H. Proehl, T. Dienel, R. Nitsche, and T. Fritz – Phys. Rev. Lett. 93 (2004) 097403

[Rit83]   A. Ritz and H. Lüth – Appl. Phys. A 31 (1983) 75

[Rob35]   J. M. Robertson, J. Chem. Soc. (1935) 615

[Ros93]   U. Rossow, U. Frotscher, W. Richter and D. R. T. Zahn – Surface Science 287/288 (1993) 718

[Ros96]   U. Rossow, W. Richter – Optical Characterization of Epitaxial Semiconductor Layers, Chapter 3, Spectroscopic Ellipsometry, Springer, Berlin (1996)

[Sak05]   T. Sakurai, S. Kawai, J. Shibata, R. Fukasawa, K. Akimoto, Jpn. J. Appl. Phys. 44 (2005) 1982.

[Sak06]   T. Sakurai, R. Fukasawa, K. Akimoto, Jpn. J. Appl. Phys. 45 (2006) 255.

[San95]   P.V. Santos, N. Esser, J. Groenen, M. Cardona, W.G. Schmidt, F. Bechstedt, Phys. Rev. B 52 (1995) 17379

[Sch00]   R. Scholz, A.Yu. Kobitski, T.U. Kampen, M. Schreiber, D.R.T. Zahn, G. Jungnickel, M. Elstner, M. Sternberg, and Th. Frauenheim, Phys. Rev. B 61 (2000) 13659.

[Sch00a]   D. Schlettwein, H. Tada, S. Mashiko, Langmuir 16 (2000) 2872

[Sch00b]   D. Schlettwein, K. Hesse, H. Tada, S. Mashiko, U. Storm, J. Binder, J.

Chem.Mater. 12 (2000) 989

[Sch01]   R. Scholz, I. Vragovic, A. Yu. Kobitski, G. Salvan, T. U. Kampen, M. Schreiber, D. R. T. Zahn, Proceedings of Enricon Fermi school, Varenna, (2001).

[Sch96]   M. Schubert – Phys. Rev. B 53 (1996) 4265

[Sid61]   A. N. Sidorov, I. P. Kotlyar Opt. I Specktroskopiya 11 (1961) 175

[Sil05]   S. Silaghi – PhD. Thesis, TU-Chemnitz 2005 Chemnitz, Germany

[Sil94]   E. A. Silinsh, V. Čápek – Organic Molecular Crystals, AIP press, New York (1994)

[Tan87]   C.W. Tang and S.A. van Slyke, Appl. Phys. Lett. 51 (1987) 913

[Tok95]   S. Tokito, J.Sakata, and Y. Taga – Thin Solid Films 256 (1995) 182

[Tok95]   S. Tokito, J. Sakata, Y. Taga: Thin Solid Films 256 (1995) 182

[Wet98]   T. Wethkamp, K. Wilmers, N. Esser, W. Richter, O. Ambacher, H. Angerer, G. Jungk, R. L. Johnson, and M. Cardona - Thin Solid Films 313-314 (1998) 745

[Woo99]   J. A. Woollam, B. Johs, C.M. Herzinger, J. Hilfiker, R. Synowicki, and C. L. Bungay – Overview of Variable Angle Spectroscopic Ellipsometry (VASE), Critical Reviews of Optical Science and Technology, Vol. CR72 (1999)

[Yim03]   S. Yim, S. Heutz, and T. S. Jones – Phys. Rev. B 67 (2003) 165308

[Yiq03]   Yiqun Wu, Donghong Gu, Fuxi Gan, Optical Materials 24 (2003) 477–482

[Yon96]   H. Yonehara, C. Pac – Thin Solid Films, 278, 1-2 (1996) 108-113

List of Tables

List of Figures

Erklärung

Ich erkläre, dass ich die vorliegende Arbeit selbständig und nur unter Verwendung der angegebenen Literatur und Hilfsmittel angefertigt habe.

April 2006

Master in Physik Ovidiu D. Gordan

Lebenslauf

Ovidiu Dorin Gordan

Date of birth	20 August 1978
Place of birth	Cluj-Napoca, Romania
Nationality	Romanian
Family status	Married
Foreign languages	English, French

Education

2003-2006	PhD. studies at the Institute of Physics, University of Technology Chemnitz, Germany
	"*Molecular Orientation and Electronic Interactions in Organic Thin Films Studied by Spectroscopic Ellipsometr*"
10.2002-07.2003	Master degree in Solid State Physics obtained at Babeş-Bolyai University Cluj-Napoca, Romania in collaboration with the Chemnitz University of Technology, Chemnitz, Germany
	"Determination of the Anisotropic Dielectric Function for Metal Free Phthalocyanine Thin Films"
	supervisor Prof. Dr. D. R. T. Zahn
	Dissertation Grade 10 (out of 10)
10.1997-07.2002	Physics engineering license
	8.72 (out of 10) best average grade on all academic years from all students (Valedictorian)
	"Magnetic Behaviour of $HoNi_{5-x}Al_x$ System With $x \leq 1.5$", supervisors: Prof. Dr. E. Burzo and Conf. Dr. R. Tetean
	Licence Grade 9.49 (out of 10) – best score from all the students of the faculty
09.1993-07.1997	Highschool: "Nicolaie Balcescu", Cluj-Napoca, Romania, informatics class
	Average grade for 4 years of study 9.23 (out of 10)
	Baccalaureate Grade: 8.94 (out of 10)
	Programming Assistant Diploma

Publication List (as of April 2006)

14) **O.D. Gordan,** T. Sakurai, M. Friedrich, K. Akimoto, and D.R.T. Zahn
Ellipsometric Study of an Organic Template Effect: $H_2Pc/PTCDA$
Organic Electronics, submitted

13) **O.D. Gordan,** C. Himcinschi, D.R.T. Zahn, C. Cobet, N. Esser, W. Braun
Reduced Intermolecular Interaction in Organic Ultrathin Films
Appl. Phys. Lett., 88, 141913 (2006)

12) **O.D. Gordan**, S. Hermann, M. Friedrich and D.R.T. Zahn
Optical properties of the interfaces in organic/organic multilayered heterostructures
Journal de Physique IV (Proceedings ICFSI-10), Vol. 132 (March 2006), 73

11) Y. Suzuki, **O.D. Gordan**, S.D. Silaghi, D.R.T. Zahn, A. Schubert, W.R. Thiel, C. Cobet, N. Esser, W. Braun
Strong Changes in the Dielectric Functions of Cytosine upon Molecular Modification
Appl. Phys. Lett., 87 (2005) 214101

10) **O.D. Gordan**, D.R.T. Zahn
The Anisotropic Dielectric Function for Copper Phthalocyanine Thin Films
New Trends in Advanced Materials (The West University of Timisoara), (2005) 83, ISBN 973-7608-41-0

9) **O.D. Gordan**, S. Hermann, M. Friedrich, D.R.T. Zahn
Comparative Study of Dielectric Function of Complex Organic Heterostructures
Phys. stat. sol. (b), 242 (13) (2005), 2688

8) C. Himcinschi, **O. Gordan**, G. Salvan, F. Müller, D.R.T. Zahn, C. Cobet, N. Esser, W. Braun
Stability of tris(8-hydroxyquinoline)-Aluminium(III) Films Investigated by Vacuum Ultraviolet Spectroscopic Ellipsometry
Appl. Phys. Lett., 86 (2005) 111907

7) S. Hermann, **<u>O.D. Gordan</u>**, M. Friedrich, D.R.T. Zahn

Optical Properties of Multilayered Alq$_3$/α-NPD Structures Investigated with Spectroscopic Ellipsometry

Phys. stat. sol. (c) 2, 12 (2005) 4037

6) **<u>O.D. Gordan</u>**, S. Hermann, M. Friedrich, D.R.T. Zahn

Optical Properties of PTCDA/CuPc Superlattices

J. Appl. Phys., 97 (2005) 063518

5) **<u>O.D. Gordan</u>**, M. Friedrich, D.R.T. Zahn

The Anisotropic Dielectric Function for Copper Phthalocyanine Thin Films

Organic Electronics, 5 (2004) 291

4) **<u>O.D. Gordan</u>**, C. Himcinschi, Yu J. Suzuki, G. Salvan, D. R. T. Zahn, C. Cobet, N. Esser, W. Richter, W. Braun

Sub-Monolayer Sensitivity in VUV Ellipsometry Investigations of Organic Thin Films

BESSY Jahresbericht (2004) 170

3) **<u>O.D. Gordan</u>**, M. Friedrich, W. Michaelis, R. Krüger, T.U. Kampen, D. Schlettwein, D.R.T. Zahn

Determination of the Anisotropic Optical Properties for Perfluorinated Vanadyl Phthalocyanine Thin Films

J. Mater. Res., 19 (2004) 2008

2) **<u>O.D. Gordan</u>**, M. Friedrich, D.R.T. Zahn

Determination of the Anisotropic Dielectric Function for Metal Free Phthalocyanine Thin Films

Thin Solid Films, 455-456 (2004) 551

1) S. D. Silaghi, Yu J. Suzuki, **<u>O. D. Gordan</u>**, C. Himcinschi, G. Salvan, M. Friedrich, T. U. Kampen, D. R. T. Zahn C. Cobet, N. Esser, W. Richter, W. Braun

VUV – Spectroscopic Ellipsometry Investigations of DNA Base Layers Grown onto Flat H-passivated Silicon Surfaces

BESSY Jahresbericht (2003) 209

Acknowledgements

First I would like to thank my wife, who came with me to Chemnitz and supported me in all the possible ways along these years. Thank you for your love, care and unconditional help.

Special thanks go to Prof. Zahn. I learnt a lot from you during these years, and it was a pleasure doing my PhD. under your supervision. While at the beginning I was stressed by your pressure of writing papers, now at the end I realised that everything was for my own advantage and it was fast and easy to write this thesis. Therefore I thank you again for your guidance, for the useful discussions and I wish you to guide many other students to their PhDs.

I would also like to thank Prof. Dr. N. Esser and Prof. Dr. F. Richter for taking the time to correct and referee my thesis.

Another special place in these acknowledgements is dedicated to Marion. If you need help go to Marion! She will never refuse you and she will kindly assist you in everything. I have to thank you and Cami for introducing me to ellipsometry and IR.

I would like to thank also the people from Berlin for their help during our often BESSY beam-times - Prof. Esser for useful discussions, Dr. Cobet and Simona for the beam-time support and Dr. Brawn for the beam time allocation. Along with these people I have to thank to Dr. Uwe Rossow and Dr. Reinhard Scholz for useful discussions.

For useful discussions and for providing some of the samples presented in this thesis I also have to thank Prof. Schlettwein, Dr. Michaelis and Dr. Sakurai. Sascha also did a great job in preparing the heterostructures and the sample holder for the *in situ* ellipsometry.

I thank Axel for all the technical help he provided in these years. Next to Axel I also thank all HLPH members and guests for the nice time spent together – Alexander, Cami, Beynor, Dan, Dirk, Ela, Geta, Giani, Henry, Ilja, Marion, Matthias, Reinhard, Sascha, Simona, Sindu, Stefan, Yu and Prof. Zahn. I appreciate the time spent with all the people involved in the Accumol Graduate College.

I will always remember with pleasure the people who shared with me the office 457– Yu, Dan and Sascha, whom I terrorized with my jokes. Thank you for the nice discussions about girls and for the long days and very long nights that we spent working together in BESSY. With you the time passed so fast. Next to them I have to mention Cami, Stefan, Simona who also joined me in BESSY.

I would also like to thank to Sybille Raschke, Kornelia Dostmann, Maud Marx and Ellen Schmidt-Kampen help in the administrative field.

I want also to thank Cami and Geta for their warm friendship, for all their help and support in my work, and for the great free time spent together.

Last but not least I want to thank my wonderful parents, my sister and Cristina's parents for their continuous support and care.